

AD-A096 633

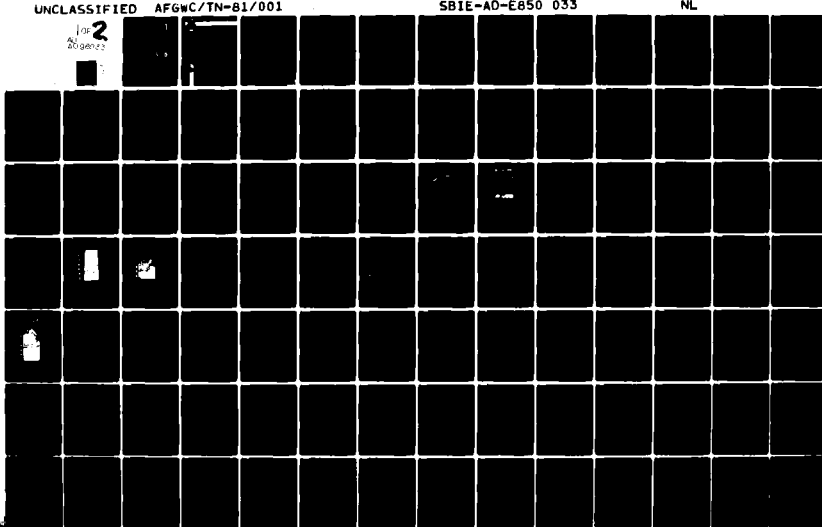
AIR FORCE GLOBAL WEATHER CENTRAL OFFUTT AFB NE  
SHORT TERM HF FORECASTING AND ANALYSIS. (U)  
JAN 81 J A MANLEY  
UNCLASSIFIED AFGWC/TN-81/001

F/G 4/1

SBIE-AD-E850 033

NL

for 2  
200000

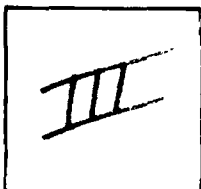


PHOTOGRAPH THIS SHEET

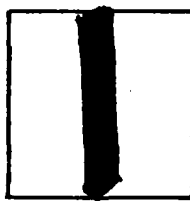
AD-E850033

AD A 096833

DTIC ACCESSION NUMBER



LEVEL



INVENTORY

Rept. No. AFGWC/TN-81-001

DOCUMENT IDENTIFICATION

Jan 81

DISTRIBUTION STATEMENT A

Approved for public release  
Distribution Unlimited

DISTRIBUTION STATEMENT

ACCESSION FOR

NTIS GRA&I

DTIC TAB

UNANNOUNCED

JUSTIFICATION

BY

DISTRIBUTION /

AVAILABILITY CODES

DIST AVAIL AND/OR SPECIAL

A

DISTRIBUTION STAMP

DTIC  
ELECTED  
S MAR 24 1981 D  
D

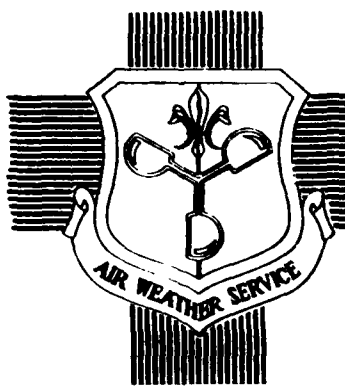
DATE ACCESSIONED

81 3 23 070

DATE RECEIVED IN DTIC

PHOTOGRAPH THIS SHEET AND RETURN TO DTIC-DDA-2

AF/C 850033  
AFG/C/TN - 81/001



SHORT TERM HF FORECASTING AND ANALYSIS

ADA096833

By

CAPT JAMES A. MANLEY

APPROVED FOR PUBLIC RELEASE; DISTRIBUTION UNLIMITED



JANUARY 1981

UNITED STATES AIR FORCE  
AIR WEATHER SERVICE (MAC)  
AIR FORCE GLOBAL WEATHER CENTRAL  
OFFUTT AFB NE 68113

81 3 23 070

REVIEW AND APPROVAL STATEMENT

This publication approved for public release. There is no objection to unlimited distribution of this document to the public at large, or by the Defense Technical Information Center (DTIC) to the National Technical Information Service (NTIS).

This technical publication has been reviewed and is approved for publication.

*Ronald L. Lininger*

RONALD L. LININGER, Lt Colonel, USAF  
Reviewing Official

FOR THE COMMANDER

*James A. Young*

JAMES A. YOUNG, Lt Colonel, USAF  
Chief, Technical Services Division



## TABLE OF CONTENTS

	<u>PAGE</u>
1. Introduction.....	1
2. Data Processing and Analysis Philosophy.....	1
3. The HF Radio Propagation Bulletin.....	4
4. Basic Principles of HF Propagation.....	9
5. Sporadic E.....	25
6. Spread F.....	31
7. Auroral Oval.....	37
8. Shortwave Fades.....	48
9. Polar Cap Absorption Events.....	48
10. MUF Forecasting.....	76
11. Ionospheric Storms.....	76
12. Communicator Reports as a Diagnostic Tool.....	91
13. HF Effects From a Nuclear Explosion.....	95

## LIST OF ILLUSTRATIONS

	<u>PAGE</u>
FIGURE 1      Sample monthly MUF-FOT prediction study.	2
2      A sample predicted path reliability prediction.	3
3      A sample primary HF propagation bulletin.	5
4      Sectors of the earth for which HF propagation forecasts are made.	6
5      Geomagnetic latitude variation with respect to geographic coordinates.	7
6      Regions of the ionosphere.	10
7      The diurnal variation of middle latitude foF2 with season and sunspot number.	13
8      MUF, LUF, foF2, and foE as a function of sunspot number.	14
9      Control points for F layer and E layer propagation modes.	17
10     Various propagation modes for HF signals.	18
11     An illustration of the wave angle, ground wave, skip distance, and skip zone.	19
12 a    Values of atmospheric noise (Autumn).	21
b    Values of atmospheric noise (Winter).	22
c    Values of atmospheric noise (Spring).	23
d    Values of atmospheric noise (Summer).	24

13	Propagation modes that can result from Sporadic E occurrence.	26
14	The seasonal and local time variation of sporadic E occurrence at Narsarssuak, Greenland, Washington, D.C., and Huancayo, Peru.	27
15 a	Percentage of time for which sporadic E exceeds 7 MHz during the summer months.	28
b	Percentage of time for which sporadic E exceeds 7 MHz during the non-summer months.	29
c	Percentage of the year for which sporadic E exceeds 7 MHz.	30
16	Graphs for determining typical foE values for different latitudes and local times.	32
17	High latitude Blanketing E occurrence in the post-midnight sector.	33
18	DMSP photograph showing discrete aurora.	34
19	DMSP photograph showing an intense substorm.	35
20	Ionospheric observations showing Spread F occurrence.	36
21	Ionospheric sounder data illustrating Spread F occurrence at the lower latitude.	38
22	A schematic illustration of the various stages of an auroral substorm.	39
23	Geomagnetic indices for 26 July 1979.	40
24	Geomagnetic indices for 27 July 1979.	41
25	Qe indices calculated from DMSP data for 26 July 1979.	42
26	Qe indices calculated from DMSP data for 27 July 1979.	43
27	The diurnal variation of the auroral oval position with respect to a given station.	45
28	An illustration of the extent of the sub-auroral trough near the maximum of a substorm.	46
29	DMSP photograph showing patch aurora associated with auroral zone absorption.	47
30 a	Solar flare associated shortwave fade 25 Oct 1972.	49
b	Solar flare associated shortwave fade 26 Oct 1972.	50
31	An illustration of solar x-ray event effects on a sulit HF circuit.	51

32	X-ray classification versus estimated SWF magnitudes and duration.	52
33	Forecaster display of LUF predictions.	53
34	A plot of the auroral oval position calculated from DMSP data.	55
35 a	Ionospheric sounder data for 14 September 1979.	56
b	Ionospheric sounder data for 15 September 1979.	57
c	Ionospheric sounder data for 16 September 1979.	58
d	Ionospheric sounder data for 17 September 1979.	59
e	Ionospheric sounder data for 18 September 1979.	60
f	Ionospheric sounder data for 19 September 1979.	61
g	Ionospheric sounder data for 20 September 1979.	62
h	Ionospheric sounder data for 21 September 1979.	63
36	Thule 30 MHz riometer absorption during the period 6-9 June 1979.	65
37 a	High latitude ionospheric sounder observations for 6 June 1979.	66
b	High latitude ionospheric sounder observations for 7 June 1979.	67
c	High latitude ionospheric sounder observations for 8 June 1979.	68
d	High latitude ionospheric sounder observations for 9 June 1979.	69
38 a	Ionospheric sounder observations (qualifiers) for 19 August 1979.	70
b	Ionospheric sounder observations (qualifiers) for 20 August 1979.	71
c	Ionospheric sounder observations (qualifiers) for 21 August 1979.	72
d	Ionospheric sounder observations (qualifiers) for 22 August 1979.	73
e	Ionospheric sounder observations (qualifiers) for 23 August 1979.	74
39	Geomagnetic activity during the period 19-23 August 1979.	75
40	The local time variation of foF2 values of three low latitude stations.	77
41	Ionospheric storm effects on the range of usable HF frequencies.	79
42	Time of peak depression during ionospheric storms.	80
43	Storm-time foF2 deviations.	81

44	Forecaster display of predicted MUF variations at different latitudes and local times.	82
45	Forecaster display of geomagnetic activity on 29 August 1979.	84
46	Forecaster display of geomagnetic activity on 30 August 1979.	85
47	Forecaster display of foF2 deviations on 29 August 1979.	86
48	Forecaster display of MUF deviations on 29 August 1979.	87
49	Forecaster display of foF2 deviations on 30 August 1979.	88
50	Forecaster display of MUF deviations on 30 August 1979.	89
51	Forecaster display of foEs values for 29 August 1979.	90
52	Forecaster display of foEs values for 30 August 1979.	92
53	Forecaster display of qualifies for 29 August 1979.	93
54	Forecaster display of qaulified for 30 August 1979.	94
55	Calculated electron densities at an altitude of 45 miles for a 1 megaton explosion.	97
56	Phenomena associated with high-altitude nuclear explosions.	98
57	Radius of debris expansion and corresponding D-region electron density as a function of time in the altitude range of 10 to 40 miles.	100
58	Radius of debris expansion and corresponding D-region electron density in the altitude range of 40 to 70 miles.	101

## INTRODUCTION

In this paper, the framework through which short term high frequency (HF) forecasts and analyses are produced by the Space Forecasting Branch of the Air Force Global Weather Central will be examined. For the forecaster who produces the short term forecast, this paper will emphasize the techniques for interpreting the data set available to him. For the user of the short term forecast, it will show the limitations of such products and hopefully improve the user's understanding and use of the forecast product.

## DATA PROCESSING AND ANALYSIS PHILOSOPHY

A comprehensive data set sufficient to specify HF propagation conditions is not available. Observations from a number of ground based ionospheric sounders are available through an international data exchange arrangement and Air Weather Service resources. Ionospheric observations from riometers and polarimeters combined with geomagnetic and auroral indices are also used to infer HF propagation conditions. Realtime satellite x-ray and particle observations are used to monitor for solar induced ionospheric disturbances. Additional information on selected HF paths is obtained through communicator reports and routine telephone contacts with HF communicators.

The major limitations of the available data set are the lack of ionospheric observations over large areas of the forecast area (northern hemisphere) and the delayed receipt (12-24 hours) of many of the observations. With these limitations, great reliance is placed on the forecaster's ability to infer ionospheric conditions, both present and future. The initial analysis process is the comparison of ionospheric sounder observations with "quiet day" baselines. These baselines, generated by the Institute of Telecommunications Services (ITS) model, serve as a climatological base from which a "first guess" ionosphere can be constructed. Computer generated displays of deviations from the ITS fields help the forecaster identify ionospheric synoptic patterns. These synoptic patterns are the basis from which HF propagation conditions are inferred. Additional information is obtained through observations of geomagnetic field variations and auroral observations obtained from the Defense Meteorological Satellite Program (DMSP). These data combined with ionospheric observations form the basis from which high latitude HF conditions are inferred. While the dynamic properties of the high latitude ionosphere prohibit a detailed description, the general state of HF propagation can be inferred from knowledge of the spatial and temporal variations of both the quiet and disturbed ionosphere.

In general, no attempt is made to quantify such analyses in terms of frequency specification for a given HF circuit. The large number of customers and circuits combined with frequency allocation restrictions would make such a task overwhelming. Rather, it is assumed the user of the short term forecast has monthly mean predictions such as those illustrated in Figure 1 and Figure 2.\* Frequency predictions such as these are generated by the ITS model and provide

\*Predictions such as these are available on a routine basis through a joint HQ AFCC and AFGWC effort. Users interested in obtaining such a product should contact HQ AFCC/XOPR at Scott AFB, IL, AUTOVON 638-5486.

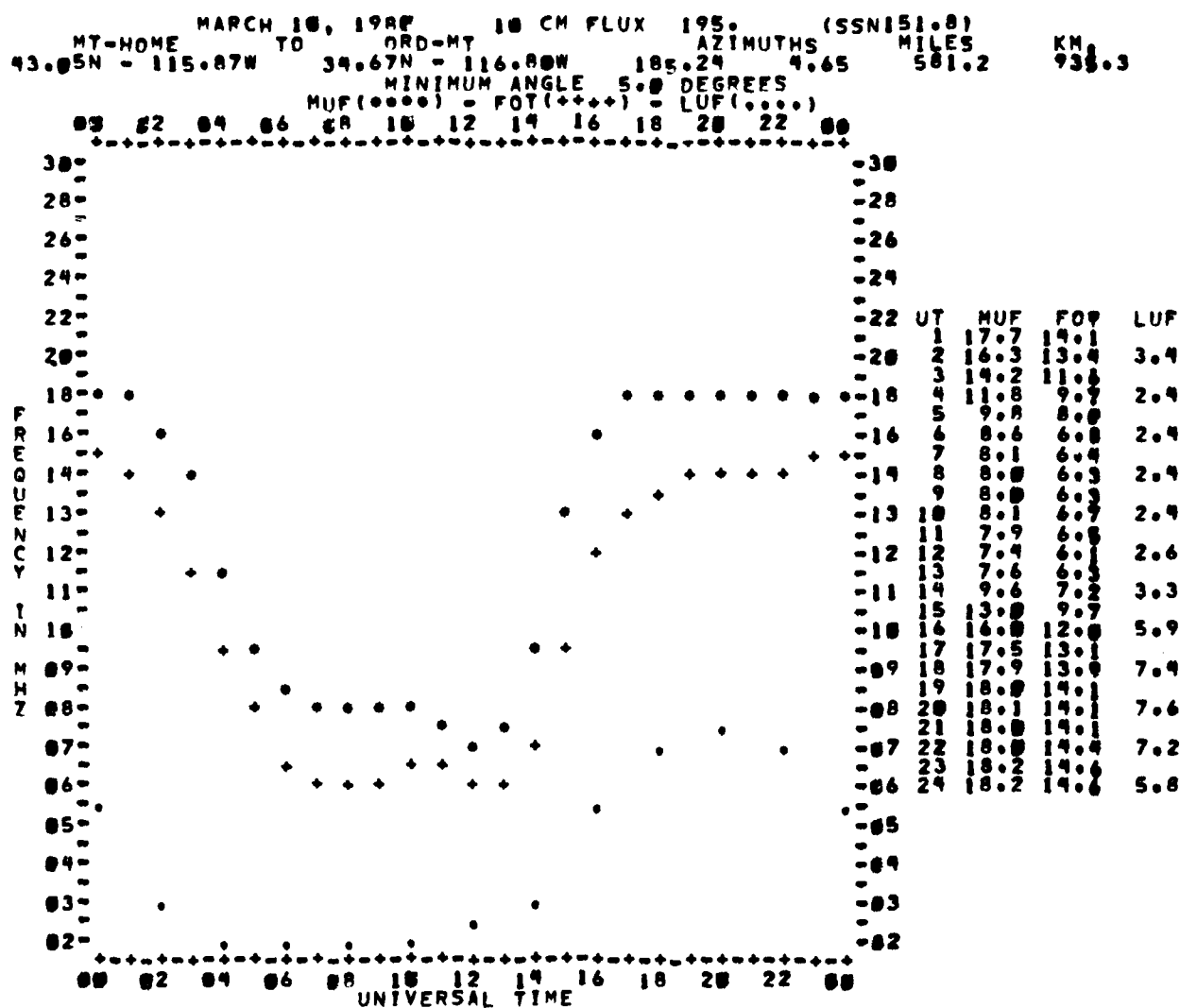


Figure 1. A sample monthly MUF - FOT prediction study.

MARCH 18, 1981 16 CM FLUX 195. (SSN151.8)

MT-HOME TO ORD-MT DISTANCE 581.2 KM  
 43.45N - 115.87W 34.67N - 116.80W 18E.24 4.65 581.2 935.3  
 MINIMUM ANGLE 5.0 DEGREES

XMTR 2.6 TO 3E.0 HOR LPA H 17.46 L 38.81 A 62.1 OFF AZ .0  
 RCVR 2.4 TO 3E.0 HOR LPA H 17.46 L 38.81 A 62.1 OFF AZ .0  
 POWER= 1.0kW 3 MHZ NOISE=-148.0dBW TIME= 99 PERCENT REQ,S/N=54.0dB  
 MULTIPATH POWER TOLERANCE=10.0 dB MULTIPATH DELAY TOLERANCE=1.50 MS.

FREQUENCIES IN MHZ

UT	MUF	5.0	6.0	7.0	8.0	9.0	10.0	11.0	12.0	13.0	14.0	15.0	16.0
82	K(2)MUF=(18.2)	K(5)MUF=(14.1)											
	IF	IF	IF	IF	IF	IF	IF	IF	IF	IF	IF	IF	MODE
	36.8	26.5	26.2	26.2	26.3	26.6	26.9	27.3	28.2	28.6	30.8	36.8	ANGLE
	.56	.99	.99	.99	.99	.99	.99	.98	.95	.92	.73	.18	F DAYS
	41.	43.	43.	42.	40.	39.	47.	38.	31.	35.	40.	41.	DBU
	81.	86.	87.	85.	86.	89.	83.	91.	88.	93.	79.	79.	S/N DB
	.47	.96	.96	.95	.93	.96	.93	.06	.92	.98	.67	.16	REL
	-	-	-	-	-	-	.91	-	-	-	-	-	MP PRO
84	K(3)MUF=(13.0)	K(5)MUF=(16.2)											
	IF	IF	IF	IF	IF	IF	IF	IF	IF	15	-	-	MODE
	37.4	27.2	27.5	28.8	28.6	29.4	30.6	32.5	37.4	37.4	11.0	-	ANGLE
	.56	.99	.99	.99	.98	.95	.86	.69	.36	.18	.5	-	F DAYS
	40.	45.	45.	43.	43.	35.	38.	33.	42.	43.	48.	-	DBU
	88.	87.	87.	87.	81.	96.	82.	93.	98.	94.	91.	-	S/N DB
	.49	.97	.97	.97	.95	.93	.84	.69	.38	.18	.5	-	REL
	-	-	-	-	-	-	-	-	-	-	-	-	MP PRO
66	K(3)MUF=( 9.6)	K(5)MUF=( 7.7)											
	IF	15	IF	IF	IF	15	15	15	15	15	-	-	MODE
	39.8	11.0	30.9	32.2	34.6	39.8	11.0	11.0	11.0	11.0	11.0	-	ANGLE
	.56	.99	.96	.87	.68	.36	.24	.18	.12	.10	.06	-	F DAYS
	36.	44.	43.	39.	34.	37.	42.	48.	46.	49.	48.	-	DBU
	87.	84.	85.	86.	81.	96.	83.	93.	91.	95.	91.	-	S/N DB
	.49	.98	.95	.86	.67	.36	.23	.18	.12	.10	.06	-	REL
	-	-	-	-	-	-	-	-	-	-	-	-	MP PRO
68	K(2)MUF=( 8.7)	K(5)MUF=( 8.6)											
	IF	15	IF	IF	IF	15	15	15	15	15	-	-	MODE
	44.7	11.0	33.3	35.0	46.7	11.0	11.0	11.0	11.0	11.0	11.0	-	ANGLE
	.53	.99	.93	.78	.48	.27	.28	.15	.09	.08	.04	-	F DAYS
	36.	44.	41.	35.	37.	46.	42.	48.	46.	49.	48.	-	DBU
	81.	81.	84.	85.	86.	98.	83.	94.	91.	95.	91.	-	S/N DB
	.49	.97	.91	.77	.47	.27	.26	.15	.09	.08	.04	-	REL
	-	-	-	-	-	-	-	-	-	-	-	-	MP PRO
10	K(2)MUF=( 8.1)	K(5)MUF=( 8.1)											
	IF	IF	IF	IF	IF	15	15	15	15	15	-	-	MODE
	41.8	33.8	34.7	36.1	39.4	41.8	11.0	11.0	11.0	11.0	-	-	ANGLE
	.54	.99	.96	.84	.55	.28	.12	.08	.04	-	-	-	F DAYS
	38.	43.	41.	33.	36.	38.	43.	48.	47.	-	-	-	DBU
	82.	81.	84.	86.	81.	91.	84.	94.	91.	-	-	-	S/N DB
	.48	.97	.95	.83	.53	.28	.12	.08	.04	-	-	-	REL
	-	-	-	-	-	-	-	-	-	-	-	-	MP PRO
12	K(2)MUF=( 8.1)	K(5)MUF=( 6.8)											
	IF	IF	IF	15	IF	15	15	15	-	-	-	-	MODE
	42.0	33.9	35.2	11.0	42.0	11.0	11.0	11.0	-	-	-	-	ANGLE
	.54	.99	.91	.67	.28	.14	.07	.04	-	-	-	-	F DAYS
	32.	43.	46.	46.	38.	47.	43.	48.	-	-	-	-	DBU
	84.	83.	86.	87.	81.	91.	83.	94.	-	-	-	-	S/N DB
	.48	.94	.88	.65	.26	.14	.07	.03	-	-	-	-	REL
	-	-	-	-	-	-	-	-	-	-	-	-	MP PRO

Figure 2. A sample predicted path reliability prediction.

the starting point for frequency management of a given HF circuit. Although the users of the short term forecast cover a broad spectrum of expertise and interests, it is assumed the user has a basic knowledge of HF propagation principles. Before presenting some of these basic principles we will describe the contents of the short term forecast.

#### THE HF RADIO PROPAGATION BULLETIN

The primary bulletin is issued at 0600Z daily in the format shown in Figure 3. Part I of this bulletin is also updated every six hours at 1200Z, 1800Z, and 0000Z. This part consists of a six hour summary and forecast of HF radio propagation conditions for 20 geographical sectors (Figure 4) in the northern hemisphere. While this format was designed for ease of use by the customer, it does present some problems. From the forecaster's viewpoint, many ionospheric variations are assessed from a framework of local time variation and a geomagnetic coordinate system (Figure 5). Neither of these is completely compatible with the grid used in Part I. For example, the area designated as auroral latitudes on the grid is governed by the auroral oval centered about the geomagnetic pole distinct from the geographic pole. In some instances, areas designated as auroral show characteristics of the middle latitude or polar ionosphere rather than those of the auroral zone.

Difficulties arise from the user's standpoint of determining conditions over long HF paths that cross several of the latitude and longitude grid areas. In general, the conditions in the sectors that contain the control points for a given circuit will best describe the propagation conditions for a user. Although the forecast is not valid for the southern hemisphere, it may be judiciously applied to circuits in that hemisphere. In particular, the southern auroral and polar cap regions will exhibit similar ionospheric conditions as the northern hemisphere. Elsewhere, caution should be exercised in using the grid for southern hemisphere circuits. Large disturbances will show up world-wide, but significant variations in intensity and characteristics may be observed between the northern and southern hemispheres associated with seasonal differences in the ionosphere. The observed propagation conditions contained in Part I are indicated by a letter using the following convention:

<u>Letter</u>	<u>Condition</u>
W	Unusable (Very Poor)
U	Fair
N	Normal (Good to Very Good)

These letters describe conditions relative to a given latitude band, i.e., normal conditions in the auroral latitude band may be considerably different from normal conditions at middle latitudes. The letter W is used to describe the poorest conditions. Intermittent periods of usable signal propagation may be possible, but consistently reliable communication is not possible. In other instances a total blackout of HF communications may be observed. The numerical indicator in this part is a coded forecast for communication from 1 (poorest condition) to 9 (excellent). The number and condition are as follows:

SUBJ: HF RADIO PROPAGATION REPORT  
 SPACE ENVIRONMENTAL SUPPORT BRANCH  
 AIR FORCE GLOBAL WEATHER CENTRAL  
 PRIMARY HF RADIO PROPAGATION REPORT ISSUED AT 230600Z NOV 80.  
 PART I. SUMMARY 230000Z to 230600Z NOV 80  
 FORECAST 230600Z to 231200Z NOV 80

QUADRANT					
	I	II	III	IV	
REGION	0 TO 90W	90 TO 180	180 TO 90E	90E TO 0	
POLAR	W3	W3	W3	W3	
AURORAL	U5	U4	U4	U4/-20	
MIDDLE	N7	U6	U6	N7	
LOW	N7	N7	N7	N7	
EQUATORIAL	N7	N7	N7	N7	

PART II. GENERAL DESCRIPTION OF HF RADIO PROPAGATION CONDITIONS OBSERVED DURING THE 24 HOUR PERIOD ENDING 22/2400Z NOV 80 AND FORECAST CONDITIONS FOR THE NEXT 24 HOURS. HF PROPAGATION CONDITIONS AT HIGH LATITUDES WERE MOSTLY FAIR TO GOOD DURING THE DAY AND FAIR AT NIGHT EARLY IN THE PERIOD. AT ABOUT 1000Z A MAJOR SOLAR EVENT OCCURRED RESULTING IN A SMALL POLAR CAP ABSORPTION EVENT BEGINNING ABOUT 1600Z. SIGNIFICANT ABSORPTION AT LATITUDES ABOVE 65 DEGREES NORTH HAS BEEN EXPERIENCED SINCE THAT TIME, BUT IS CURRENTLY SUBSIDING. THIS POLAR CAP ABSORPTION (PCA) EVENT SEVERELY DEGRADED HF CONDITIONS THROUGHOUT THE SECOND HALF OF THE PERIOD. AT AURORAL LATITUDES CONDITIONS WERE MOSTLY POOR THROUGHOUT THE PERIOD WITH MUFS DEPRESSED ABOUT 35 PERCENT IN THE SUNSET TO MIDNIGHT HOURS. MIDDLE LATITUDE CONDITIONS WERE GENERALLY GOOD WITH MUFS DEPRESSED ABOUT 25 PERCENT IN THE SUNSET TO MIDNIGHT HOURS. CONDITIONS AT LOW AND EQUATORIAL LATITUDES WERE GOOD THROUGHOUT THE PERIOD. FOR THE COMING 24 HOURS HF CONDITIONS SHOULD IMPROVE IN THE POLAR LATITUDES AS THE ABSORPTION DECREASES. FOR THE REMAINING LATITUDES UNAFFECTED BY THE PCA, HF CONDITIONS SIMILAR TO THOSE MENTIONED ABOVE SHOULD PERSIST.

PART III. SUMMARY OF SOLAR FLARE INDUCED IONOSPHERIC DISTURBANCES WHICH MAY HAVE PRODUCED SHORT WAVE FADES IN THE SUNLIT HEMISPHERE DURING THE 24 HOUR PERIOD ENDING 22/2400Z.

START(Z)	END(Z)	CONFIRMED	FREQUENCIES AFFECTED
0958	1111	YES	UP TO 18 MHZ

PROBABILITY FOR THE NEXT 24 HOURS MODERATE.

PART IV. OBSERVED FORECAST F 10 and K/AP. THE OBSERVED 10.7 CM FLUX FOR 22 NOV 80 WAS 192. THE PREDICTED 10.7 CM FLUX FOR 23, 24, and 25 NOV ARE 191. 190, and 189. THE OBSERVED K/AP VALUES FOR 22 NOV 80 WERE 01/03. THE FORECAST K/AP VALUES FOR 23, 24, AND 25 NOV ARE 03/10, 03/15, AND 04/25.

Figure 3. A sample primary HF propagation report.

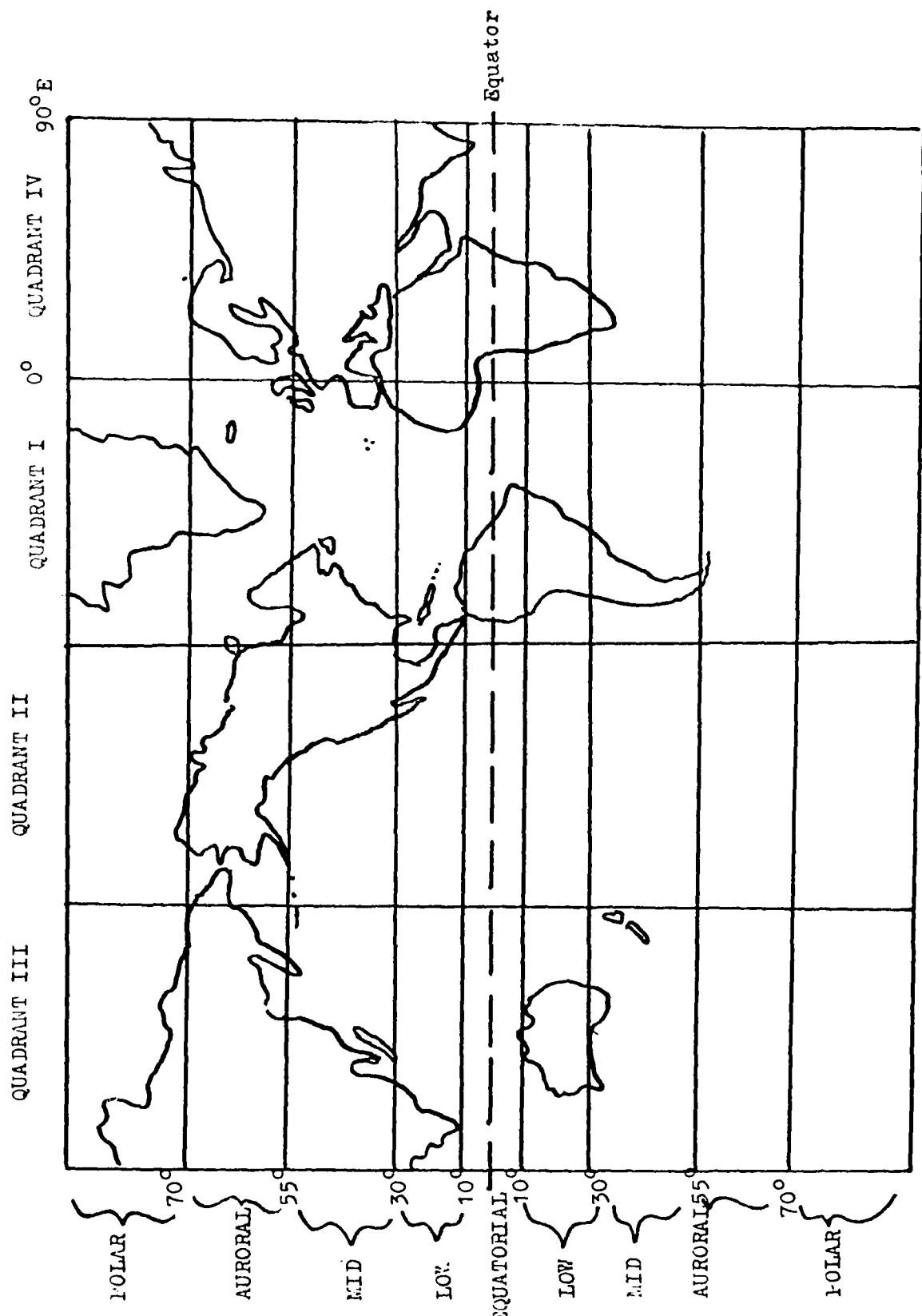


Figure 4. Sectors of the earth for which HF propagation forecasts are made.

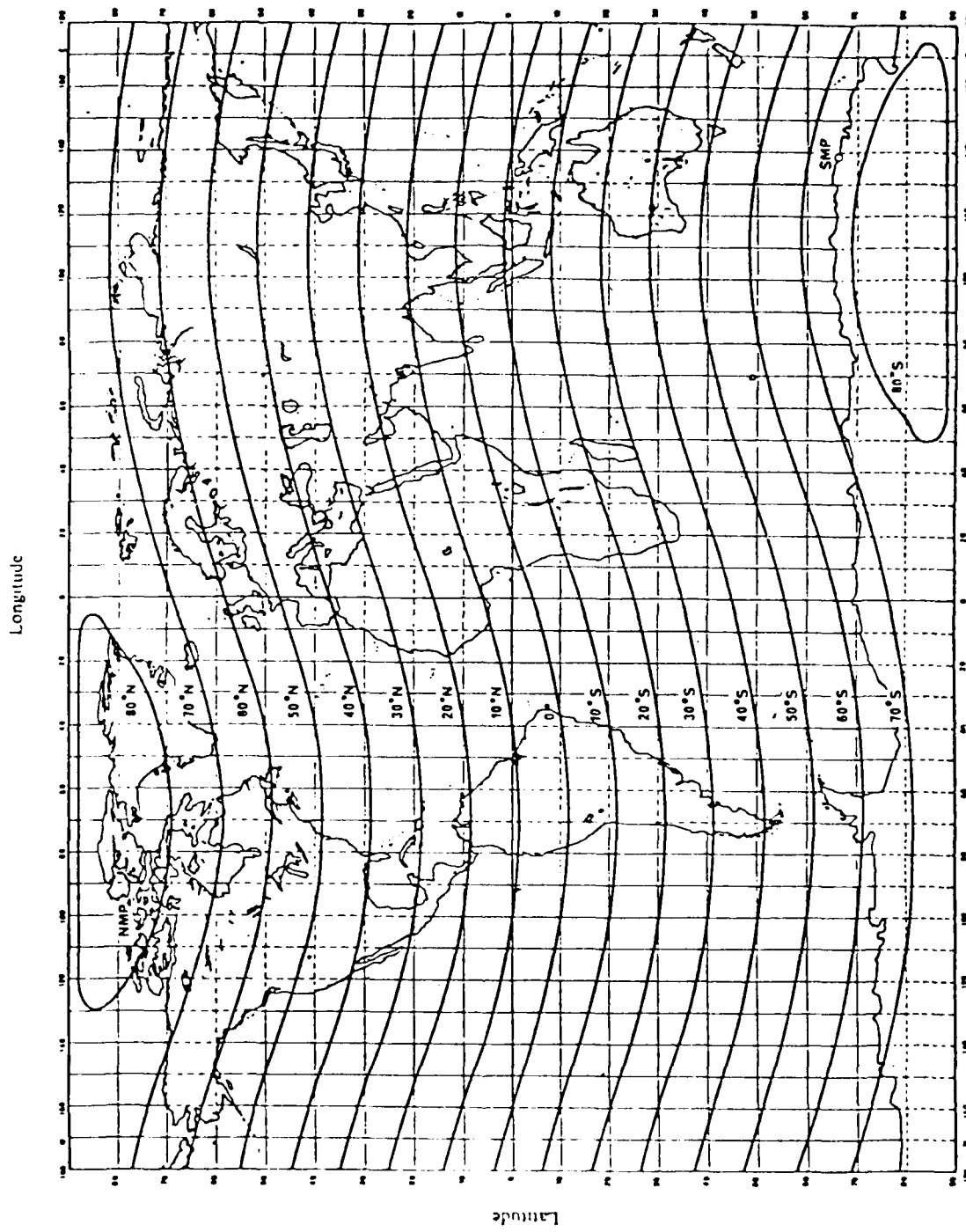


Figure 5. Geomagnetic latitude variation with respect to geographic coordinates.

1 - Useless	6 - Fair to Good
2 - Very Poor	7 - Good
3 - Poor	8 - Very Good
4 - Poor to Fair	9 - Excellent
5 - Fair	

In general, propagation conditions will fall into categories 4, 5, 6, and 7 with the other numbers describing extremes in propagation conditions.

Also included in this section is a six hour prediction of percent deviation in the maximum usable frequency (MUF) on paths in the appropriate sector. Communicators may use these figures in conjunction with the monthly mean predictions mentioned above to plan which frequencies to use during the forecast period. The percent deviation and their description are listed below:

Near Normal - generally within 15% of normal  
 Slight - less than 35% from normal  
 Moderate - 35% to 50% from normal  
 Severe - greater than 50% from normal

Part II of the 0600Z bulletin contains a general written description of ionospheric conditions and their effects on communications during the previous Zulu day. A brief description of expected conditions for the current day is also included. This section can be used by communications managers for circuit analysis and quality control. During disturbed conditions, remarks in an abbreviated Part II may be appended to the bulletins transmitted at 1200Z, 1800Z, and 0000Z. Part III contains a summary of observed solar events that may have disrupted sunlit HF circuits, i.e., a shortwave fadeout (SWF). If a confirmed disruption of an HF circuit was reported, a yes will appear in the confirmed column. The description of frequency affected will include the highest known frequency affected. In some instances, user circuits may have experienced disruptions on frequencies higher than those reported to AFGWC. This section also contains a probability of the occurrence of a SWF during the next 24 hours according to the following categories:

<u>Probabiltiy</u>	<u>Description</u>
$\leq 1\%$	Nil
$\geq 1\% \text{ but } \leq 20\%$	Slight
$\geq 20\% \text{ but } \leq 50\%$	Moderate
$\geq 50\%$	Strong

Part IV contains information that can be of use to communicators in planning operations during the three day forecast period. This includes observations and forecasts for the 10.7cm solar radio emission as well as the Ap and K geomagnetic indices. The 10.7cm radio flux may be used as an indicator of the general level of solar activity. Variations of 10 units or more above the 90 day mean indicate a reasonable chance of solar related disruptions occurring. Conversely, values significantly below the 90 day mean can be interpreted as an expectation of low solar activity. Geomagnetic activity indices can be used to project propagation conditions in general, with the lower indices indicating

good conditions, the higher values indicating poorer conditions. The predicted K values can be also be used in conjunction with monthly mean predictions such as Figure 2 for frequency selection and reliability determination. The following is a brief description of the geomagnetic indices:

<u>Condition</u>	<u>Minimum Ap</u>
Quiet	0
Unsettled	7
Active	15
Minor Storm	30
Major Storm	50

Ap Range for a given K value

<u>Ap</u>	<u>K</u>	<u>Ap</u>	<u>K</u>
0-2	0	33-56	5
3-5	1	57-94	6
6-9	2	95-154	7
10-18	3	155-236	8
19-32	4	237	9

BASIC PRINCIPLES OF HF PROPAGATION

High frequency communication is possible because there exists, in the earth's upper atmosphere, a region consisting of several electrified layers which are capable of bending HF radio waves and returning them to the earth at a great distance. The electrified characteristics of these layers, which are collectively referred to as the ionosphere, are subject to wide variations. This is so because the ionosphere is formed by ultraviolet radiation from the sun, and the intensity of this radiation changes radically with time and geographical location. The amount of radiation illuminating the ionosphere varies hourly, seasonally, and geographically, depending upon the relationship between the sun and the earth. In addition, year-to-year changes, over an approximate 11-year cycle, affect the ionosphere's ability to reflect radio waves.

The range of ultraviolet radiation from the sun comprises a relatively wide band of frequencies. Since the gases composing the upper atmosphere respond to different frequencies in the ultraviolet spectrum, there is a tendency for ionization to occur at several different levels, or layers, from approximately 30 to beyond 400 miles above the surface of the earth. While these ionized regions are usually referred to as "layers", they are not completely separated from one another. Each layer overlaps to some extent, forming a continuous but non-uniform area with at least four levels of peak intensity designated D, E, F<sub>1</sub> and F<sub>2</sub> (Figure 6).

The D layer is the lowest region of pronounced ionization. It extends from about 30 to 55 miles above the earth's surface and exists mainly during the daylight hours. Although it is the ionized region nearest the earth, there is presently less known about it than any other region of the ionosphere. The amount of ionization in this region is very low compared to other layers. It reaches maximum intensity at local noon when the sun is highest in the sky.

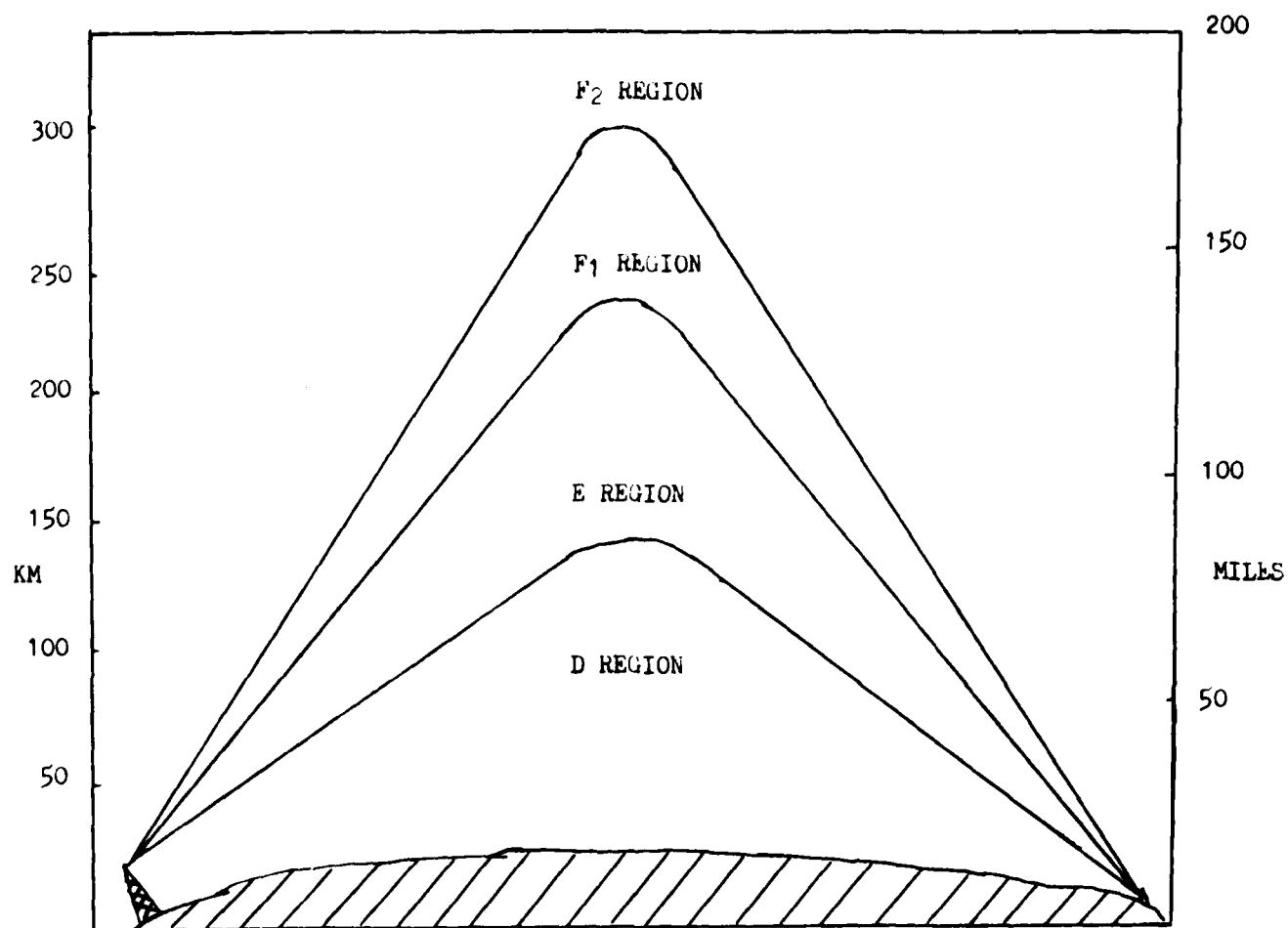


Figure 6. Regions of the ionosphere.

This dependency of the D region on solar zenith angle produces strong seasonal variations. A notable exception to the seasonal variation of electron density is an abnormal increase of this density and radio wave absorption during the winter months. This phenomena is most often observed near 55 degrees geographic latitude, but also exists in general poleward of 35 degrees. This anomalous state begins earlier and ends later at the higher latitude region. The phenomenon is poorly understood but it is thought to be mainly of a meteorological nature, possibly associated with stratospheric warming. Other D region absorption events associated with various ionosphere disturbances will be discussed in a later section.

The upper part of the D region blends into another distinct region called the E layer. This layer of the ionosphere occurs mainly during the daylight hours at heights between 55 and 100 miles. The intensity of the ionization in the E region is considerably greater than the D layer, and follows closely the sun's position in the sky. Maximum ionization occurs near noon when the sun is directly overhead. As soon as the sun sets, recombination takes place and a part of the E layer disappears during the hours of darkness. The E layer shows a strong correlation with the overall level of solar activity. The diurnal, seasonal, and cyclical variations are quite predictable during undisturbed conditions. The exception to this is the occurrence of various abnormalities known as Sporadic E. This phenomenon will be discussed in more detail in a later section. The occurrence of Sporadic E, while generally transient in nature and spatially limited, does pose some real problems to HF communicators.

The F layers are the most important regions of the ionosphere for long-distance HF communication. During the daylight hours there are two well defined regions. The F<sub>1</sub> layer begins slightly above the upper boundary of the E layer and extends up to about 150 miles. The F<sub>2</sub> layer height varies seasonally, ranging up to about 200 miles during the winter and 300 miles during the summer. Although more highly ionized, the F<sub>1</sub> layer behaves very much like the E layer. Maximum ionization occurs near noon, when the sun is more directly overhead, and nearly disappears during the hours of darkness. Unlike the other layers, ionization in the F<sub>2</sub> region exists at all times. This region is the most highly ionized and the most important region in the ionosphere.

During the nighttime hours the F<sub>2</sub> layer height varies approximately between 150 and 250 miles. Because the recombination rate of this region is relatively slow, the layer exists around the clock. Were it not for this fact, long-distance HF communication would be virtually impossible during the hours of darkness.

The seasonal behavior of the F<sub>2</sub> layer is rather complicated. Unexpectedly, the critical frequencies ( $foF_2$ )\* of the winter daytime are high. During the long hours of winter darkness, on the other hand, the ionosphere has

---

\*The highest frequency of a vertically incident signal so returned by each of the layers of the ionosphere is called the critical frequency for that layer.

more time to lose its electrical charge, and nighttime critical frequencies dip to very low values. In the summer, heating causes the  $F_2$  layer to expand during the daylight hours, resulting in a much lower ionization density than during the winter. As a result, summer daytime  $F_2$  layer critical frequencies are lower than the winter values. Because of the shorter nights during the summer, recombination does not occur to the extent that it does during the winter. This results in  $F_2$  layer nighttime critical frequencies during the summer months that are significantly higher than during the winter months. These relative differences are illustrated in Figure 7.

The anomalous high  $foF_2$  values during the winter are actually the combined effects of two anomalies. The December anomaly shows a higher than expected midday maximum in  $foF_2$  during the months of November, December, and January. This anomaly is observed between  $50^{\circ}N$  and  $35^{\circ}S$ . The other anomaly, called the Winter Anomaly, occurs throughout the hemisphere in its winter, but it is most pronounced near  $50^{\circ}$  from the geomagnetic equator. The significance of this to the HF communicator is that rapid changes in the range of usable frequencies will be occurring during the hours near sunrise and sunset at the control points of a given circuit.

The solar cycle variation of HF propagation conditions may also be inferred from Figure 7. In addition, Figure 8 illustrates the variability of different propagation factors with sunspot number. Caution should be exercised in using sunspot number (SSN) as an index of ionospheric variability. SSN is not a particularly good measure of solar effects on the ionosphere. While the peaks of solar cycles result in much different propagation conditions than solar minima, the ionosphere can also vary significantly for any given SSN.

The critical frequency of the  $F_2$  layer is an important determinant of the maximum usable frequency or MUF. The MUF is defined as the highest frequency for ionospheric transmission over a given path. In addition to the  $foF_2$ , the MUF is dependent upon the height of the reflecting layer and the path length. For a radio wave to be reflected between two distant points via the ionosphere, its frequency must be less than or equal to the MUF. As the operating frequency is raised towards the MUF, the signal will be received with increasing signal strength. When the frequency exceeds the MUF, ionization at the point of reflection will not be strong enough to bend the wave back to the earth, and it will continue through the ionosphere into space. To insure satisfactory communication between two points, the operating frequency must be as near to the MUF as possible, but should never exceed it. It should also be noted that the power radiated does not enter into the determination of the MUF.

--- Predictions of MUF similar to those illustrated in Figures 1 and 2 are made for the monthly median value, which is the value equalled or exceeded 50 percent of the days during the month at a specified time of day. The frequency of optimum transmission (FOT), sometimes called the optimum working frequency, is defined as the value of MUF equalled or exceeded 90 percent of the days during the month. The FOT for  $F_2$  layer propagation may be estimated by multiplying the monthly median MUF by 0.85. Day to day variations of E layer MUF and  $F_1$  layer MUF can be considered negligible for operational use. Thus the FOT for the E and  $F_1$  layers may be considered to be the monthly median MUF for those layers.

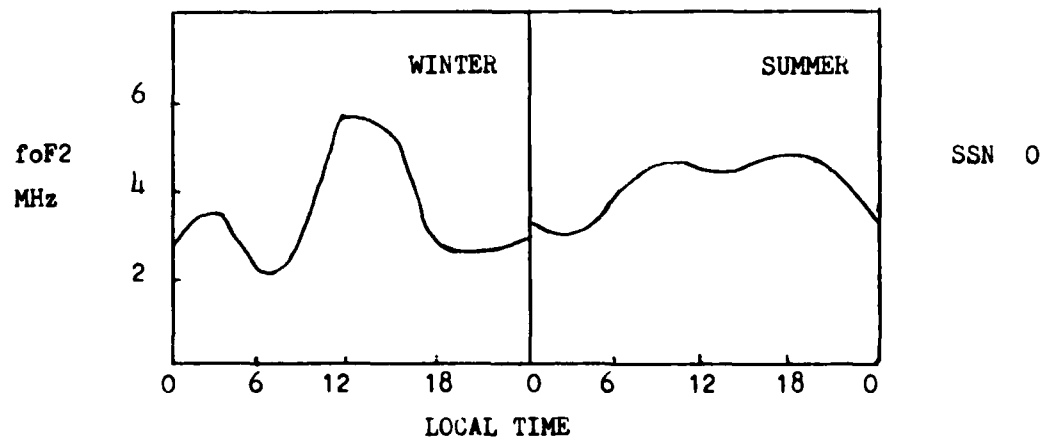
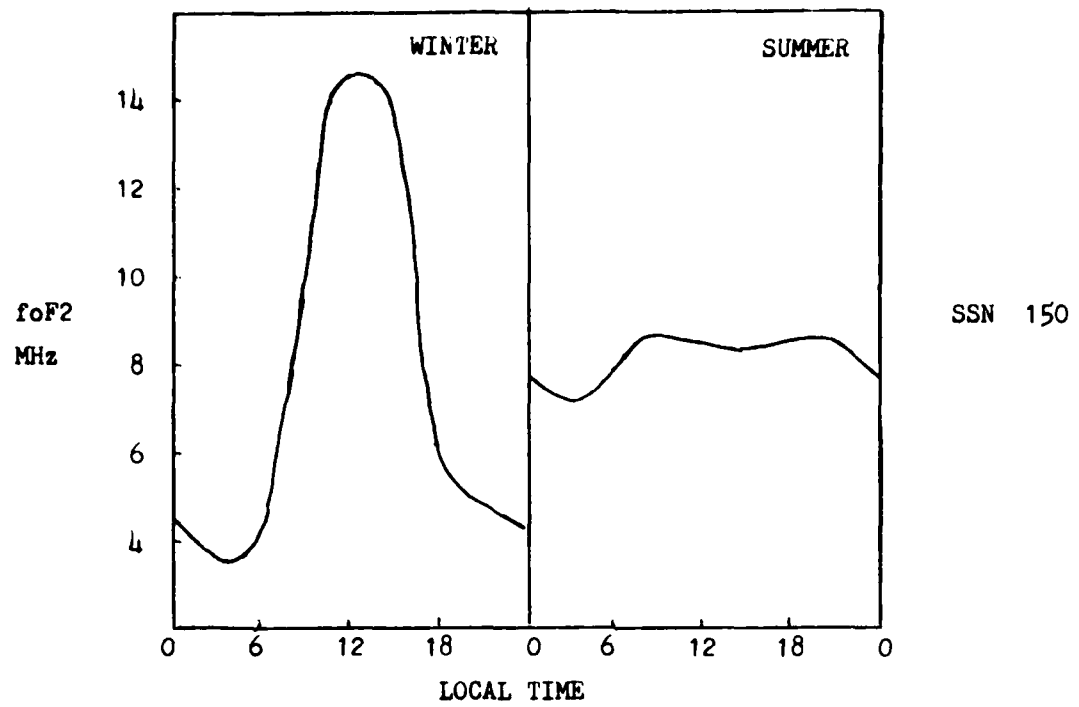


Figure 7. The diurnal variation of middle latitude foF2 with season and sunspot number. foF2 is in MHz and the diurnal time is in hours, local time.

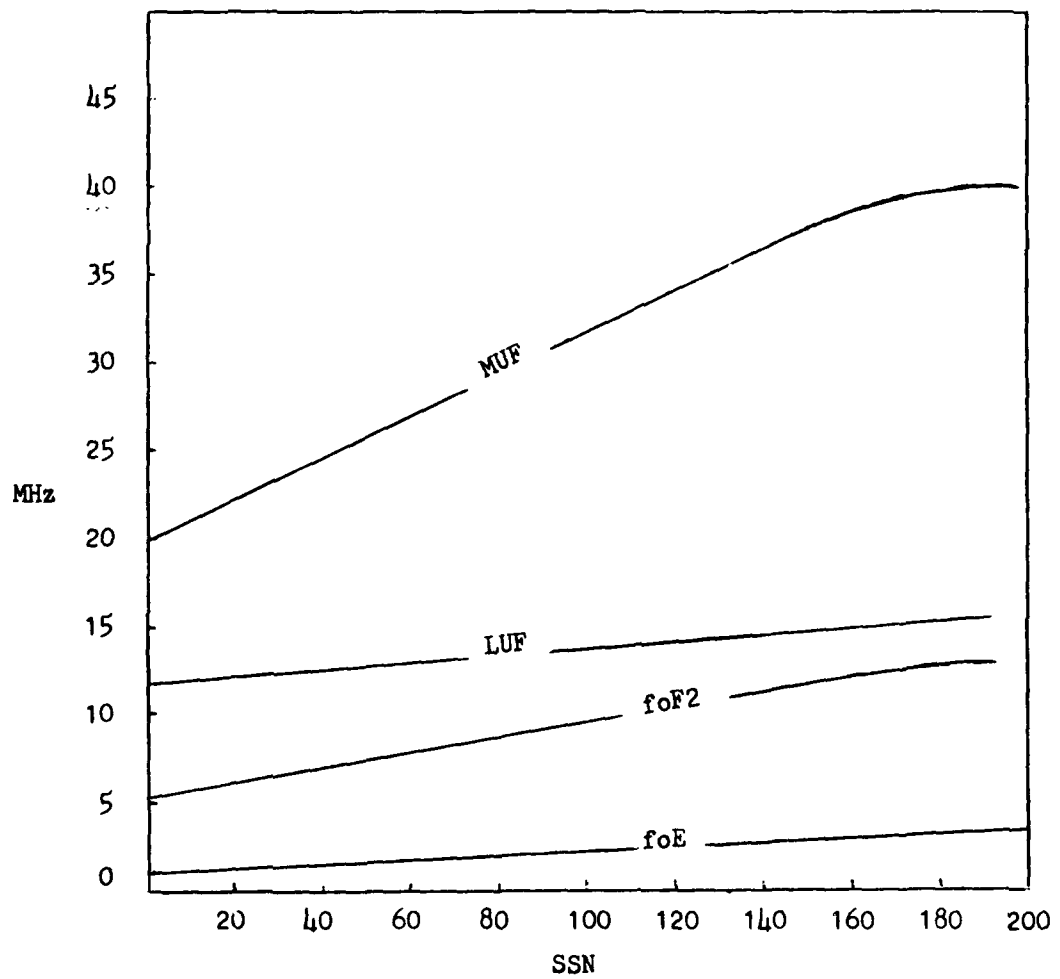


Figure 8. MUF, LUF, foF2, and foE as a function of sunspot number.

The lowest usable frequency, or LUF, is the lowest frequency that can be used for satisfactory communication over a particular path at a particular time. The LUF is a function of the strength of the transmitted signal strength. The strength of the received signal depends upon the power of the transmitter, the gain and directivity of the transmitting and receiving antennas, the path length, and ionospheric absorption. At frequencies below the LUF, satisfactory reception will not be possible since the received signal will be lost in the prevailing noise level. As the operating frequency is raised above the LUF, the signal to noise ratio (S/N) increases.

Ionospheric absorption is one of the main reasons the signal strength is reduced as it passes through the ionosphere. As the radio wave enters the ionosphere it imparts energy to the electrons that exist there. Part of this energy is not propagated with the radio wave and the amount of energy in the radio wave when it emerges from the ionosphere is less than when it entered, resulting in decreased signal strength. The energy lost depends on the number of the electrons present and the radio wave frequency.

The amount of ionospheric absorption varies inversely as the square of the frequency i.e., the higher the frequency, the less the absorption. If the frequency is doubled, ionospheric absorption will decrease by a factor of four. For example, the absorption on 28 MHz is 1/4 the intensity of the absorption found on 14 MHz. When both bands are open at the same time, it will require considerably more power on 14 MHz to equal the strength of the 28 MHz transmission over the same path. During undisturbed ionospheric conditions the level of absorption varies with local time, season of the year and geographic location. The absorption is inversely proportional to the angle that the sun makes with respect to the earth. Thus, absorption is more intense in the equatorial regions than in the temperate latitudes, and is generally greater during the summer months than in winter. Absorption is also higher during the maximum of the solar cycle when solar radiation is the strongest. Strong absorption conditions prevail in certain areas during disturbed ionospheric conditions. These effects will be discussed in more detail in a later section.

A propagation path for an HF circuit is the route by which the radio wave travels from a transmitter to a receiver. More than one propagation path is often possible for a particular operating frequency and circuit. In general, the longer the distance and the lower the operating frequency below the MUF, the greater the number of possible paths. Radio waves arriving at the receiver after travelling different paths may interfere with each other (multipath). These effects can adversely affect telegraph and voice circuits. These effects can be minimized by using a frequency near the MUF and the proper antenna selection. Ionospheric variabilities, however, preclude the entire elimination of such effects.

A particular propagation path may be pictured as a succession of one or more hops, or reflections between the ionosphere and ground. The ionosphere is assumed to be concentric with the earth, and the propagation takes places along a great circle path. For the average heights of the ionospheric layers, the maximum great circle distance for a one-hop  $F_2$  layer reflection is about 4,000 kilometers, and for a one-hop E layer reflection, the maximum distance

is roughly 2,000 kilometers. The MUF for the 4,000 km hop is about three times the critical frequency ( $foF_2$ ); for the E layer reflection, the MUF is about five times the critical frequency ( $foE$ ).

As the number of hops in a single path and the number of possible paths increase, the propagation characteristics become more complex. The ionospheric point of reflection that affects the MUF is called the control point. For one-hop paths, this is taken as the path midpoint. For distances beyond 4,000 km, a two control point assumption is made. This assumes there are  $F_2$  layer control points on the great circle path 2,000 km from each terminal. Ionospheric conditions at these control points determine the usable range of frequencies. For E layer propagation modes, the distances for the control points are 1,000 km from the transmitter and receiver terminals (See Figure 9). For an entire circuit the MUF is approximated by the highest frequency which can arrive or depart from both ends of the circuit.

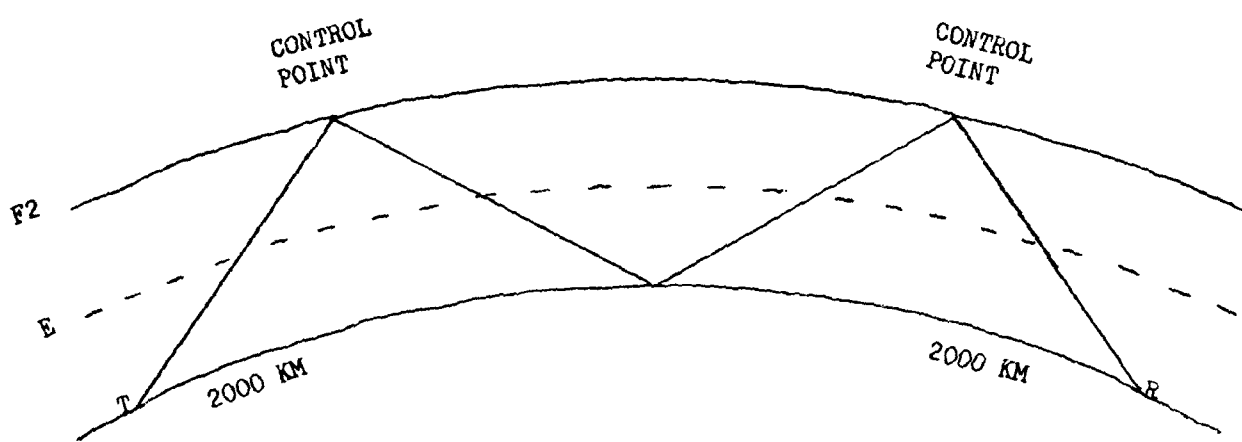
A wide variety of propagation modes can be experienced depending upon ionospheric conditions. Under normal daytime conditions, the E region generally supports propagation over distances up to 2,000 km. The  $F_1$  region supports propagation paths between 2,000 and 3,000 km, while for distances greater than 3,000 km, the  $F_2$  layer is the primary reflection layer.

The predominant modes are usually the simplest modes under normal ionospheric conditions. Assuming a height of 100 km for the E region and 300 km for the F region the simplest modes are as follows:

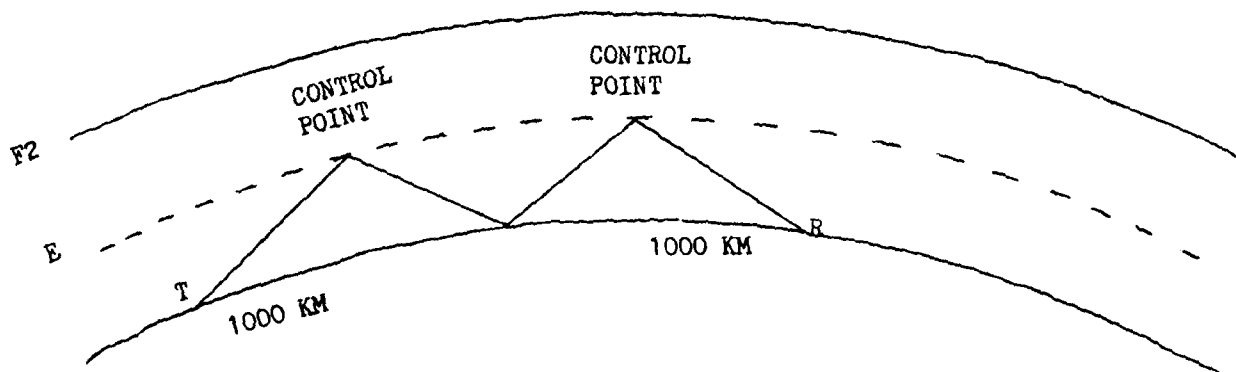
Range (km)	Modes
0000-2000	1E and 1F
2000-4000	2E and 1F
4000-6000	3E and 2F
6000-8000	4E and 2F

Complex ionospheric conditions such as Sporadic E occurrence or large horizontal ionospheric gradients often result in more complex propagation modes. Some of these are illustrated in Figure 10.

Another aspect of radio wave propagation concerns the angle of radiation or wave angle. If a radio signal is directed toward the ionosphere at a smaller angle with respect to the tangent plane touching the earth at the point of transmission, it will cover more distance and need less bending to return to the earth. This is illustrated in Figure 11. A signal transmitted at some small angle will be returned at point D. As the wave angle is increased, the distance between A and D will decrease. If the transmitted frequency is high enough for the existing ionospheric conditions, a critical wave angle will be reached such that the radio wave will not be returned to the earth. Thus, there exists a so called zone of silence, or skip zone, between the point where the last ray is returned to the ground and the distance beyond which the ground wave (AB) is no longer detectable. This distance between A and C is called the skip distance. Thus, the distance B to C defines the skip zone where neither ground-wave or sky wave signals are detectable. The ground-wave range (AB) for a given transmitter is dependent solely on frequency such that the higher the



a. F layer propagation.



b. E layer propagation.

Figure 9. Control points for F layer propagation (a.) and E layer propagation (b.) modes.

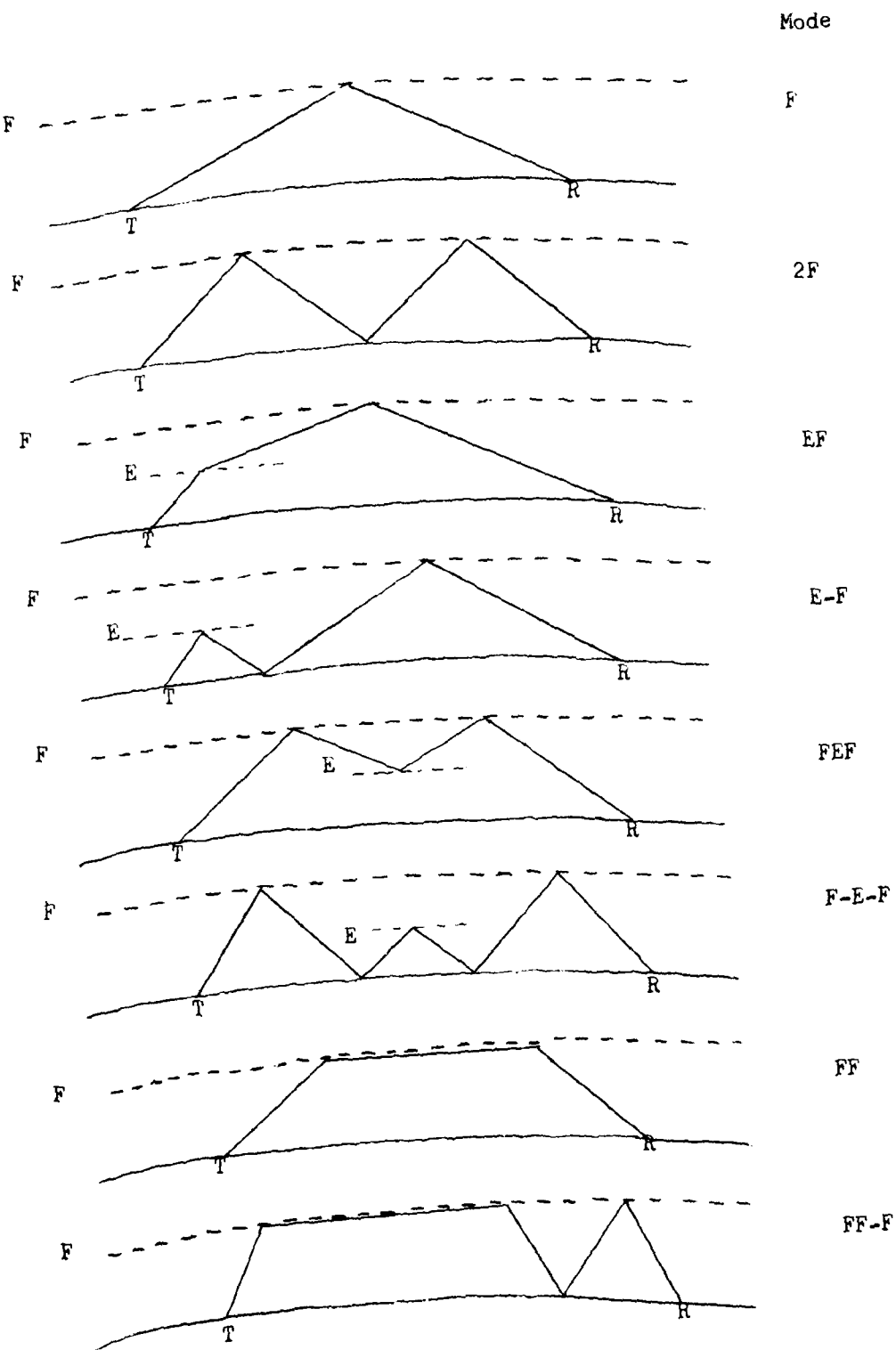


Figure 10. Some of the various propagation modes for HF signals.

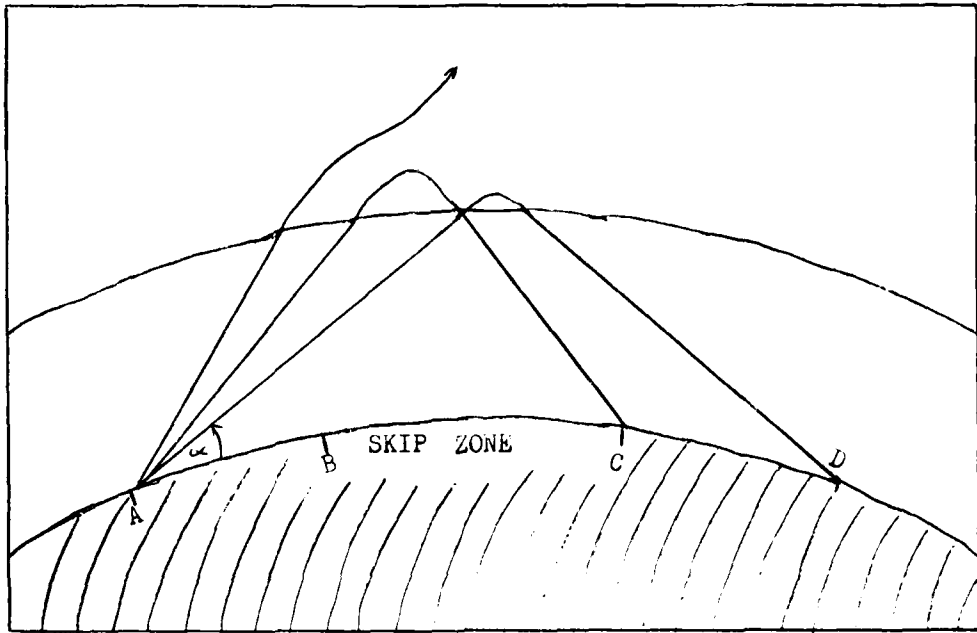


Figure 11. An illustration of the wave angle  $\alpha$ , ground wave (AB), skip distance (AC), and skip zone (BC).

frequency, the shorter the distance. Assuming constant ionospheric conditions, the skip zone increases in area as the frequency radiated by the transmitter is increased.

Before discussing the effects of ionospheric disturbances, a brief review of some of the phenomena which influence day to day propagation is in order. These include fading, multipath interference, noise, ducting, and non-great circle propagation.

FADING. Fading is a rapidly initiated temporary decrease in received signal strength. Fading effects in HF circuits may be due to variations associated with geography, geometry, and time varying ionospheric conditions. Additional influences include diurnal, annual, and solar cycles. Fading can be sudden or gradual, and intermittently or continuously fluctuating. The signal strength can fade partially or completely. In general, fading is frequency dependent with the fastest fading occurring on the higher frequencies.

SELECTIVE FADING. This phenomena is independent fading of individual narrow frequency bands of a modulated signal spectrum. This is sometimes manifested as sound distortion on a double sideband signal in which the lower frequency sideband fades at a much slower rate than the upper sideband. Selective fading can be a form of flutter fading or may be due to multipath phase interference or marginal amplitude conditions. The occurrence of this phenomenon is more often intermittent than continuous.

FLUTTER FADING. This condition consists of rapid variations in signal level. The fluctuation rate is between 10 and 100 Hz. This type of fading is most often observed in the auroral zone and on transequatorial circuits.

MULTIPATH TRANSMISSIONS. Multipath transmissions are signals received from a single transmitting source, arriving at slightly different times as a result of propagation over several different modes or paths. Because of the time difference in arrival of the many waves that make up the transmitted signal, the waves can either amplify or weaken each other, and the effect is a fluctuating signal. This type of fading is produced by small scale irregularities in the electron density of the reflective layer.

INTERFERENCE. Interference is the term used to describe the presence of unwanted manmade signals. It is often the result of frequency congestion in certain radio bands. Interfering signals add to the natural noise level and reduce the signal to noise ratio at the receiving point. In addition, the unwanted signals can contribute to the various fading effects described above.

NOISE. Atmospheric radio noise is due mainly to the long distance propagation of the radiation associated with electrical discharges in thunderstorms. Since thunderstorms occur mostly over land areas, the highest noise levels are usually found there. The noise distribution over the earth's surface is a function of radio frequency, time of day, and season. Figures 12 a-d illustrate the relative seasonal variation of radio noise.

DUCTING. Ducting is a propagation mode that results in a radio wave being guided parallel to the ionospheric reflecting surface over long distances before it is refracted back to the ground. This condition is usually

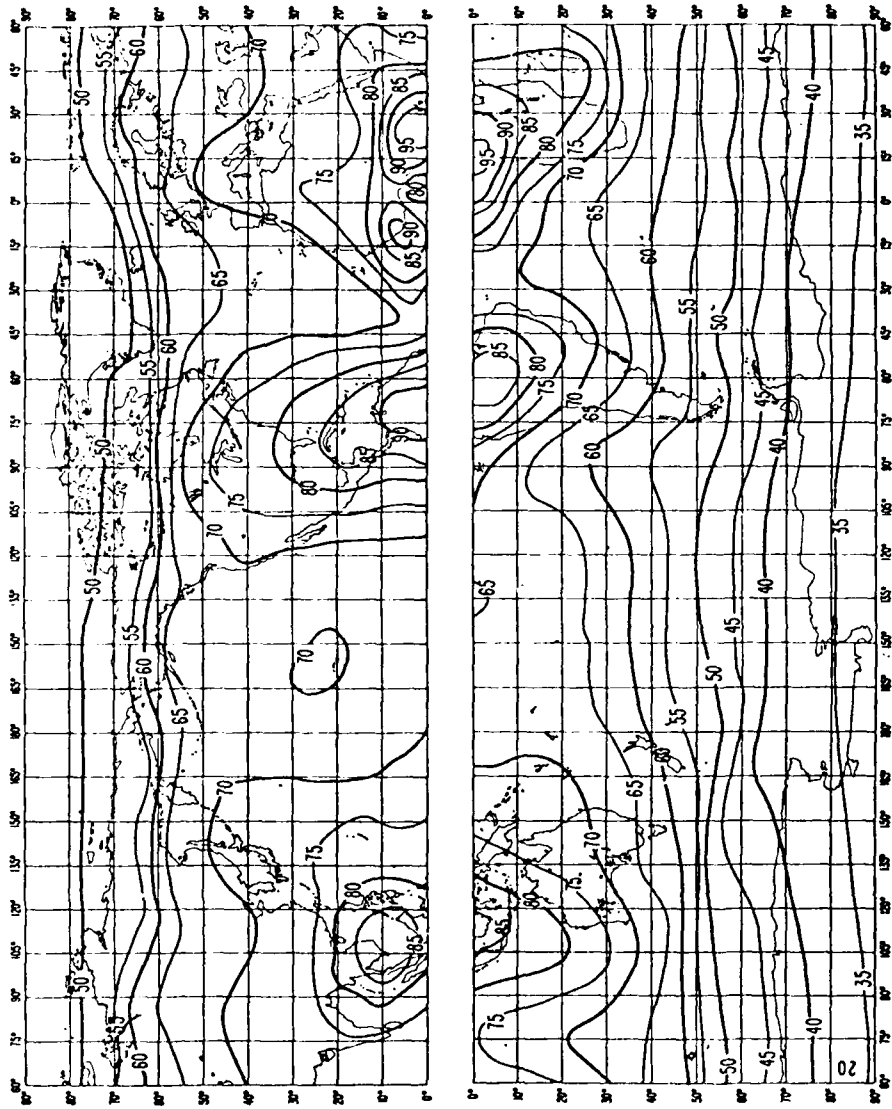


Figure 12a. Expected values of atmospheric noise in terms of an effective antenna noise factor. (Autumn, 0000-0400L).  
(from CCIK Report 322, 1963)

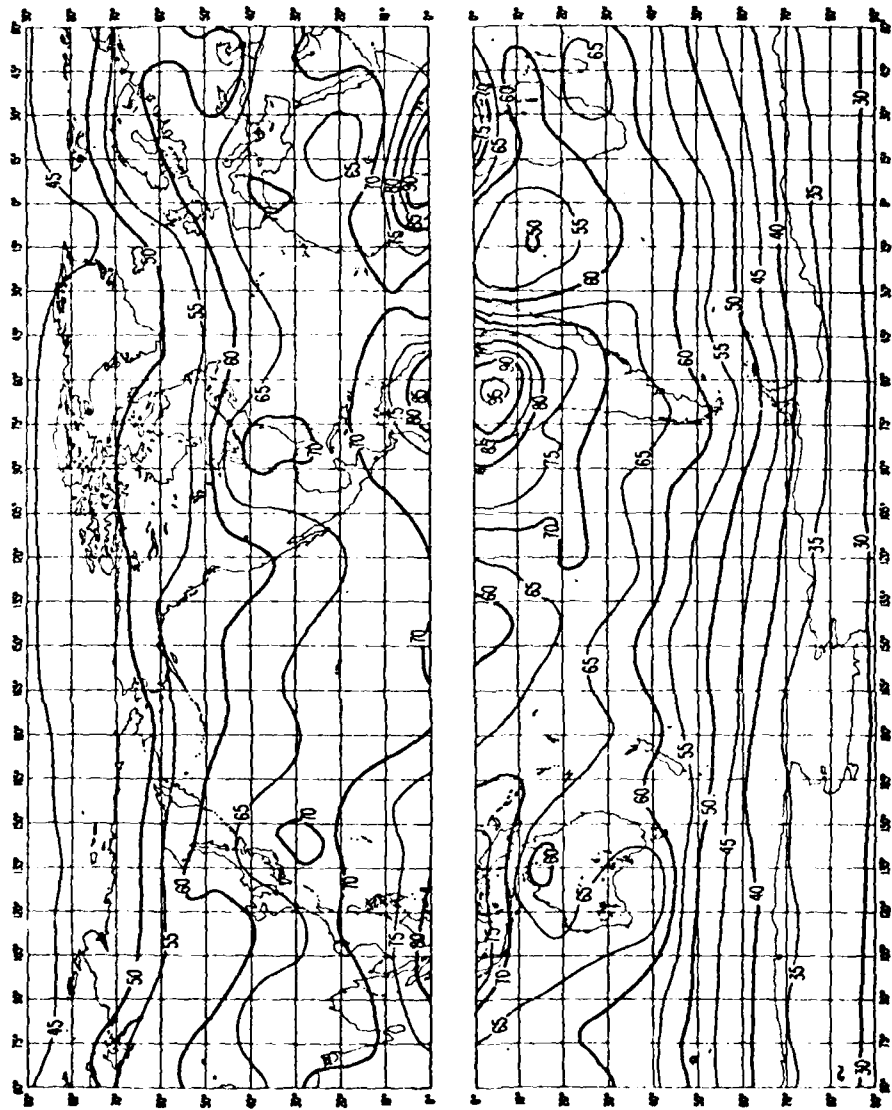


Figure 12b. Expected values of atmospheric noise in terms of an effective antenna noise factor. (Winter, 0000-0400L).  
(from CCIR Report 322, 1963)

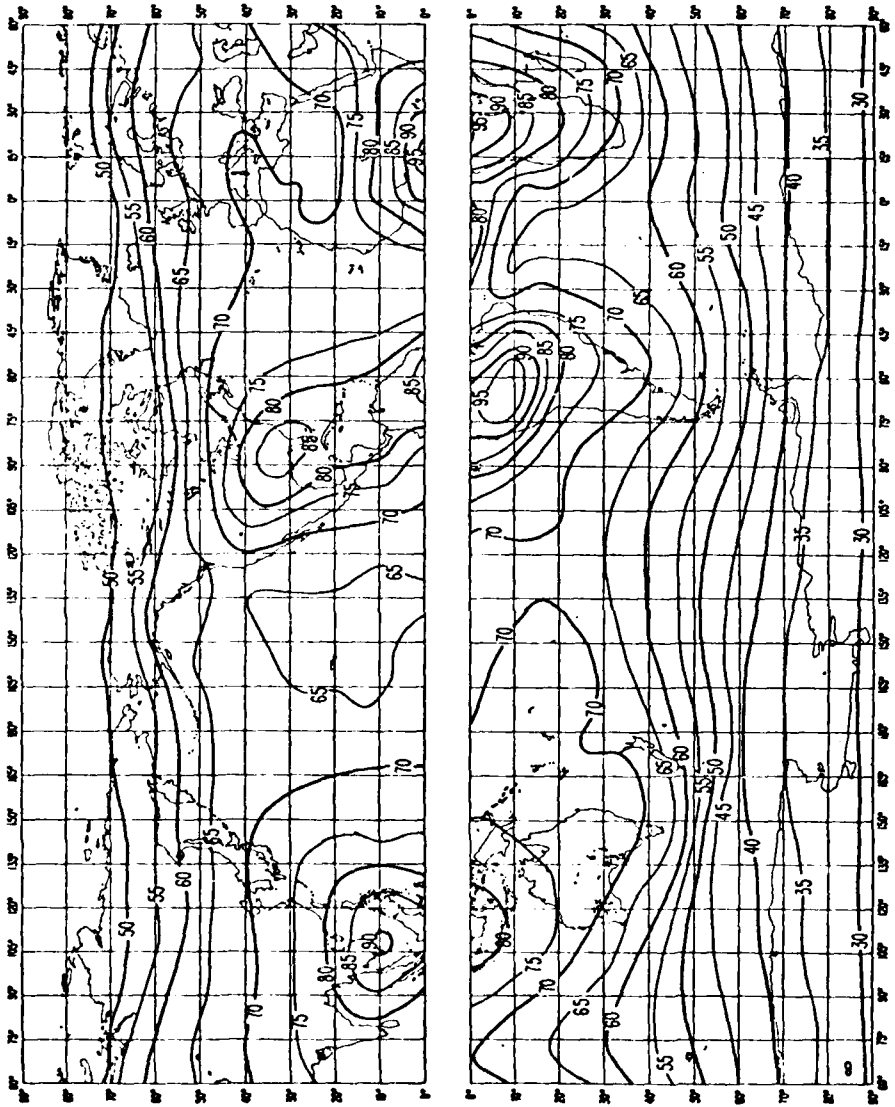


Figure 12c. Expected values of atmospheric noise in terms of an effective antenna noise factor. (Spring, 0000-0400L).  
(from CCIR Report 322, 1963)

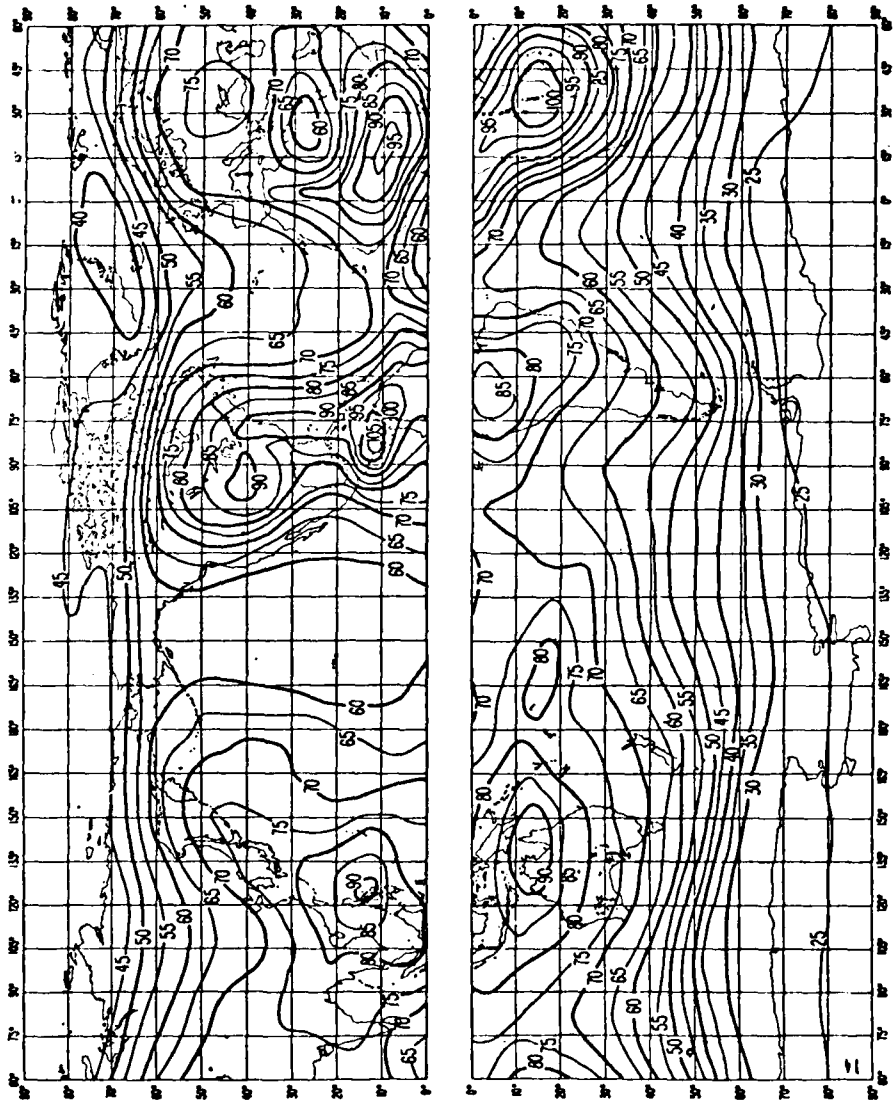


Figure 12d. Expected values of atmospheric noise in terms of an effective antenna noise factor. (Summer, 0000-0400L).  
(from CCIR Report 322, 1963)

associated with the higher part of the HF frequency spectrum extending up into the VHF range. Very great distances can be traversed in one hop in this manner. This propagation mode is associated with strong F layer electron gradients and is most common on transequatorial and auroral zone paths. This mode is not a very reliable mode of transmission because of the uncertainty in the refracting conditions.

NON-GREAT CIRCLE PROPAGATION. A normal HF propagation path follows approximately a great circle path between the transmitter and receiver, but in areas where there are strong horizontal gradients in the ionospheric electron density and ionospheric irregularities, the radio signal can deviate significantly from a great circle path. The two areas where this occurrence is most common are the auroral oval and the equatorial regions. On paths near the equatorward boundary of the auroral oval, departures on the order of 1,000 km may be observed. In general, the lower the transmission frequency, the greater the deviation from a great circle path. Azimuthal deviations of up to 90 degrees from the normal great circle path can be observed.

#### SPORADIC E.

Sporadic E is one of the most important transient phenomena observed in the ionosphere. It is a cloud of abnormally high density with a spatial extent of tens to hundreds of kilometers. Since the electron density is so great, the maximum frequency reflected can, on occasion, exceed the maximum frequency ( $foF_2$ ) of the F region. Several types of Sporadic E have been identified, and the effects on an HF radio signal can vary considerably. Sometimes the Sporadic E is nearly transparent and does not affect signals using the F region. At other times it is thin and produces only minor signal propagation problems. The most severe case is Blanketing Sporadic E in which the electron cloud is sufficiently dense to prevent signals from using the F region (Figure 13).

The cause of Sporadic E is not well understood, but several processes are associated with some occurrences of this phenomena. Large, squall-line thunderstorms are sometimes associated with Sporadic E as well as strong wind shears at certain altitudes. Meteor showers, perturbations of ionospheric/magnetospheric current systems, and auroral substorm occurrence are other phenomena that are associated with Sporadic E production.

For radio communicators the major problem with Sporadic E is the uncertainty in its temporal and spatial variations. On some days, and in certain locations, Sporadic E conditions can provide better than normal propagation with stronger signal strengths. On other occasions it can wreak havoc with HF circuits through its rapidly varying changes and multipath and ducting effects.

Figure 14 illustrates the statistical occurrence of Sporadic E at three stations. The Sporadic E at the high temperate zone may be considered representative of the middle latitudes. From this, one can see that Sporadic E is essentially a daytime phenomenon at the equatorial latitudes at all times of the year. It also occurs most frequently between sunset and midnight in the auroral latitudes but infrequently at other times of the day. In the middle latitudes, Sporadic E occurs more often during the summer daytime hours.



Figure 13. Some propagation modes that can result from Sporadic E occurrence.

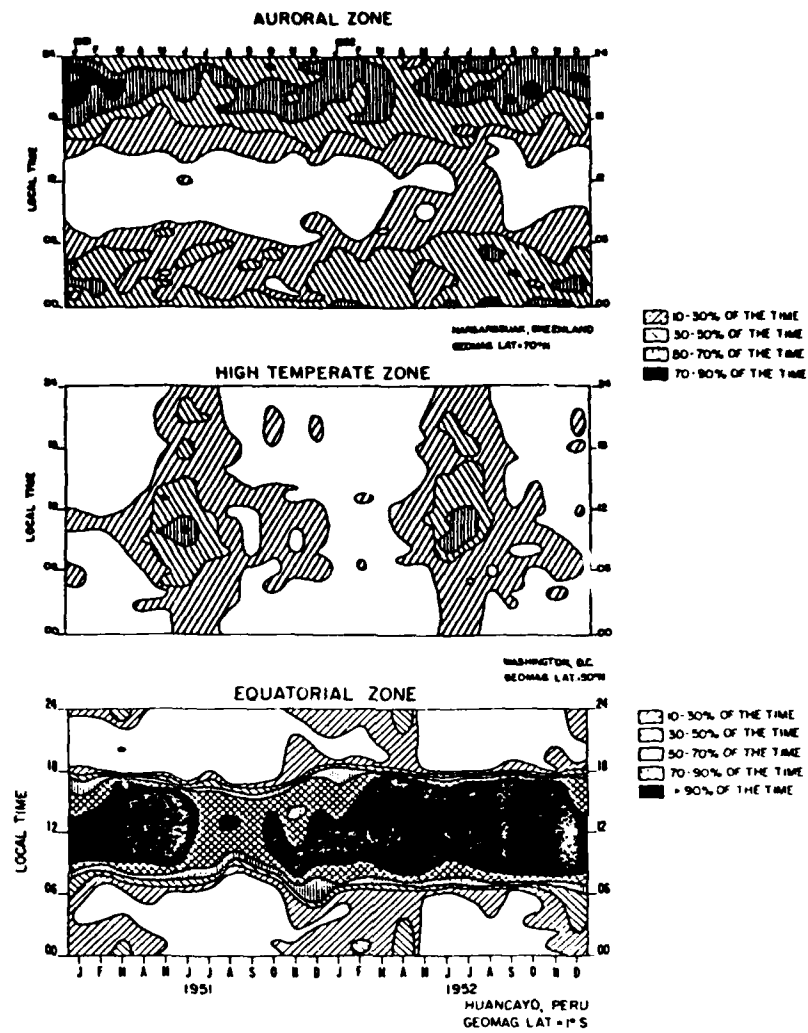


FIGURE 3.30. Fraction of time  $fE_s > 5$  Mc/s.

(After E. K. Smith, 1957, Worldwide occurrence of sporadic E, NBS Circ. 582.)

Figure 14. The seasonal and local time variation of Sporadic E occurrence at Narsarssuak, Greenland, Washington, D.C., and Huancayo, Peru. (from Davies)

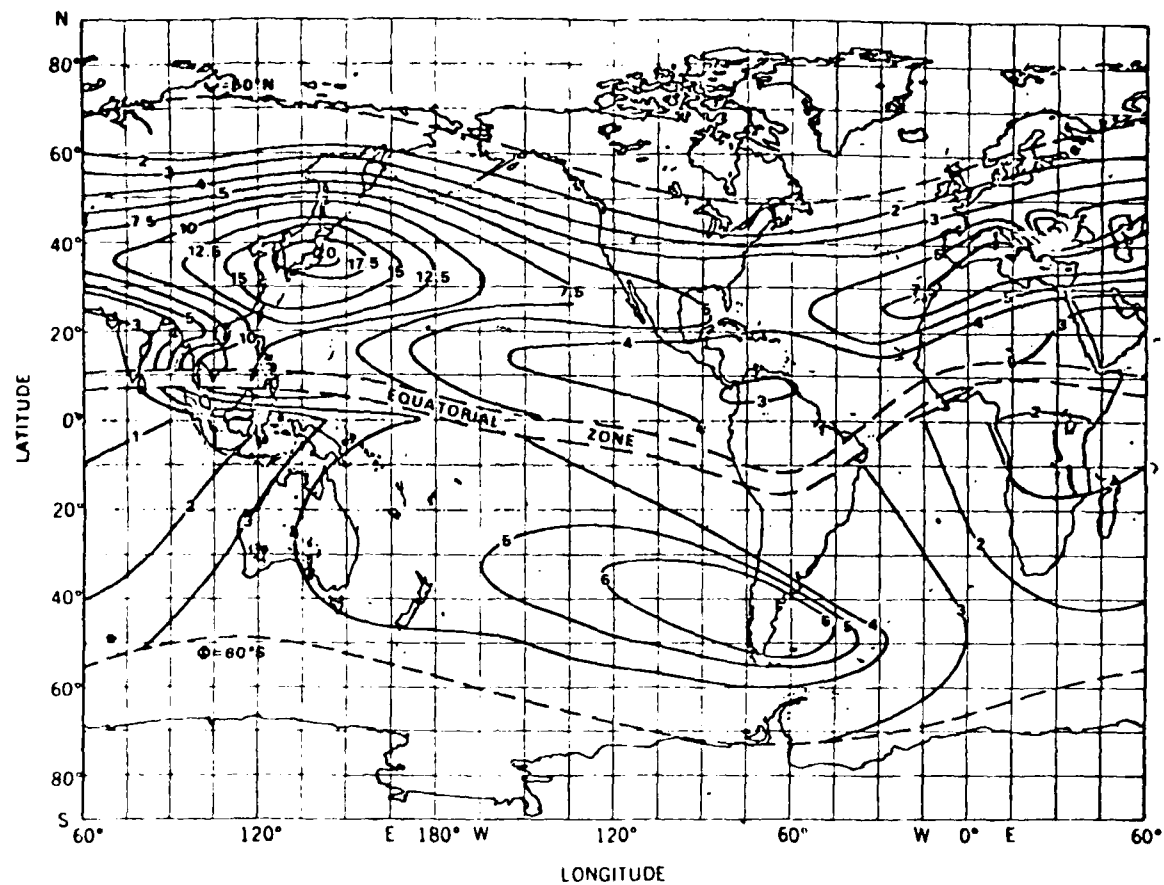


Figure 15a. Percentage of time for which sporadic E (f0Es) exceeds 7 MHz during the summer months (May-August north of the equator and November-February south of the equator). (E. K. Smith 1978).

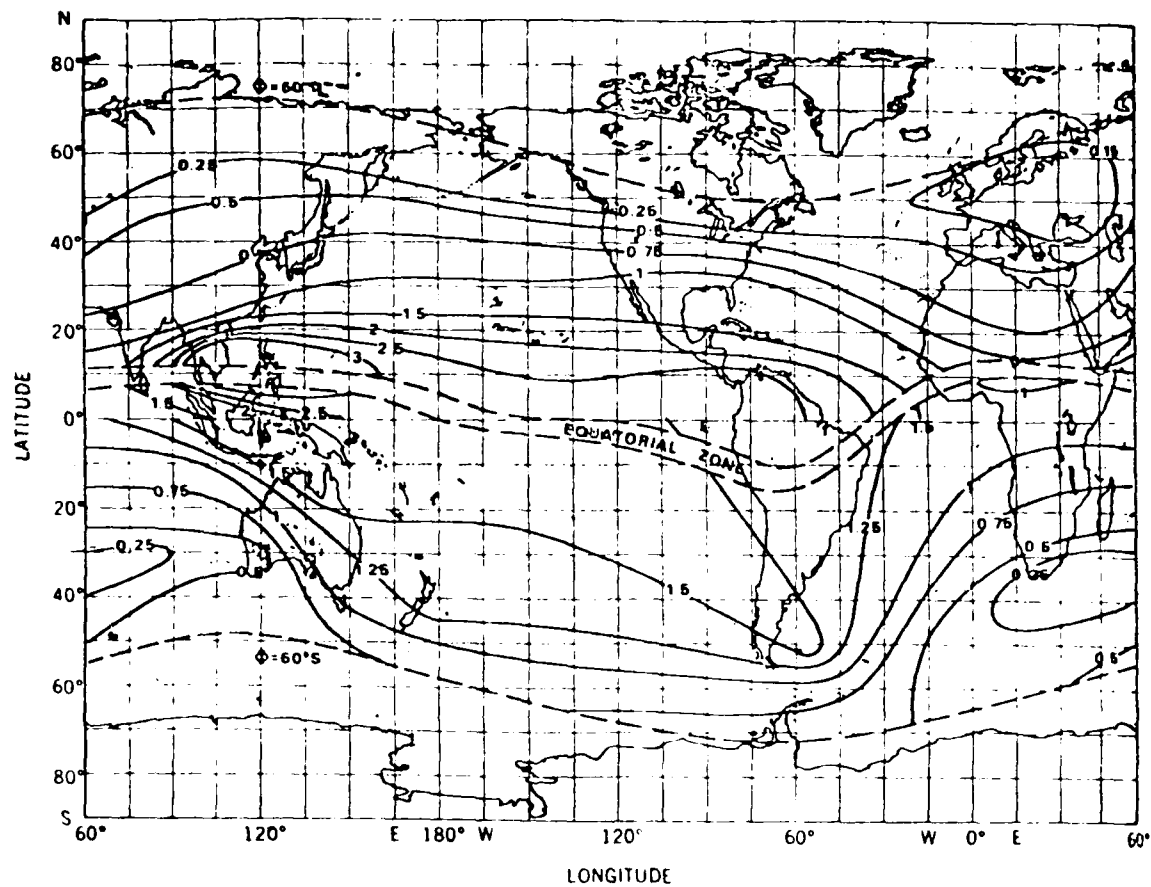


Figure 15b. Percentage of time for which sporadic E (fOEs) exceeds 7 MHz during the non summer months (September-April in the northern hemisphere and March-October in the southern hemisphere). (after E.K. Smith 1978).

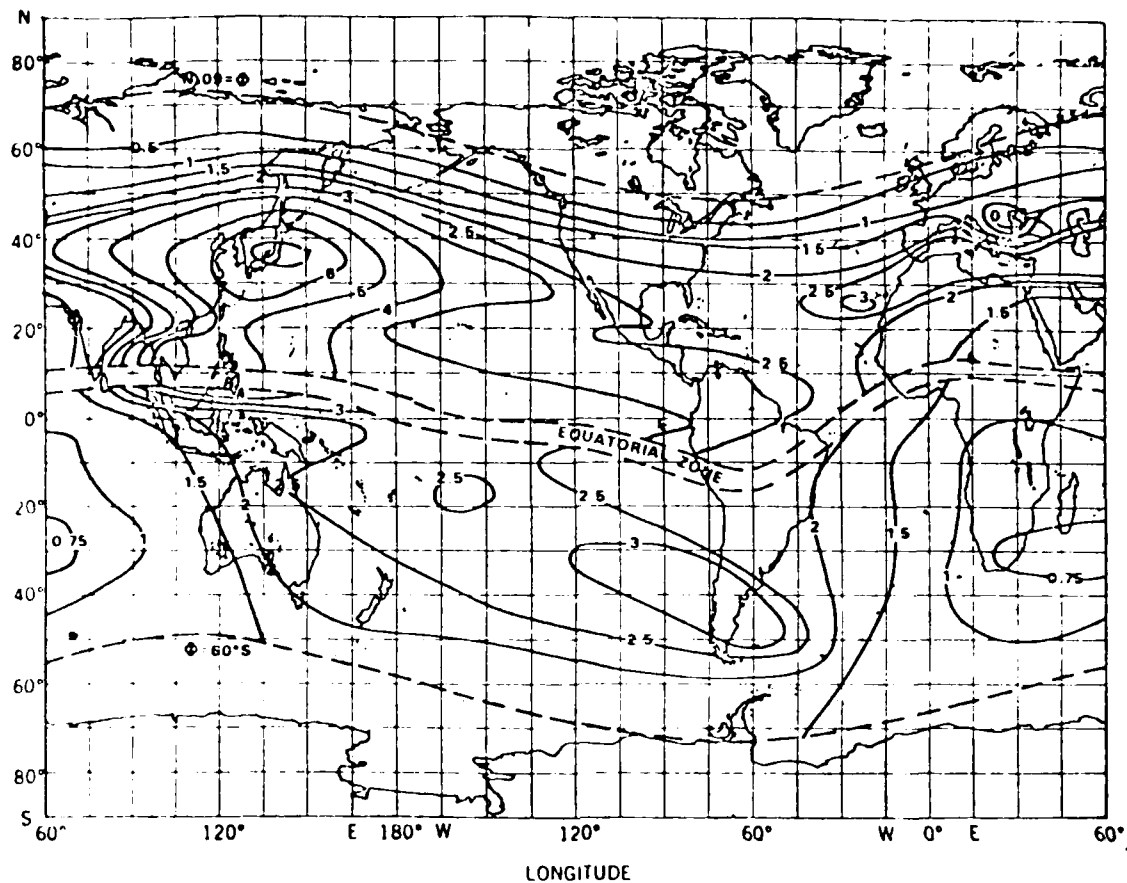


Figure 15c. Percentage of the year for which sporadic E (fOEs) exceeds 7 MHz.  $\Phi$  is in geomagnetic coordinates. (after E. K. Smith, 1978).

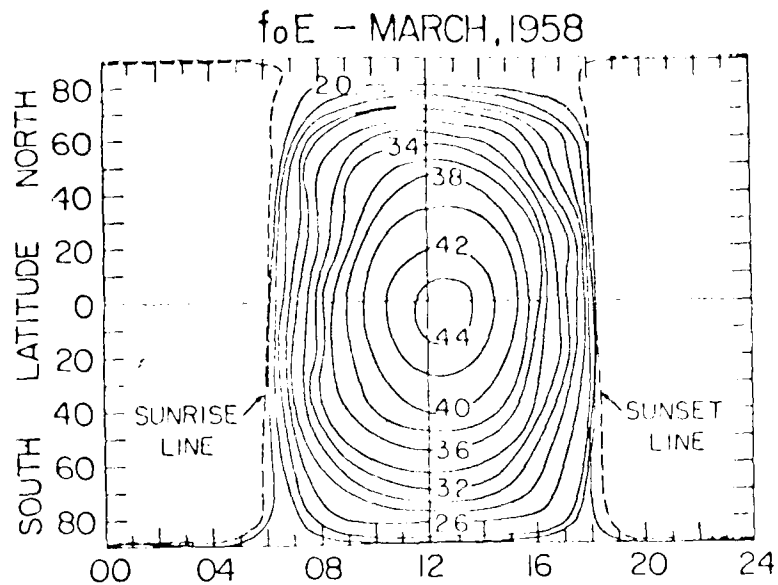
In Figures 15a, b, and c, Sporadic E maps for the areas between 5 - 60 degrees N and 5 - 60 degrees S geomagnetic latitude are shown. Note the higher occurrence of Sporadic E over the western Pacific area. By comparing observed foEs and Blanketing E observations with the expected climatological occurrence, the forecaster can determine the areas of higher than normal Sporadic E. If the ionosphere has been stable and is expected to remain so, then a forecast of significant Sporadic E would be made for the same latitudinal band and local time of the identified area of higher than normal Sporadic E. This would mean an expected occurrence of Blanketing Sporadic E for 25 to 50 percent of the time or an foEs on the order of 3 MHz or more higher than climatology. Graphs for determining climatological foE are contained in Figures 16a and b.

High latitude Sporadic E occurrence is closely related to geomagnetic/auroral substorm activity. Even during quiet geomagnetic conditions some auroral substorms occur. Sporadic E associated with these substorms is most often observed in the late evening sector. When more disturbed conditions prevail, the substorms become larger and more frequent in occurrence. As a result, the auroral oval expands both in size and equatorward extent. Under these conditions, Sporadic E occurrence extends into the post-midnight sectors (Figure 17). By monitoring geomagnetic and DMSP data, the forecaster can identify the position of the auroral oval and the likely geographic areas where Sporadic E occurred. During more disturbed conditions, Sporadic E can be expected to occur on upper middle latitude paths as the equatorward expansion of the auroral oval extends into these latitudes. The location of areas of Sporadic E occurrence can be even more closely identified by using the visual transparencies from the DMSP satellites (Figures 18 and 19). The most intense discrete (bright) auroras are usually associated with the highest foE (on the order of 8 MHz), while the areas of continuous aurora have foE values of about 2 to 3 MHz. A limiting factor in this analysis process is that the processing time of much of the DMSP data is on the same order of time as the substorm itself. Thus, a single data source is really insufficient. Complementing data, such as high latitude magnetometers and riometers as well as ground based ionospheric sounders, are needed to monitor the temporal and spatial extent of high latitude Sporadic E occurrence.

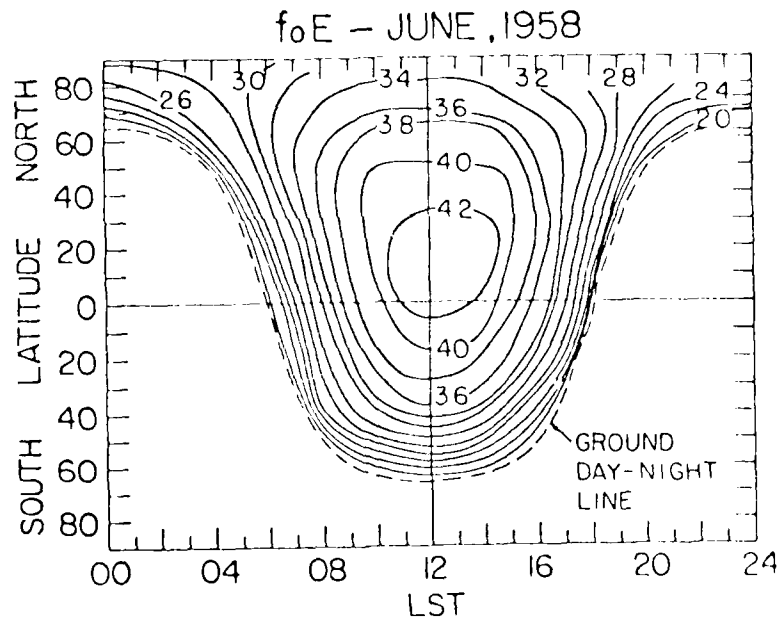
#### SPREAD F

The Spread-F condition is a phenomenon associated with irregularities at F region altitudes. East to west dimensions of Spread F may range up to 400 km. Spread F occurs at all latitudes, but is principally observed in high latitude and equatorial regions. In the polar regions, Spread F is observed nearly continuously. Partial trapping of radio waves sometimes results in long delay times of the received signal. The characteristics of high latitude and equatorial Spread F differ significantly. At the higher latitudes, Spread F occurs more often during increased geomagnetic activity, often spreading into the upper middle latitudes. The occurrence of Spread F may be observed at any hour of the day but is strongest at night and is more commonly observed during the winter (Figure 20).

At equatorial latitudes, Spread F occurs within 30 degrees north and 30 degrees south of the geomagnetic equator with the maximum occurrence in a belt 15 degrees north and south of the geomagnetic equator. The diurnal variation is controlled by sunset, i.e., Spread F irregularities are normally not



16a.



16b.

Figure 16. Graphs for determining typical  $f_{\text{OE}}$  values for different latitudes and local times. Fig 16a. can be used during spring and autumn. Fig 16b can be used in the summer, and also in the winter when inverted.  $f_{\text{OE}}$  values are in megahertz. (from Davies)

QUAL	00L	13 FEB	01L	02L	03L	04L	05L	06L	07L	08L	09L	10L	11L
MANILA	8		0	0	0	6	0	0	0	0	0	0	0
TAIPEI	0		0	0	0	0	0	0	0	0	0	0	0
MAUI	0		0	0	0	0	0	0	0	0	0	0	0
KOKOBU													
NI COSI	3		3	3	3	3	3	3	3	3	3	3	3
ASHKHA	0		0	0	0	0	0	0	0	0	0	0	0
VANDEN	0		0	0	0	0	0	0	0	0	0	0	0
ALMAA													
POITIE	0		0	0	0	0	0	0	0	0	0	0	0
KHABAR	0		0	0	0	0	0	0	0	0	0	0	0
BOULDE													
WALLOP	0		0	0	0	0	0	0	0	0	0	0	0
KIEV	0		0	0	0	0	0	0	0	0	0	0	0
IRKUTS													
MOSCOW													
DOURBE	0		0	0	0	0	0	0	0	0	0	0	0
SLOGUH	0		0	0	0	0	0	0	0	0	0	0	0
MAGADA	0		0	0	0	0	0	0	0	0	0	0	0
OTTAWA	0		0	0	0	0	0	0	0	0	0	0	0
SVERDL	0		0	0	0	0	0	0	0	0	0	0	0
TOMSK	0		0	0	0	0	0	0	0	0	0	0	0
GOOSE	6		6	6	6	6	6	6	6	6	6	6	6
YAKUTS	0		0	0	0	0	0	0	0	0	0	0	0
COLLEG	0		0	0	0	0	0	0	0	0	0	0	0
DAFES	0		0	0	0	0	0	0	0	0	0	0	0
MURMAN	3		3	3	3	3	3	3	3	3	3	3	3
CHURCH	0		0	0	0	0	0	0	0	0	0	0	0
NARSSA	0		0	0	0	0	0	0	0	0	0	0	0
SALEKH	6		6	6	6	6	6	6	6	6	6	6	6
DIKON	2		2	2	2	2	2	2	2	2	2	2	2
KRENKE	0		0	0	0	0	0	0	0	0	0	0	0
GODHAV	6		6	6	6	6	6	6	6	6	6	6	6
RESOLU	6		6	6	6	6	6	6	6	6	6	6	6
QUANO	6		6	6	6	6	6	6	6	6	6	6	6

17 a.

QUAL	29 JAN	00L	01L	02L	03L	04L	05L	06L	07L	08L	09L	10L	11L
MANILA	0	0	0	0	0	0	0	0	0	0	0	0	0
TAIPEI	0	0	0	0	0	0	0	0	0	0	0	0	0
MAUI	0	0	0	0	0	0	0	0	0	0	0	0	0
KOKOBU													
NI COSI	0	0	0	0	0	0	0	0	0	0	0	0	0
ASHKHA	0	0	0	0	0	0	0	0	0	0	0	0	0
VANDEN	0	0	0	0	0	0	0	0	0	0	0	0	0
ALMAA													
POITIE	0	0	0	0	0	0	0	0	0	0	0	0	0
KHABAR	0	0	0	0	0	0	0	0	0	0	0	0	0
BOULDE													
WALLOP	0	0	0	0	0	0	0	0	0	0	0	0	0
KIEV	0	0	0	0	0	0	0	0	0	0	0	0	0
IRKUTS													
MOSCOW													
DOURBE	0	0	0	0	0	0	0	0	0	0	0	0	0
SLOGUH	0	0	0	0	0	0	0	0	0	0	0	0	0
MAGADA	0	0	0	0	0	0	0	0	0	0	0	0	0
OTTAWA	0	0	0	0	0	0	0	0	0	0	0	0	0
SVERDL	0	0	0	0	0	0	0	0	0	0	0	0	0
TOMSK	0	0	0	0	0	0	0	0	0	0	0	0	0
GOOSE	6	6	6	6	6	6	6	6	6	6	6	6	6
YAKUTS	0	0	0	0	0	0	0	0	0	0	0	0	0
COLLEG	0	0	0	0	0	0	0	0	0	0	0	0	0
DAFES	0	0	0	0	0	0	0	0	0	0	0	0	0
MURMAN	1	1	1	1	1	1	1	1	1	1	1	1	1
CHURCH													
NARSSA	6	6	6	6	6	6	6	6	6	6	6	6	6
SALEKH	2	2	2	2	2	2	2	2	2	2	2	2	2
DIKON	0	0	0	0	0	0	0	0	0	0	0	0	0
KRENKE	0	0	0	0	0	0	0	0	0	0	0	0	0
GODHAV	6	6	6	6	6	6	6	6	6	6	6	6	6
RESOLU	6	6	6	6	6	6	6	6	6	6	6	6	6
QUANO	6	6	6	6	6	6	6	6	6	6	6	6	6

17 b.

Figure 17. High latitude Blanketing E ( qualifier 1 ) occurrence in the post - midnight sector during quiet-geomagnetic conditions ( 17a. Feb 13, 1980, Ap = 4 ) and during intense substorm activity ( 17b. Jan 29, 1980, Ap = 19 ).

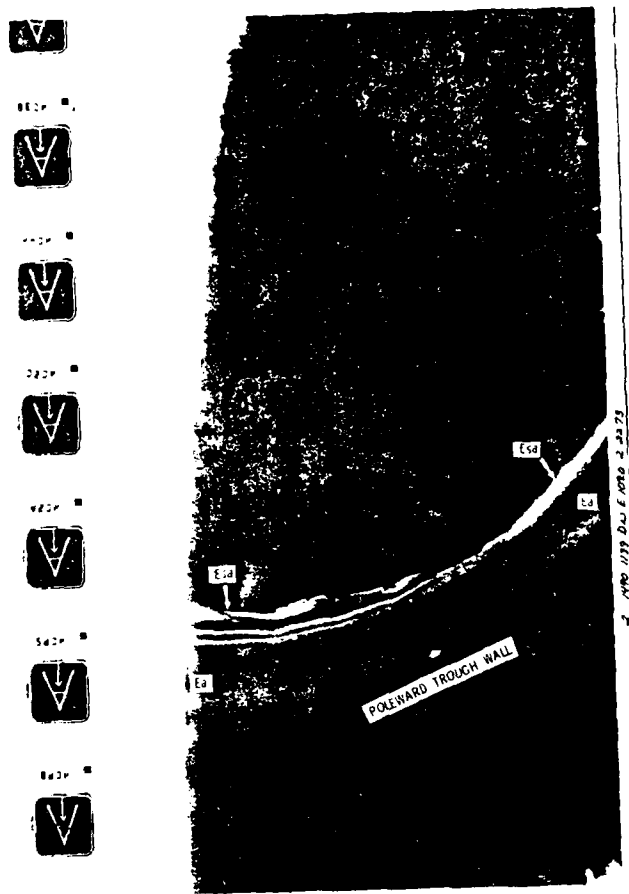


Figure 18. DMSP photograph. Esa mark the areas of discrete aurora and most intense sporadic E. Ea indicates areas of continuous aurora and less intense sporadic E.

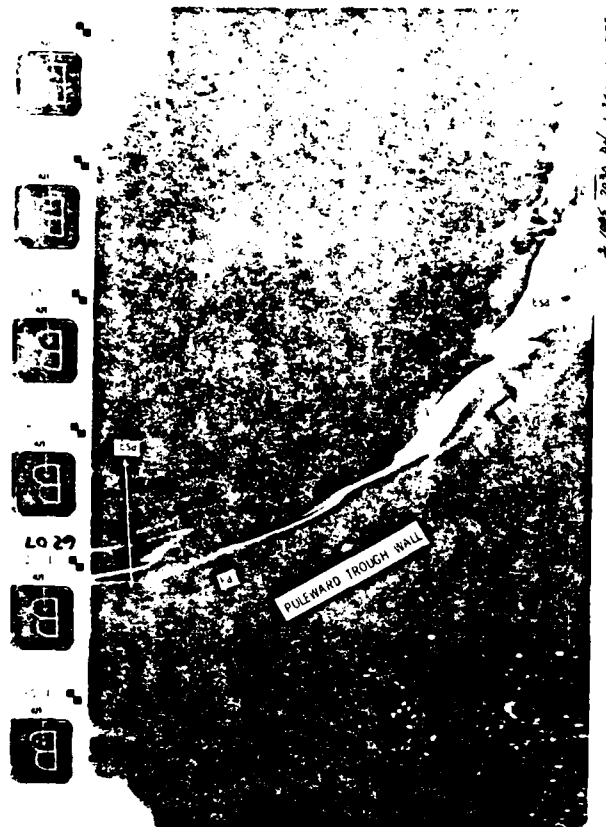


Figure 19. DMSP aurora photograph showing an intense substorm. The entire area of very bright aurora is dominated by intense sporadic E.

	11 DEC	12L	13L	14L	15L	16L	17L	18L	19L	20L	21L	22L	23L
MANILA	0	0	0	0	0	0	0	0	0	0	0	0	0
TAIPEI	0	0	0	0	0	0	0	0	0	0	0	0	0
MAUI	0	0	0	0	0	0	0	0	0	0	0	0	0
KOKOBIN	0	0	0	0	0	0	0	0	0	0	0	0	0
NICOSIA	0	0	0	0	0	0	0	0	0	0	0	0	0
ASHKHA	0	0	0	0	0	0	0	0	0	0	0	0	0
VANDEN	0	0	0	0	0	0	0	0	0	0	0	0	0
ALMA A	0	0	0	0	0	0	0	0	0	0	0	0	0
POITIE	0	0	0	0	0	0	0	0	0	0	0	0	0
KHABAR	0	0	0	0	0	0	0	0	0	0	0	0	0
BOULDE	0	0	0	0	0	0	0	0	0	0	0	0	0
WALLOP	0	0	0	0	0	0	0	0	0	0	0	0	0
KIEV	0	0	0	0	0	0	0	0	0	0	0	0	0
IRKUTS	0	0	0	0	0	0	0	0	0	0	0	0	0
MOSCOW	0	0	0	0	0	0	0	0	0	0	0	0	0
DOURBE	0	0	0	0	0	0	0	0	0	0	0	0	0
COLLOUGH	0	0	0	0	0	0	0	0	0	0	0	0	0
MAGADA	0	0	0	0	0	0	0	0	0	0	0	0	0
OTTAWA	0	0	0	0	0	0	0	0	0	0	0	0	0
SVERDL	0	0	0	0	0	0	0	0	0	0	0	0	0
TOMSK	0	0	0	0	0	0	0	0	0	0	0	0	0
GOOSE	0	0	0	0	0	0	0	0	0	0	0	0	0
YAKUTS	0	0	0	0	0	0	0	0	0	0	0	0	0
COLLEG	0	0	0	0	0	0	0	0	0	0	0	0	0
CAPE S	0	0	0	0	0	0	0	0	0	0	0	0	0
MURMAN	0	0	0	0	0	0	0	0	0	0	0	0	0
CHURCH	0	0	0	0	0	0	0	0	0	0	0	0	0
NARSSA	0	0	0	0	0	0	0	0	0	0	0	0	0
SALEKH	0	0	0	0	0	0	0	0	0	0	0	0	0
DIXON	0	0	0	0	0	0	0	0	0	0	0	0	0
KRENKE	0	0	0	0	0	0	0	0	0	0	0	0	0
GODHAV	0	0	0	0	0	0	0	0	0	0	0	0	0
RESOLU	0	0	0	0	0	0	0	0	0	0	0	0	0

Figure 20. Ionospheric observations showing Spread F occurrence (qualifier 6) during a typical undisturbed winter day.

observed before local sunset in the equatorial regions. It is usually observed between 1900 and 0400 local time with the peak occurrence between 2100 and 2400 local. The seasonal variation shows maximum occurrence in the spring and autumn. During solar maximum Spread F is observed more often during the pre-midnight hours, and in the post-midnight hours during solar minimum conditions. The pre-midnight Spread F condition is stronger in the eastern hemisphere than in the western hemisphere. In contrast to the high latitude Spread F phenomenon, equatorial Spread F is predominant during very quiet geomagnetic conditions (Figure 21).

Spread F is an important consideration on long north-south transequatorial circuits. Significant great circle deviations are often observed under Spread F conditions associated with reflection and scattering. This phenomenon starts in the section east of the great circle for a given circuit and moves westward with local sunset in the equatorial regions. Deviations of up to 50 degrees east and west of the great circle path may be observed. Time delay of the signal arrival is greater on paths east of the great circle path than on ones west of it. The signal strength is stronger and the occurrence more frequent for paths west of the great circle path. For paths west of the great circle route, extensions of the maximum usable frequency are often observed. Flutter fading of the signal amplitude also characterizes transequatorial propagation under Spread F conditions.

#### AURORAL OVAL

The auroral oval is an oval shaped belt which encircles the polar regions in which auroras occur. There are auroral ovals in both the northern and southern hemispheres. Auroras occur simultaneously in both hemispheres and follow nearly the same spatial and temporal variations. The centroid of the quiet auroral oval is displaced approximately three degrees in latitude toward the night hemisphere. The auroral oval is actually the instantaneous location of auroras and can be viewed as fixed with the earth rotating beneath it. The statistical locations for maximum occurrence of auroras is located in a narrow band near 67 degrees geomagnetic latitude and is called the auroral zone.

Auroral activity is present to some degree at all times in the auroral oval. Auroral activity is ordered in a framework of the substorm concept. This activity consists of the activation of quiet aurora into an expansive phase of intense activity followed by a recovery phase back to quiet aurora. During large disturbances, the intensity of the substorms is more severe and substorm occurrence more frequent. This substorm concept provides a convenient way of ordering auroral activity in both local time and storm time conditions.

During quiet geomagnetic conditions, the auroral oval contracts poleward. At such times, auroral substorms are less frequent, generally less intense, and of shorter duration. During disturbed conditions, the auroral oval expands equatorward (Figure 22). Such changes in position can occur in less than an hour. During disturbed conditions, the auroral substorms are more intense, more frequent, and of longer duration.

An example of auroral substorm activity during 26-27 July 1979 is illustrated in Figures 23, 24, 25, and 26. Figures 23 and 24 are forecaster displays of geomagnetic activity on 26 and 27 July respectively. The onset of

	19 JUL												
MANILA	002	012	022	032	042	052	062	072	082	092	102	112	000
TAIPEI	000	000	000	000	000	000	000	000	000	000	000	000	000
MAUI	000	000	000	000	000	000	000	000	000	000	000	000	000
KOKOBU	000	000	000	000	000	000	000	000	000	000	000	000	000
NIKOSI	000	000	000	000	000	000	000	000	000	000	000	000	000
ASHKHA	000	000	000	000	000	000	000	000	000	000	000	000	000
VANDEN	000	000	000	000	000	000	000	000	000	000	000	000	000
ALMAA	000	000	000	000	000	000	000	000	000	000	000	000	000
POITIE	000	000	000	000	000	000	000	000	000	000	000	000	000
KHABAR	000	000	000	000	000	000	000	000	000	000	000	000	000
BOULDE	000	000	000	000	000	000	000	000	000	000	000	000	000
WALLOP	000	000	000	000	000	000	000	000	000	000	000	000	000
KIEV	000	000	000	000	000	000	000	000	000	000	000	000	000
MOSCOW	000	000	000	000	000	000	000	000	000	000	000	000	000
DOLIRBE	000	000	000	000	000	000	000	000	000	000	000	000	000
SLOUGH	000	000	000	000	000	000	000	000	000	000	000	000	000
MAGADA	000	000	000	000	000	000	000	000	000	000	000	000	000
SVERDL	000	000	000	000	000	000	000	000	000	000	000	000	000
TOMSK	000	000	000	000	000	000	000	000	000	000	000	000	000
GOOSE	000	000	000	000	000	000	000	000	000	000	000	000	000
YAKUTS	000	000	000	000	000	000	000	000	000	000	000	000	000
COLLEG	000	000	000	000	000	000	000	000	000	000	000	000	000
CAPE	000	000	000	000	000	000	000	000	000	000	000	000	000
MIRMAN	000	000	000	000	000	000	000	000	000	000	000	000	000
CHIURCH	000	000	000	000	000	000	000	000	000	000	000	000	000
NARSSA	000	000	000	000	000	000	000	000	000	000	000	000	000
CALEKH	000	000	000	000	000	000	000	000	000	000	000	000	000
DI XON	000	000	000	000	000	000	000	000	000	000	000	000	000
KRENKE	000	000	000	000	000	000	000	000	000	000	000	000	000
GO.DHAU	000	000	000	000	000	000	000	000	000	000	000	000	000
RESOLU	000	000	000	000	000	000	000	000	000	000	000	000	000
	122	132	142	152	162	172	182	192	202	212	222	232	000

Figure 21. Ionospheric sounder data illustrating the occurrence of Spread F (qualifier 6) at the low latitudes during very quiet geomagnetic conditions.

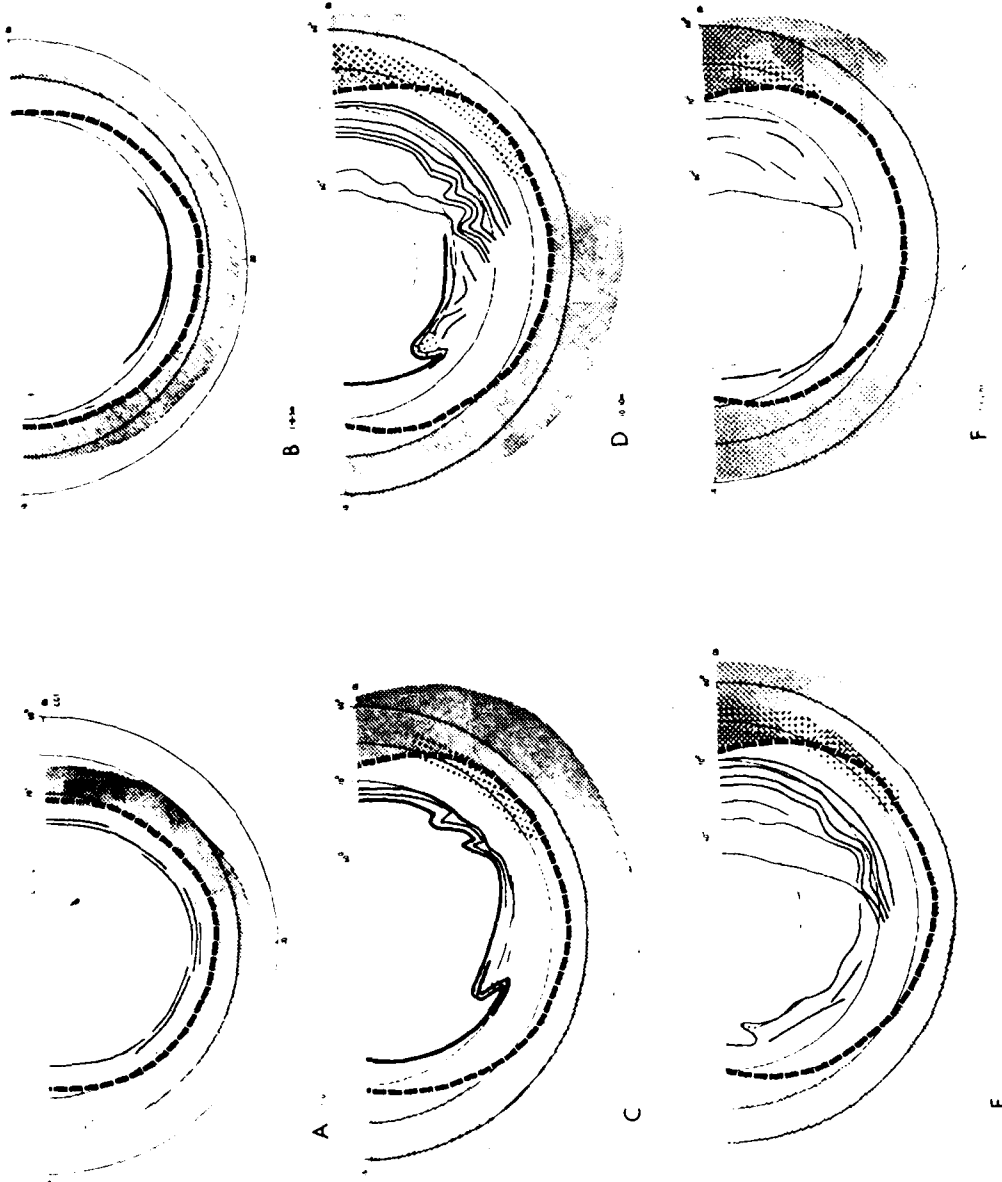


Figure 22. A schematic illustrating the various stages of an auroral substorm and the equatorward expansion of the auroral oval. The heavy dashed line is the equatorward boundary of the oval. The dark solid lines represent areas of strong absorption and bright aurora. The large dots represent areas of strong absorption and bright aurora. The lightly shaded areas indicate the sub-auroral trough region. (from Pike)

## GEOMAGNETIC INDEX DISPLAY FOR 790726

STATION		K-INDICES										REMARKS
STATION	NUMBER	03	06	09	12	15	18	21	24			
THULE	04205	3	3	3	5	4	3	5	5			
KRENKEL	36801	3	4	4	5	3	3	4	5			
DI XON	38701	2	2	4	4	3	4	7	7			
TI XIE BAY	43701											
COLLEGE	25602	2	2	3	3	3	2	3	3			
GOOSE BAY	71816	1	1	2	1	2	3					
MURMANSK	33702	0	1	1	2	1	1	5	6			
ANCHORAGE	25601	3	4	3	3	3	3	4	3			
LORING	72712	3	2	3	2	2	3	4	5			
TUNGUSKA	39601	0	1	3	3	1	1	5	6	*SSC*		(1833)
LENINGRAD	33603											
MAGADAN	45601											
SVERDLOVSK	36602	1	2	1	2	2	2	3	6	GRAD SC		(1900)
UPPERHEYFORD	03655	0	1	2	2	2	3	3	3			
WINGST	31523											
MOSCOW	34502			2	2	2	2	4	5	*SSC*		(1830)
FREDRICKSBURG	18403	0	1	3	2	1	0	4	5	*SSC*		(1833)
BOULDER	72469	3	1	3	2	1	1	4	4			
IRKUTSK	40501	2	1	1	2	1	2	4	4	*SSC*		(1830)
PE TROPAVLOVK	46501	2	1	2	1	1	1	4		*SSC*		(1830)
CHAMBON	30503			1	1	1	1	4	4	*SHARP SSC*		(1833)
KAKIOKA	44402											
ERGUELEN	77501				1	1	1	5	6	BAY (PSC)		(2323)
3-HOURLY AP		7	5	10	9	7	10	25	36			
3-HOURLY KP		20	1+	2+	2+	20	2+	4-	4+			
24-HR AVE AP		7	6	7	7	7	8	10	14			

Figure 23. Forecaster display of geomagnetic indices for 26 July 1979.

## GEOMAGNETIC INDEX DISPLAY FOR 27 JULY 1979

STATION	NUMBER	K-INDICES								REMARKS
		03	06	09	12	15	18	21	24	
THULE	04205	4	4	3	5	7	7	5	4	
KOPENKEL	36801	5	5							
DIXON	38701									
TIXIE BAY	43701									
COLLEGE	25602	5	4	2	2	3	3	3	2	
GOOSE BAY	71816	6	5	1	2	3	3	5		
MURMANSK	33702									
ANCHORAGE	25601	6	6	3	2	3	4	4	3	
LORING	72712	6	6	1	3	3	4	4	4	
TUNGUSKA	39601									
LENINGRAD	33603									
MAGADAN	45601									
VERDLOVSK	36602									
UPPERHEYFORD	03655	3	3	3	3	2	3	2	2	
WINGST	31523									
MOSCOW	34502	5	3							
FREDRICKSBURG	18403	5	5	1	2	2	3	3	4	
BOULDER	72469	5	6	2	2	2	4	3	3	
IRKUTSK	40501									
PETROPAVLOVSK	46501									
CHAMBON	30503	4	3							
KAKIOKA	44402									
MERGUELEN	77501	7	4	1						
3-HOURLY AP	53	48	6	10	11	18	19	12		
3-HOURLY KP	50	50	2-	2+	2+	3+	3+	3-		
24-HR AVE AP	19	25	24	24	25	26	25	22		

Figure 24. Geomagnetic indices for 27 July 1979.

## AURORAL QE INDEX FOR 26JUL74

DATE	TIME	LAT	LON	QE	CHAR	CGLT	CGLAT	QUAL	TYPE	SAT
26JUL79	0214	57.1	282.5	- .9		2123.0	67.9	70	J	F4
26JUL79	0356	59.7	256.6	.8		2001.0	66.3	0	J	F4
26JUL79	0539	65.5	227.4	3.4		1856.6	63.9	70	J	F4
26JUL79	0640	-76.1	258.4	4.4		0124.6	63.1	70	J	F4
26JUL79	0709	63.6	226.9	3.5		2027.7	63.9	0	J	F2
26JUL79	0722	72.1	193.8	3.9		1825.5	63.5	0	J	F4
26JUL79	0824	-69.0	222.8	4.3		0112.2	63.1	70	J	F4
26JUL79	0925	-57.9	158.4	1.2		2058.3	65.9	0	J	F2
26JUL79	1029	73.1	188.4	- .4		2109.5	67.4	0	J	F2
26JUL79	1107	-57.0	167.2	2.0	2	2318.9	65.2	0	H	
26JUL79	1211	71.1	158.0	3.6		2139.3	63.8	0	J	F2
26JUL79	1246	-53.0	112.2	4.3		1922.2	63.2	0	J	F2
26JUL79	1248	-52.0	144.8	3.5	3	2245.7	63.8	0	H	F1
26JUL79	1334	-50.4	136.5	4.3		2244.5	63.1	70	J	F4
26JUL79	1353	70.6	131.8	3.6		2210.0	63.8	0	J	F2
26JUL79	1428	-50.4	119.7	3.8	3	2202.7	63.6	0	H	F1
26JUL79	1429	-55.5	87.0	6.3		1835.6	61.3	70	J	F2
26JUL79	1515	-50.4	112.3	3.7		2208.3	63.6	0	J	F4
26JUL79	1535	70.7	107.2	2.5		2236.3	64.8	0	J	F2
26JUL79	1611	-52.0	93.9	4.8	2	2114.8	62.7	0	H	F1
26JUL79	1613	-66.9	55.2	6.6		1709.2	61.1	0	J	F2
26JUL79	1656	-53.9	89.8	3.2		2133.2	64.1	0	J	F4
26JUL79	1837	-56.9	66.9	5.8		2125.0	61.8	0	J	F4
26JUL79	1938	-62.0	37.2	9.5	4	2019.1	58.5	0	H	F1
26JUL79	2017	-59.9	43.2	8.4		2125.6	59.5	0	J	F4
26JUL79	2158	-62.3	18.7	11.3		2136.9	56.9	0	J	F4
26JUL79	2302	-75.8	293.0	12.6		1912.2	55.7	70	J	F2
26JUL79	2305	-74.5	260.1	12.7	3	1812.3	55.6	0	H	F3
26JUL79	2339	-65.7	354.8	13.1		2206.6	55.2	70	J	F4

Figure 25. QE indices calculated from DMSP aurora data. These indices help define the equatorward boundary of the auroral oval.

## AURORAL RE INDEX FOR 27JUL79

DATE	TIME	LAT	LON	RE	CHAR	CGLT	CGLAT	DUAL	TYPE	SAT
27JUL79	0009	51.4	322.0	10.8		2252.1	57.3	0	J	F2
27JUL79	0119	-71.5	334.1	10.9		2249.8	57.2	0	J	F4
27JUL79	0300	-71.4	305.8	12.7		2325.5	55.6	0	J	F4
27JUL79	0333	46.1	268.3	12.2		2104.8	56.0	70	J	F4
27JUL79	0407	-63.8	193.9	6.9	3	1905.8	60.8	0	H	
27JUL79	0438	-80.6	305.5	2.4		0056.3	64.9	70	J	F4
27JUL79	0703	70.2	201.7	4.4		1836.4	63.0	70	J	F4
27JUL79	0726	-61.4	185.1	3.8		2124.1	63.6	70	J	F2
27JUL79	0804	-72.7	232.2	3.3		0137.1	64.1	70	J	F4
27JUL79	0831	67.6	210.0	2.9		2036.8	64.4	0	J	F2
27JUL79	0907	-57.6	163.0	2.0		2103.9	64.8	70	J	F2
27JUL79	1012	71.0	188.8	2.0		2103.7	65.2	0	J	F2
27JUL79	1047	-54.8	140.0	2.0		2022.5	65.2	0	J	F2
27JUL79	1154	70.8	161.9	3.9		2134.2	63.5	0	J	F2
27JUL79	1228	-52.1	116.9	4.8		1935.4	62.7	0	J	F2
27JUL79	1335	70.7	136.1	3.7		2204.1	63.7	0	J	F2
27JUL79	1411	-56.1	91.0	4.9		1834.5	62.6	0	J	F2
27JUL79	1457	-49.1	116.2	5.1		2214.5	62.4	70	J	F4
27JUL79	1517	69.3	109.3	4.1		2225.6	63.4	0	J	F2
27JUL79	1553	-50.0	99.6	5.9	3	2134.2	61.7	0	H	F1
27JUL79	1638	-51.2	92.9	5.3		2140.4	62.2	70	J	F4
27JUL79	1735	-54.0	72.0	7.9	2	2050.7	59.9	0	H	F1
27JUL79	2214	61.4	339.8	4.5		2216.5	62.9	0	J	F4
27JUL79	2318	-72.1	8.5	5.9		2201.8	61.7	0	J	F4
27JUL79	2348	59.6	331.0	3.8		2321.6	63.6	0	J	F2

Figure 26. Qe indices for 27 July 1979.

intense substorm occurs near 26/1830Z. Geomagnetic indices worldwide, and particularly at the high latitudes, show a significant increase during the following hours.

These disturbed conditions persist through 27/0600Z and end rather abruptly prior to 27/0900Z. Figures 25 and 26 are forecaster displays of Qe indices obtained from DMSP auroral photos and precipitating electron sensor measurements. A one unit increase in Qe values corresponds to roughly a one degree southward expansion of the auroral oval. Thus, we see from the Qe values that the auroral oval has expanded equatorward roughly seven degrees in latitude from its pre-substorm position.

The shape and dynamic characteristics of the auroral oval pose serious problems for both the forecaster and user of HF propagation forecasts. For the forecaster, certain stations such as College, Alaska are part time auroral stations. During very quiet conditions, College is in the middle latitude ionosphere during much, but not all, of the day (Figure 27). During very disturbed conditions the station often is a polar ionospheric station. Thus the forecaster must analyse data that varies with geomagnetic coordinates and local time and relate this to a geographic coordinate/Zulu time forecast grid.

The effects on HF propagation associated with the auroral oval are often severe. Strong enhancements of Sporadic E are associated with discrete aurora occurrence. In the night sector, enhanced ionization in the F region changes abruptly to an area of electron depletion called the sub-auroral F layer trough. This trough extends up to 10 degrees (1000 km) south of the equatorward boundary of the auroral oval in the northern hemisphere (see Figure 28). The equatorward expansion, or passage of this trough region, results in decreased foF<sub>2</sub> and often drastic changes in the MUF over a relatively short time. Thus, circuits with control points in these areas will show a decreased range of usable frequencies. Many North Atlantic circuits are susceptible to this type of effect. It should also be noted that circuits typically thought of as middle latitude, e.g., California to Korea, have their control points just south of the auroral oval. During large disturbances the equatorward expansion of the auroral oval can even affect these circuits.

Non-great-circle propagation is often observed on transauroral circuits during intense substorm activity. Communicators possessing directional antennas may be able to reduce outages during these times by combining the use of such equipment with the knowledge of the existence of non-great-circle propagation conditions.

During intense auroral substorms, increased absorption is observed where bright aurora occurs and also just equatorward of the oval in the daytime sector. This phenomena is known as auroral zone absorption (AZA). During the pre-midnight hours it maximizes about 1 to 2 degrees south of the bright optical aurora. During the daytime, AZA occurs in the same relative geographic location as the nighttime absorption but is roughly 10 degrees equatorward of the daytime position of the auroral oval. Absorption is also observed in the morning sector associated with patch type aurora (Figure 29). Areas of AZA can be identified by using high latitude riometers and ionospheric sounders in conjunction with the observed/expected position of the auroral oval.

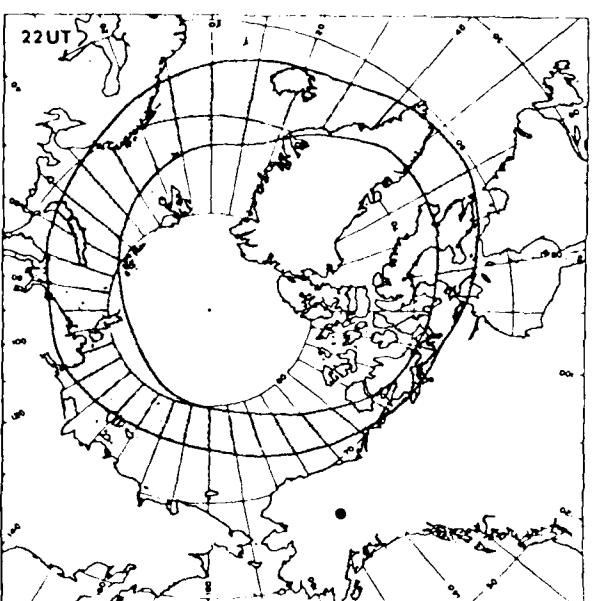
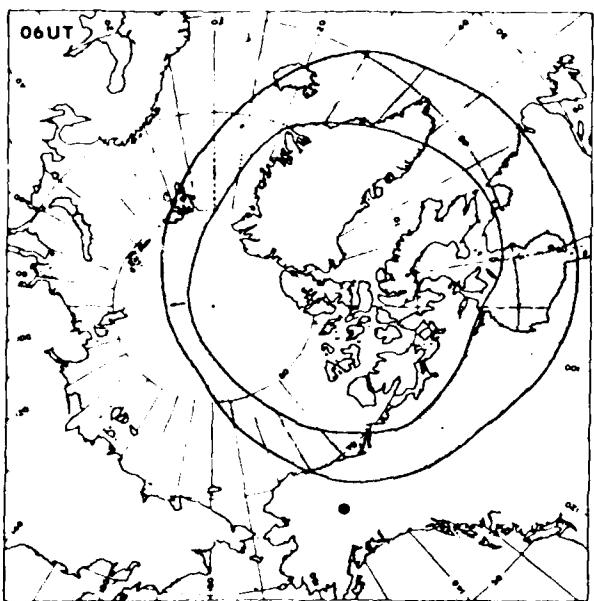
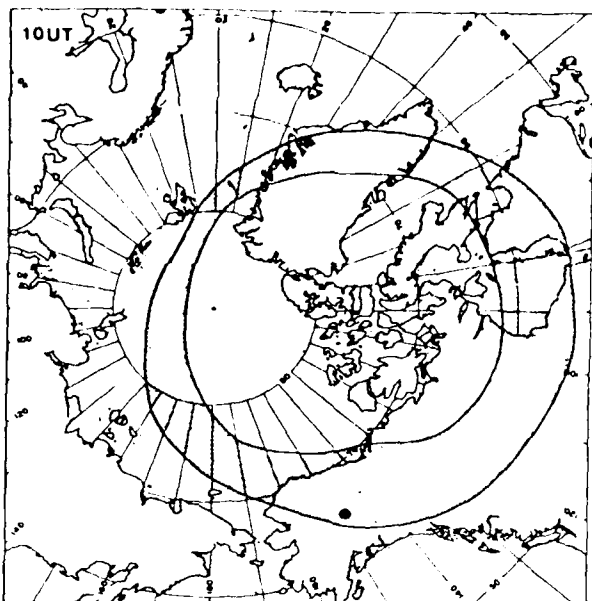
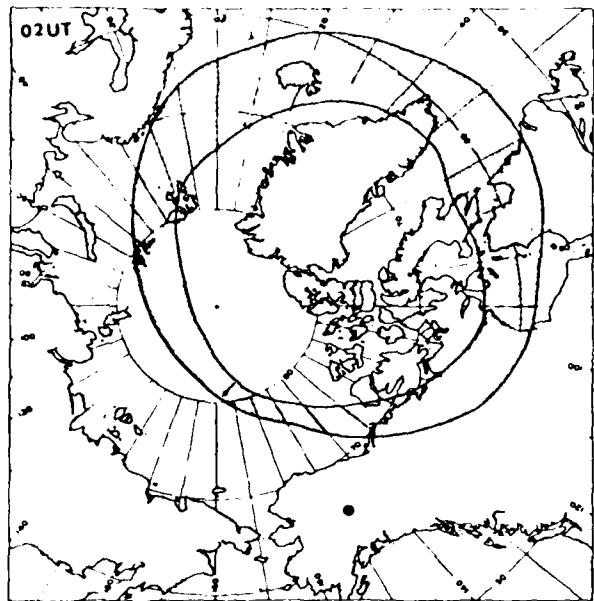


Figure 27. An illustration of the diurnal variation of the auroral oval position with respect to a given station.

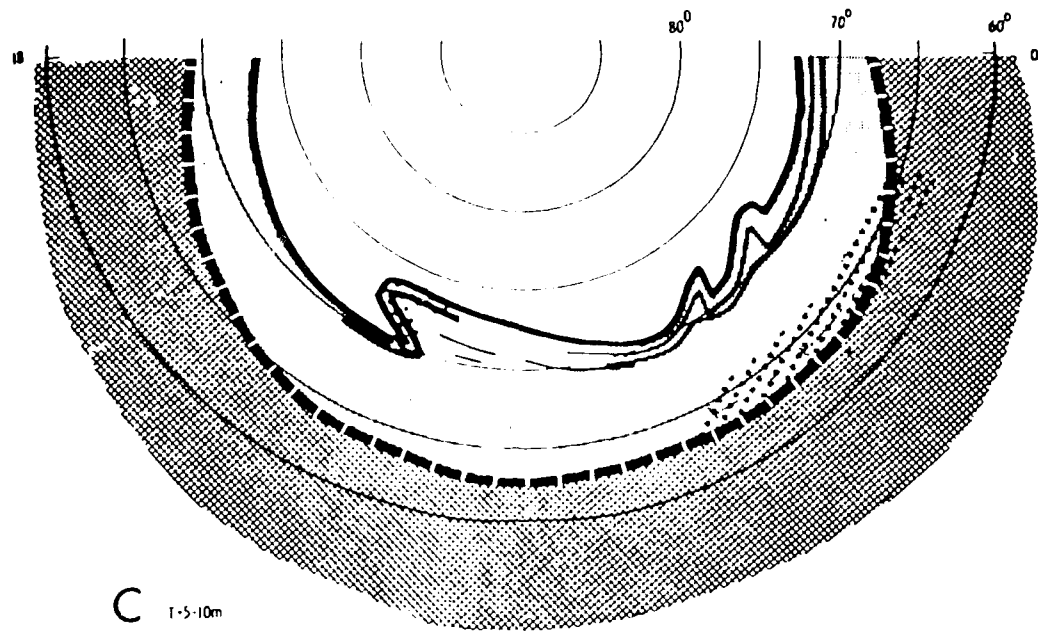


Figure 28. An illustration of the extent of the sub-auroral trough (dark shaded area) near the maximum of a substorm. The heavy dashed line is the equatorward boundary of the oval. The dark solid lines indicate the areas of brightest aurora and the lightly shaded area less bright aurora. The dots indicate areas of strong absorption. (from E.P. Pike)



Figure 29. DMSP photograph showing patch type aurora associated with auroral zone absorption.  
(from Pike)

### SHORTWAVE FADE (SWF)

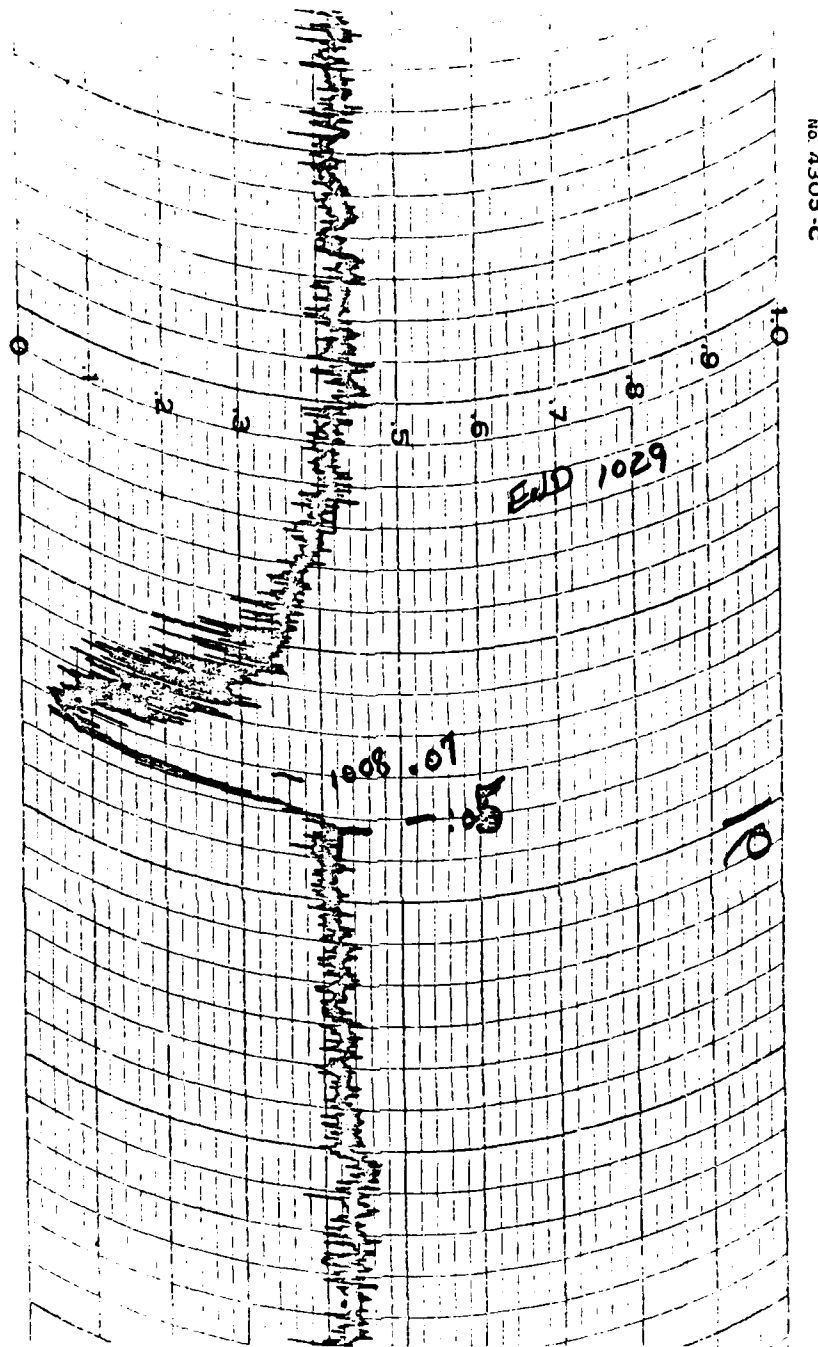
A shortwave fade is a decrease or loss in signal strength of an HF signal caused by increased absorption due to 1-10 Angstrom X-ray enhancement in the D-region of the ionosphere. Additional x-ray enhancements in the 10-100 Angstrom range also contribute to the absorption effects. Many SWF events are characterized by a sudden onset and are a particular case of the more generalized phenomenon known as a Sudden Ionospheric Disturbance (SID). Shortwave fades may have a more gradual onset depending upon the characteristic of the solar x-ray event producing it. Figures 30a and b illustrate typical shortwave fade events. The duration of a SWF varies from several minutes to several hours depending upon the intensity of the solar event, frequency being used, and the propagation path. The intensity of such events may vary from very minor absorption on frequencies in the low part of the HF spectrum to a total blackout of the HF spectrum.

From a communicator's standpoint, this phenomenon poses a serious problem in the disruption of HF transmissions, particularly during solar maximum. If any part of the path is in sunlight, some absorption can be expected. The more time the signal passes through the D-region, the more absorption occurs (Figure 31). In general, the lower frequencies are absorbed first and recover last. Corrective action would be a switch to a higher frequency or, where possible, to a different propagation path that is in darkness. In some cases, e.g., during E mode propagation, the lower frequencies on a given path may show less absorption than the higher ones because of fewer passages through the D-region.

Real-time monitoring of solar x-ray data used in conjunction with certain forecaster aids can provide the means for making reasonable estimates of the frequencies affected and the duration of the SWF. Figure 32 contains a table relating x-ray event classification and SWF frequency and duration. This is empirically based on forecaster experience. Another computer generated display developed by an adaptation of Rose, et al (1974) provides estimates of the LUF for a predetermined set of paths (Figure 33). Input data includes the date, month, GMT time and x-ray flux. While frequencies higher than the ones indicated may show some absorption, the display provides a reasonable starting point for estimating the lower limit of the usable frequencies during a given x-ray event. Additional paths may be specified and displayed by the forecaster as required.

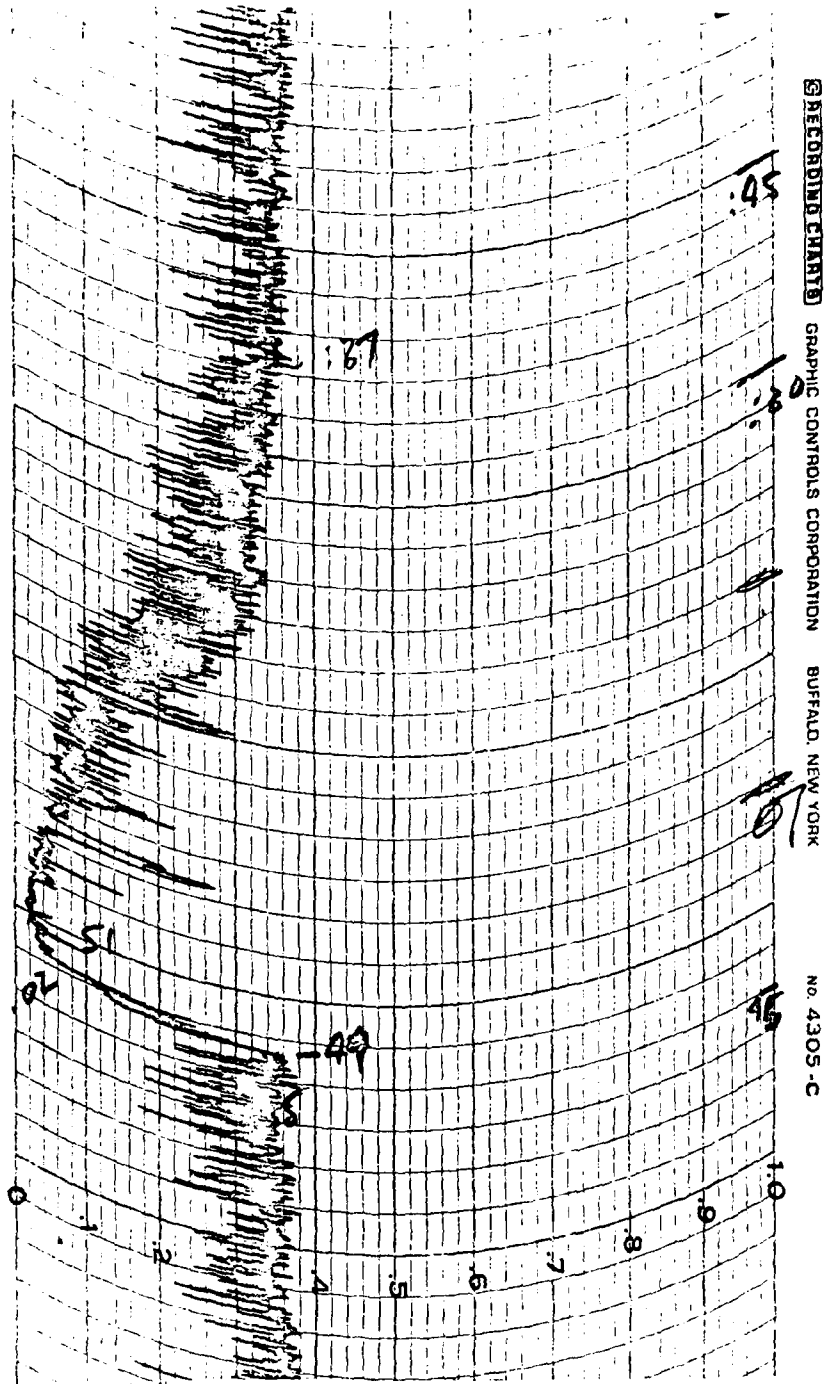
### POLAR CAP ABSORPTION (PCA) EVENTS

The PCA phenomenon is an increased absorption of HF radio waves in the polar regions associated with enhanced ionization from solar flare produced protons. The onset of a polar cap absorption event may occur from a fraction of an hour to several hours after the associated flare occurrence. This is a function of the arrival time of the solar produced particles. In some cases the onset of the PCA event may be delayed several days depending upon the location of the flare on the sun and earth-sun geometry. The duration of the PCA is typically about three days, but may be as short as one day and as long as 10 days. The magnitude and duration of the absorption is directly related to the energies and numbers of incoming particles. The absorption usually reaches maximum 5-6 hours after onset, and generally follows the time and



DATE: 25 OCT 1972  
PATH: LONDON-ATHENS 15.070 mHz  
START: 1005 GMT  
MAX: 1008  
END: 1029

Figure 30a. A solar flare associated shortwave fade.



DATE: 26 OCT 1972  
PATH: PEKING-ATHENS 15.590 mHz  
START: 0647 GMT  
MAX: 0651  
END: 0737

Figure 30b. A solar flare associated shortwave fade.

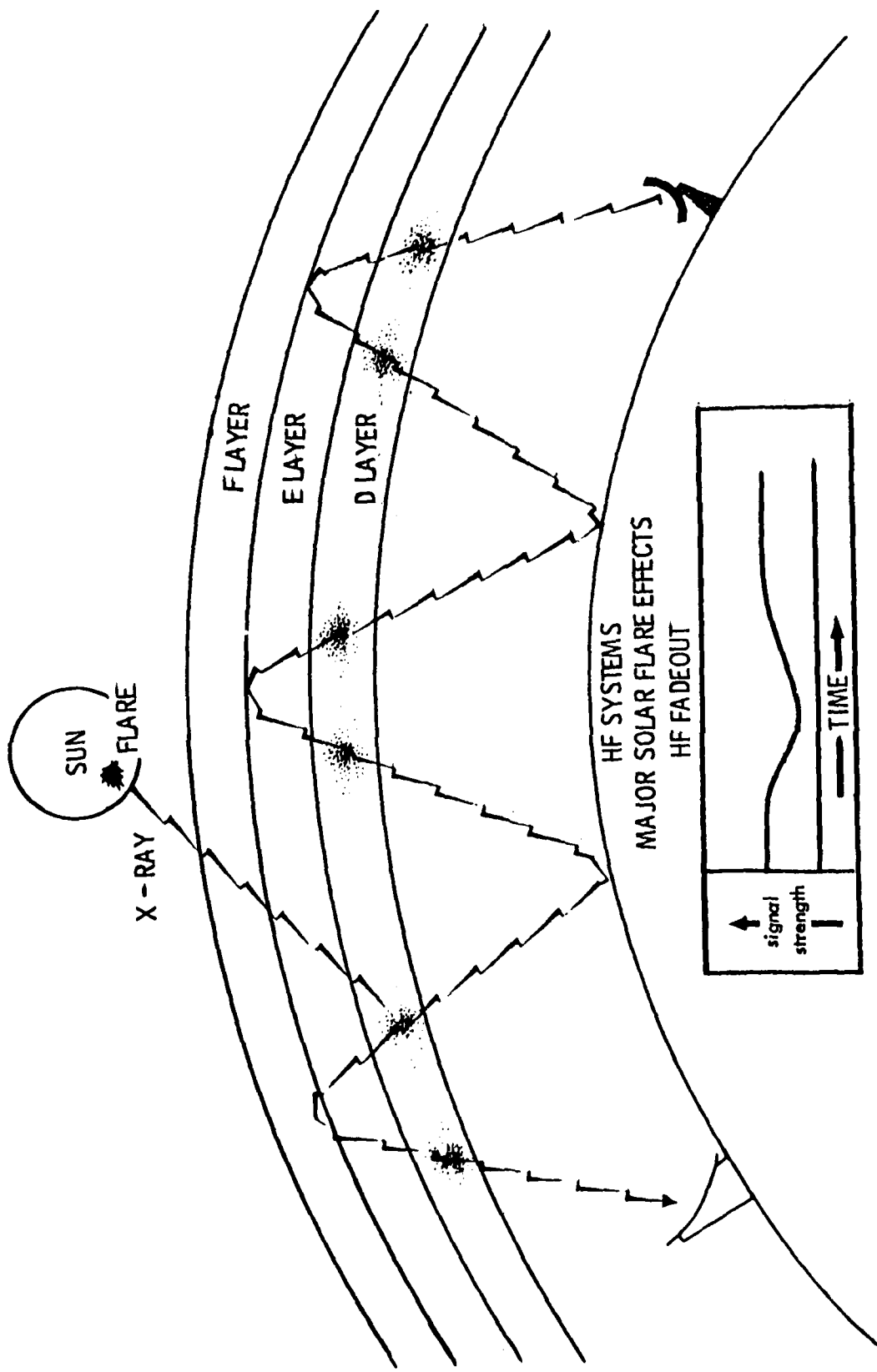


Figure 31. An illustration of solar x-ray event effects on a sunlit HF circuit. Each additional signal passage through the D region produces additional absorption.

### X-RAY CLASSIFICATION vs SWF

Estimated magnitudes/durations for SWF events are as follows:

<u>X-RAY CLASS</u>	<u>FREQUENCY</u>	<u>DURATION</u>	<u>X-RAY CLASS</u>	<u>FREQUENCY</u>	<u>DURATION</u>
M1	12 MHz	20 min	X1	20 MHz	40 min
M2	13 MHz	20 min	X2	23 MHz	50 min
M3	14 MHz	25 min	X3	25 MHz	60 min
M4	15 MHz	25 min	X4	27 MHz	75 min
M5	15 MHz	30 min	X5	28 MHz	90 min
M6	16 MHz	30 min	X6	29 MHz	100 min
M7	17 MHz	35 min	X7	30 MHz	100 min
M8	18 MHz	35 min	X8	30 MHz	120 min
M9	19 MHz	40 min	X9	30 MHz	120 min

Note: These estimates assume a fully sunlit, single hop HF radio path.  
(Developed by CMSgt Edward D Beard USAF (Ret)).

The X-ray classification is as follows:

CLASS C = Any solar x-ray burst with a peak flux at 1-8 $\text{\AA}$  less than  $10^{-2}$  erg cm $^{-2}$  sec $^{-1}$ , but greater than  $10^{-3}$ .

CLASS M = A solar x-ray burst with peak flux at 1-8 $\text{\AA}$  greater than or equal to  $10^{-2}$  but less than  $10^{-1}$  erg cm $^{-2}$  sec $^{-1}$ . EX: M5 =  $5.0 \times 10^{-2}$  erg cm $^{-2}$  sec $^{-1}$ .

CLASS X = A solar x-ray burst with peak flux at 1-8 $\text{\AA}$  greater than or equal to  $10^{-1}$  erg cm $^{-2}$  sec $^{-1}$ . EX: X8 =  $8.0 \times 10^{-1}$  erg cm $^{-2}$  sec $^{-1}$ .

Figure 32. X-ray classification versus estimated SWF magnitudes and duration.

Location of Subsolar PT is: Lat = -15.3 Lon = 355.9 at date/time=791104/1200

Path=KNDY-ASCN	Location:	28.50	279.50	-8.00	345.60
Flux=5.0000-01	LUF=31	100 Percent of Path in Sunlight			
Path=KNDY-MAHE	Location:	28.50	279.50	-4.70	55.60
Flux=5.0000-01	LUF=29	100 Percent of Path in Sunlight			
Path=ASCN-MAHE	Location:	-8.00	345.60	-4.70	55.60
Flux=5.0000-01	LUF=31	100 Percent of Path in Sunlight			
Path=CROU-AZORES	Location:	52.00	359.00	39.60	333.00
Flux=5.0000-01	LUF=25	100 Percent of Path in Sunlight			
Path=MORC-DIEGO	Location:	35.00	354.00	-7.00	72.00
Flux=5.0000-01	LUF=28	100 Percent of Path in Sunlight			
The Path -22.34	114.05 to 11.40	121.00 is in darkness			
Path=ANDRW-PUERTO	Location:	40.00	283.00	18.00	294.00
Flux=5.0000-01	LUF=19	100 Percent of Path in Sunlight			
Path=ATHENS-LONDN	Location:	38.00	23.00	52.00	359.00
Flux=5.0000-01	LUF=25	100 Percent of Path in Sunlight			
Path=ATHENS-MOSCW	Location:	38.00	23.00	55.00	37.60
Flux=5.0000-01	LUF=25	100 Percent of path in Sunlight			
Path=TEHRAN-LONDN	Location:	36.00	52.00	52.00	359.00
Flux=5.0000-01	LUF=21	100 Percent of Path in Sunlight			
Path=TEHRAN-MOSCW	Location:	36.00	52.00	55.00	37.60
Flux=5.0000-01	LUF=15	100 Percent of Path in Sunlight			
Path=RAMEY-LONDN	Location:	18.00	293.00	52.00	359.00
Flux=5.0000-01	LUF=22	100 Percent of path in Sunlight			

Figure 33. Forecaster display of LUF predictions used during shortwave fade events.

magnitude profiles of the incoming protons. The absorption will gradually decrease as the number of incoming particles decreases. The amount of absorption shows large diurnal variations, with daytime absorption values 2-5 times those at night. During those times of the year when the polar cap is completely sunlit or completely dark, these variations are much less pronounced.

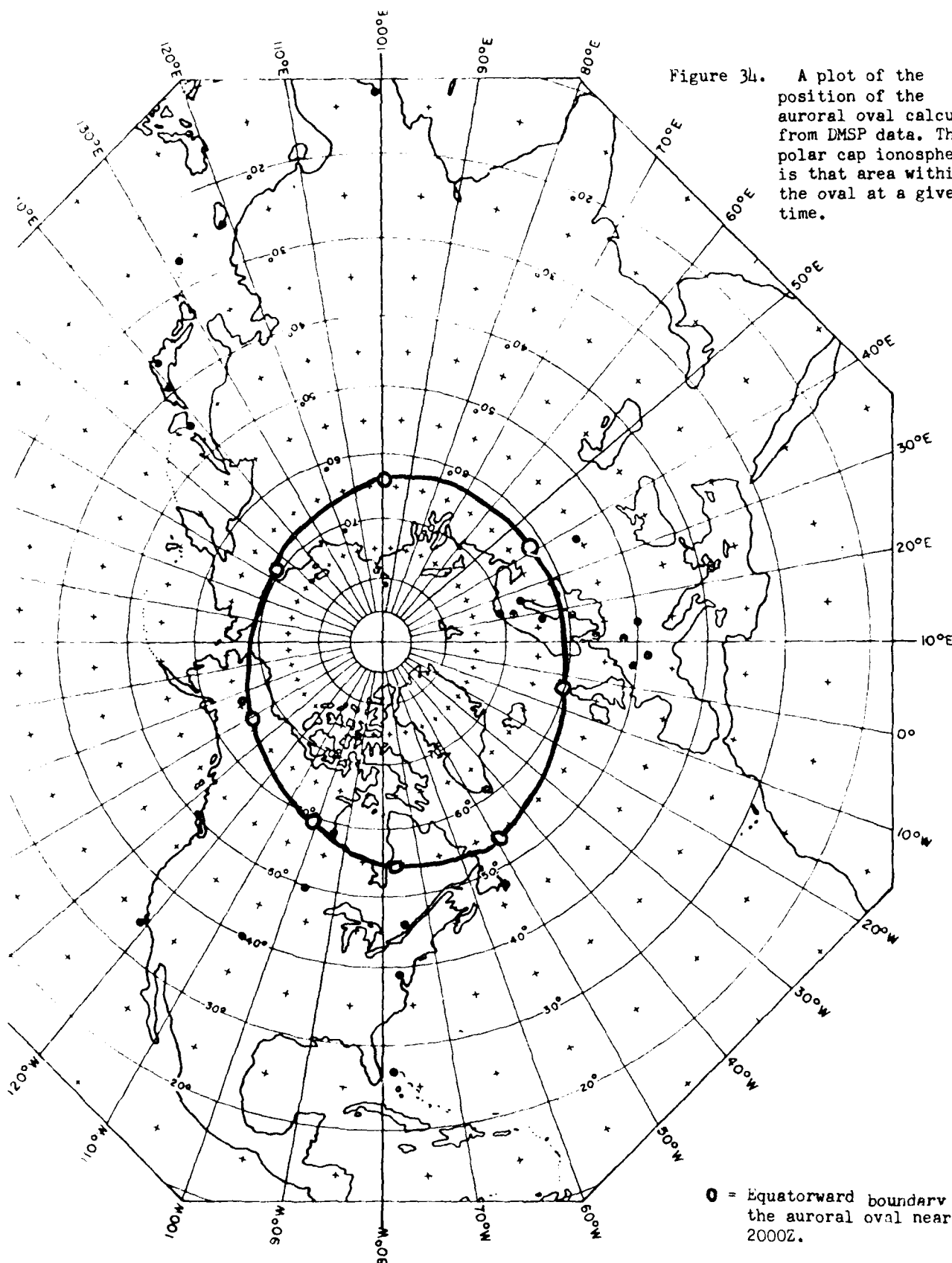
The geographical extent of the PCA covers the area poleward of the auroral oval. Typically the area is poleward of 65 degrees latitude. The PCA will occur simultaneously in both the northern and southern hemispheres. Often the PCA starts in a small area near the auroral oval, spreads into a "U" shaped area about the geomagnetic pole and expands to engulf the entire polar area. During the decay phase, the PCA breaks into small regions within the polar cap and gradually subsides.

Difficulties arise in monitoring the spatial extent of PCA because of the sparsity of data from the polar regions. The PCA will extend to lower latitudes when the geomagnetic field is disturbed and the auroral oval expands equatorward. The polar cap area can be identified at a given time by using auroral observations from the DMSP satellite to define the auroral oval position (Figure 34). During periods of high geomagnetic activity, the flux of precipitating protons producing the PCA tends to be uniform over the polar cap, whereas when the geomagnetic field is quiet, there tends to be a minimum of proton flux over the geomagnetic pole and a maximum near the auroral oval. Thus, during periods of high magnetic activity, the amount of absorption will be more uniform over the polar area and less patchy than during quiet magnetic conditions.

Polar cap absorption events are usually monitored using riometers (relative ionospheric opacity meter), and ground based ionospheric sounders. The riometer measurements are in the form of absorption of the background galactic noise near 30 MHz. Near realtime measurements are available from Thule, Greenland and a chain of riometers in Alaska. Arbitrary thresholds of 2.0 decibels absorption for daytime and 0.5 decibels at night are used for PCA detection. Caution should be exercised in using the Alaskan data, since auroral zone absorption effects may be confused with PCA absorption. Ionospheric sounder data is also useful in the detection and monitoring of PCA events, but is, in general, less timely in receipt. Using these two data sets, we'll examine several PCA events.

#### Case 1

The first case concerns the period 14-21 September 1979. Figures 35a through 35h are displays of reported ionospheric sounders for the period of interest. During the 14th and the first half of the 15th, the high latitude ionosphere is dominated by Spread F conditions as indicated by qualifier 6 in the displays. The first indication of increased absorption in the polar region occurs at 15/1400Z with absorption (qualifier 2) being reported at Quaq, Greenland. This is followed several hours later by absorption at Godhavn, Greenland. This absorption does not persist and it is nearly 24 hours before a definite pattern of a PCA develops. The pattern that emerges from 16-18 September is one in which absorption is reported in the Western Hemisphere



QIAL	14 SEP	007000	022000	037000	047000	057000	062000	077000	087000	097000	107000	117000
MANILA	1226	1326	1476	1576	1676	1726	1876	1976	2076	2176	2276	2370
MAUI	00	00	00	00	00	00	00	00	00	00	00	00
KOKOBU	00	00	00	00	00	00	00	00	00	00	00	00
NI COSI	00	00	00	00	00	00	00	00	00	00	00	00
AS HKHA	00	00	00	00	00	00	00	00	00	00	00	00
VA NDEN	00	00	00	00	00	00	00	00	00	00	00	00
AL MA A	00	00	00	00	00	00	00	00	00	00	00	00
PO ITIE	00	00	00	00	00	00	00	00	00	00	00	00
BO ULD E	00	00	00	00	00	00	00	00	00	00	00	00
WALL OP	00	00	00	00	00	00	00	00	00	00	00	00
KIEV	00	00	00	00	00	00	00	00	00	00	00	00
IR KIITS	00	00	00	00	00	00	00	00	00	00	00	00
MO SCOW	00	00	00	00	00	00	00	00	00	00	00	00
DO URBE	00	00	00	00	00	00	00	00	00	00	00	00
PU NIGH	00	00	00	00	00	00	00	00	00	00	00	00
MA GADA	00	00	00	00	00	00	00	00	00	00	00	00
OT TAWA	00	00	00	00	00	00	00	00	00	00	00	00
SV ERDL	00	00	00	00	00	00	00	00	00	00	00	00
TO MSK	00	00	00	00	00	00	00	00	00	00	00	00
GO OSE	00	00	00	00	00	00	00	00	00	00	00	00
YA KIITS	00	00	00	00	00	00	00	00	00	00	00	00
COLLEG	00	00	00	00	00	00	00	00	00	00	00	00
CAPE S	00	00	00	00	00	00	00	00	00	00	00	00
MIRMAN	00	00	00	00	00	00	00	00	00	00	00	00
CH URCH	00	00	00	00	00	00	00	00	00	00	00	00
SA LEKH	00	00	00	00	00	00	00	00	00	00	00	00
DI XON	00	00	00	00	00	00	00	00	00	00	00	00
KRENKE	00	00	00	00	00	00	00	00	00	00	00	00
GO DH AV	00	00	00	00	00	00	00	00	00	00	00	00
RE SOLU	00	00	00	00	00	00	00	00	00	00	00	00
QIANO	00	00	00	00	00	00	00	00	00	00	00	00

Figure 35a. Ionospheric sounder data for 14 September 1979.

Figure 35b. Ionoospheric sounder data for 15 September 1979.

Figure 35c. Ionospheric sounder data for 16 September 1979.

QSL	17	SEP	007	017	027	037	047	052	062	072	082	097	107	117
MANILA														
TA IPEI														
MAUI														
KOKOBU														
NI CO SI														
AS HK HA														
VA NDEN														
AL MA A														
PO IT IE														
BO UIL DE														
WALL OP														
KI EV														
IR KUTS														
MO SCOW														
DO URB E														
EL DUGH														
MAGADA														
OT TAWA														
EVER DL														
TO MSK														
GO OSE														
YA KU TS														
COLLEG														
MIRMAN														
NA RSSA														
SA LEKH														
DI XON														
KR ENKE														
GA DHAV														
RE SOLU														
QU ANO														
MANILA	122		137		147		157		167		172		182	
TA IPEI	6		6		6		6		6		6		6	
MAUI	8		8		8		8		8		8		8	
KOKOBU	0		0		0		0		0		0		0	
NI CO SI	0		0		0		0		0		0		0	
AS HK HA	0		0		0		0		0		0		0	
VA NDEN	0		0		0		0		0		0		0	
AL MA A	0		0		0		0		0		0		0	
PO IT IE	0		0		0		0		0		0		0	
BO UIL DE	0		0		0		0		0		0		0	
WALL OP	0		0		0		0		0		0		0	
KI EV	0		0		0		0		0		0		0	
IR KUTS	0		0		0		0		0		0		0	
MO SCOW	0		0		0		0		0		0		0	
DO URB E	0		0		0		0		0		0		0	
EL DUGH	0		0		0		0		0		0		0	
MAGADA	0		0		0		0		0		0		0	
OT TAWA	0		0		0		0		0		0		0	
EVER DL	0		0		0		0		0		0		0	
TO MSK	0		0		0		0		0		0		0	
GO OSE	0		0		0		0		0		0		0	
YA KU TS	0		0		0		0		0		0		0	
COLLEG	0		0		0		0		0		0		0	
MIRMAN	0		0		0		0		0		0		0	
CHUR CH	0		0		0		0		0		0		0	
NA RSSA	0		0		0		0		0		0		0	
SA LEKH	0		0		0		0		0		0		0	
DI XON	0		0		0		0		0		0		0	
KR ENKE	0		0		0		0		0		0		0	
GA DHAV	0		0		0		0		0		0		0	
RE SOLU	0		0		0		0		0		0		0	
QU ANO	2		2		2		2		2		2		2	

Figure 35d. Ionospheric sounder data for 17 September 1979.

Figure 35e. Ionospheric sounder data for 18 September 1979.

QAL	19 SEP	00Z	01Z	02Z	03Z	04Z	05Z	06Z	07Z	08Z	09Z	10Z	11Z
MANILA		000	017	000	027	037	047	057	062	077	087	097	107
TAIPEI		000	0	000	0	0	0	0	0	0	0	0	0
MAUI		000	0	000	0	0	0	0	0	0	0	0	0
KOKOBU		000	0	000	0	0	0	0	0	0	0	0	0
NICOSI		000	0	000	0	0	0	0	0	0	0	0	0
ASHKHA		000	0	000	0	0	0	0	0	0	0	0	0
VANDEN		000	0	000	0	0	0	0	0	0	0	0	0
ALMAA		000	0	000	0	0	0	0	0	0	0	0	0
POITIE		000	0	000	0	0	0	0	0	0	0	0	0
KHABAR		000	0	000	0	0	0	0	0	0	0	0	0
BOULDE		000	0	000	0	0	0	0	0	0	0	0	0
WALLOP		000	0	000	0	0	0	0	0	0	0	0	0
KIEV		000	0	000	0	0	0	0	0	0	0	0	0
IRKUTS		000	0	000	0	0	0	0	0	0	0	0	0
MOSCOW		000	0	000	0	0	0	0	0	0	0	0	0
DOURBE		000	0	000	0	0	0	0	0	0	0	0	0
SLOUGH		000	0	000	0	0	0	0	0	0	0	0	0
MAGADA		000	0	000	0	0	0	0	0	0	0	0	0
SVERDL		000	0	000	0	0	0	0	0	0	0	0	0
TOMSK		000	0	000	0	0	0	0	0	0	0	0	0
GOOSE		000	0	000	0	0	0	0	0	0	0	0	0
YAKUTS		000	0	000	0	0	0	0	0	0	0	0	0
COLLEG		000	0	000	0	0	0	0	0	0	0	0	0
MURMAN		000	0	000	0	0	0	0	0	0	0	0	0
NARSSA		000	0	000	0	0	0	0	0	0	0	0	0
SALEKH		000	0	000	0	0	0	0	0	0	0	0	0
DIxon		000	0	000	0	0	0	0	0	0	0	0	0
KRENKE		000	0	000	0	0	0	0	0	0	0	0	0
GO DHAV		000	0	000	0	0	0	0	0	0	0	0	0
RE SOLU		000	0	000	0	0	0	0	0	0	0	0	0
QIANQ		22	22	22	22	22	22	22	22	22	22	22	22
MANILA	122	122	132	142	152	162	172	182	192	202	212	222	232
TAIPEI	6	6	6	6	6	6	6	6	6	6	6	6	6
MAUI	000	0	0	0	0	0	0	0	0	0	0	0	0
KOKOBU	000	0	0	0	0	0	0	0	0	0	0	0	0
NICOSI	000	0	0	0	0	0	0	0	0	0	0	0	0
ASHKHA	000	0	0	0	0	0	0	0	0	0	0	0	0
VANDEN	000	0	0	0	0	0	0	0	0	0	0	0	0
ALMAA	000	0	0	0	0	0	0	0	0	0	0	0	0
POITIE	000	0	0	0	0	0	0	0	0	0	0	0	0
KHABAR	000	0	0	0	0	0	0	0	0	0	0	0	0
BOULDE	000	0	0	0	0	0	0	0	0	0	0	0	0
WALLOP	000	0	0	0	0	0	0	0	0	0	0	0	0
KIEV	000	0	0	0	0	0	0	0	0	0	0	0	0
IRKUTS	000	0	0	0	0	0	0	0	0	0	0	0	0
MOSCOW	000	0	0	0	0	0	0	0	0	0	0	0	0
DOURBE	000	0	0	0	0	0	0	0	0	0	0	0	0
SLOUGH	000	0	0	0	0	0	0	0	0	0	0	0	0
MAGADA	000	0	0	0	0	0	0	0	0	0	0	0	0
OT TAWA	000	0	0	0	0	0	0	0	0	0	0	0	0
SVERDL	000	0	0	0	0	0	0	0	0	0	0	0	0
TOMSK	000	0	0	0	0	0	0	0	0	0	0	0	0
GOOSE	000	0	0	0	0	0	0	0	0	0	0	0	0
YAKUTS	000	0	0	0	0	0	0	0	0	0	0	0	0
COLLEG	000	0	0	0	0	0	0	0	0	0	0	0	0
MURMAN	000	0	0	0	0	0	0	0	0	0	0	0	0
CHURCH	000	0	0	0	0	0	0	0	0	0	0	0	0
NARSSA	90	90	90	90	90	90	90	90	90	90	90	90	90
SALEKH	90	90	90	90	90	90	90	90	90	90	90	90	90
KRENKE	90	90	90	90	90	90	90	90	90	90	90	90	90
GO DHAV	9	9	12	2	2	2	2	2	2	2	2	2	2
RE SOLU	2	2	2	2	2	2	2	2	2	2	2	2	2
QIANQ	2	2	2	2	2	2	2	2	2	2	2	2	2

Figure 35f. Ionospheric sounder data for 19 September 1979.

QAL	20 SEP												117
MANILA	007	20	017	027	037	047	057	062	072	087	097	107	600
TAIPEI	0	000	000	000	000	000	000	000	000	000	000	0	000
MAUI	0	0	0	0	0	0	0	0	0	0	0	0	000
KOKOBU	0	0	0	0	0	0	0	0	0	0	0	0	000
NI COSI	0	0	0	0	0	0	0	0	0	0	0	0	000
AS HKHA	0	0	0	0	0	0	0	0	0	0	0	0	000
VANDEN	0	0	0	0	0	0	0	0	0	0	0	0	000
ALMA A	0	0	0	0	0	0	0	0	0	0	0	0	000
POITIE	0	0	0	0	0	0	0	0	0	0	0	0	000
BOULDE	0	0	0	0	0	0	0	0	0	0	0	0	000
WALLOP	0	0	0	0	0	0	0	0	0	0	0	0	000
KIEV	0	0	0	0	0	0	0	0	0	0	0	0	000
IRKUTS	0	0	0	0	0	0	0	0	0	0	0	0	000
MOSCOW	0	0	0	0	0	0	0	0	0	0	0	0	000
DOURBE	6	6	6	6	6	6	6	0	0	0	0	0	000
ALOUGH	0	0	0	0	0	0	0	0	0	0	0	0	000
AGAGADA	0	0	0	0	0	0	0	0	0	0	0	0	000
OT TAWA	0	0	0	0	0	0	0	0	0	0	0	0	000
SVERDL	0	0	0	0	0	0	0	0	0	0	0	0	000
TO MSK	0	0	0	0	0	0	0	0	0	0	0	0	000
GOOSE	0	0	0	0	0	0	0	0	0	0	0	0	000
YAKUTS	0	0	0	0	0	0	0	0	0	0	0	0	000
COLLEG	0	0	0	0	0	0	0	0	0	0	0	0	000
CAPE S	0	0	0	0	0	0	0	0	0	0	0	0	000
MIRMAN	0	0	0	0	0	0	0	0	0	0	0	0	000
CHIUCH	0	0	0	0	0	0	0	0	0	0	0	0	000
NAPSSA	0	0	0	0	0	0	0	0	0	0	0	0	000
SALEKH	0	0	0	0	0	0	0	0	0	0	0	0	000
KRENKE	0	0	0	0	0	0	0	0	0	0	0	0	000
GO DHAV	0	0	0	0	0	0	0	0	0	0	0	0	000
RE SOLU	0	0	0	0	0	0	0	0	0	0	0	0	000
QIANQ	0	0	0	0	0	0	0	0	0	0	0	0	000
MANILA	122	137	147	157	167	177	187	197	207	217	227	237	0
TAIPEI	6	6	6	8	6	8	6	6	6	6	0	0	0
MAUI	0	0	0	0	0	0	0	0	0	0	0	0	0
KOKOBU	0	0	0	0	0	0	0	0	0	0	0	0	0
NI COSI	0	0	0	0	0	0	0	0	0	0	0	0	0
AS HKHA	0	0	0	0	0	0	0	0	0	0	0	0	0
VANDEN	0	0	0	0	0	0	0	0	0	0	0	0	0
ALMA A	0	0	0	0	0	0	0	0	0	0	0	0	0
POITIE	0	0	0	0	0	0	0	0	0	0	0	0	0
BOULDE	0	0	0	0	0	0	0	0	0	0	0	0	0
WALLOP	0	0	0	0	0	0	0	0	0	0	0	0	0
KIEV	0	0	0	0	0	0	0	0	0	0	0	0	0
IRKUTS	0	0	0	0	0	0	0	0	0	0	0	0	0
MOSCOW	0	0	0	0	0	0	0	0	0	0	0	0	0
DOURBE	0	0	0	0	0	0	0	0	0	0	0	0	0
ALOUGH	0	0	0	0	0	0	0	0	0	0	0	0	0
AGAGADA	0	0	0	0	0	0	0	0	0	0	0	0	0
OT TAWA	0	0	0	0	0	0	0	0	0	0	0	0	0
SVERDL	0	0	0	0	0	0	0	0	0	0	0	0	0
TO MSK	0	0	0	0	0	0	0	0	0	0	0	0	0
GOOSE	0	0	0	0	0	0	0	0	0	0	0	0	0
YAKUTS	0	0	0	0	0	0	0	0	0	0	0	0	0
COLLEG	0	0	0	0	0	0	0	0	0	0	0	0	0
CAPE S	0	0	0	0	0	0	0	0	0	0	0	0	0
MIRMAN	0	0	0	0	0	0	0	0	0	0	0	0	0
CHIUCH	0	0	0	0	0	0	0	0	0	0	0	0	0
NAPSSA	0	0	0	0	0	0	0	0	0	0	0	0	0
SALEKH	0	0	0	0	0	0	0	0	0	0	0	0	0
KRENKE	0	0	0	0	0	0	0	0	0	0	0	0	0
GO DHAV	0	0	0	0	0	0	0	0	0	0	0	0	0
RE SOLU	0	0	0	0	0	0	0	0	0	0	0	0	0
QIANQ	0	0	0	0	0	0	0	0	0	0	0	0	0

Figure 35g. Ionospheric sounder data for 20 September 1979.

QSL AL	002	21	SEP	017	022	037	047	057	067	077	087	097	107	117
MANILA	0	002	000	000	000	000	000	000	000	000	000	000	000	000
TAIPEI	0	000	000	000	000	000	000	000	000	000	000	000	000	000
MAUI	0	000	000	000	000	000	000	000	000	000	000	000	000	000
NIKOSI	0	000	000	000	000	000	000	000	000	000	000	000	000	000
ASIAKH	0	000	000	000	000	000	000	000	000	000	000	000	000	000
VANDEN	0	000	000	000	000	000	000	000	000	000	000	000	000	000
ALMAA	0	000	000	000	000	000	000	000	000	000	000	000	000	000
POITIE	0	000	000	000	000	000	000	000	000	000	000	000	000	000
BOULDE	0	000	000	000	000	000	000	000	000	000	000	000	000	000
WALLOP	0	000	000	000	000	000	000	000	000	000	000	000	000	000
KIEV	0	000	000	000	000	000	000	000	000	000	000	000	000	000
IRKUTS	0	000	000	000	000	000	000	000	000	000	000	000	000	000
MOSCOW	0	000	000	000	000	000	000	000	000	000	000	000	000	000
DOLURBE	0	000	000	000	000	000	000	000	000	000	000	000	000	000
ELDUGH	0	000	000	000	000	000	000	000	000	000	000	000	000	000
MAGADA	0	000	000	000	000	000	000	000	000	000	000	000	000	000
OT TAWA	0	000	000	000	000	000	000	000	000	000	000	000	000	000
SVERDL	0	000	000	000	000	000	000	000	000	000	000	000	000	000
TO MSK	0	000	000	000	000	000	000	000	000	000	000	000	000	000
GOOSE	0	000	000	000	000	000	000	000	000	000	000	000	000	000
YAKUTS	0	000	000	000	000	000	000	000	000	000	000	000	000	000
COLLEG	0	000	000	000	000	000	000	000	000	000	000	000	000	000
CAPE	0	000	000	000	000	000	000	000	000	000	000	000	000	000
MURMAN	0	000	000	000	000	000	000	000	000	000	000	000	000	000
NASSA	0	000	000	000	000	000	000	000	000	000	000	000	000	000
SALEKH	0	000	000	000	000	000	000	000	000	000	000	000	000	000
KRENKE	0	000	000	000	000	000	000	000	000	000	000	000	000	000
GO DHAV	0	000	000	000	000	000	000	000	000	000	000	000	000	000
RE SOLU	0	000	000	000	000	000	000	000	000	000	000	000	000	000
	122	137	142	157	162	177	187	197	207	217	227	237	247	257
MANILA	0	000	000	000	000	000	000	000	000	000	000	000	000	000
TAIPEI	0	000	000	000	000	000	000	000	000	000	000	000	000	000
MAUI	0	000	000	000	000	000	000	000	000	000	000	000	000	000
NIKOSI	0	000	000	000	000	000	000	000	000	000	000	000	000	000
VANDEN	0	000	000	000	000	000	000	000	000	000	000	000	000	000
ALMAA	0	000	000	000	000	000	000	000	000	000	000	000	000	000
BOULDE	0	000	000	000	000	000	000	000	000	000	000	000	000	000
WALLOP	0	000	000	000	000	000	000	000	000	000	000	000	000	000
IRKUTS	0	000	000	000	000	000	000	000	000	000	000	000	000	000
MOSCOW	0	000	000	000	000	000	000	000	000	000	000	000	000	000
DOLURBE	0	000	000	000	000	000	000	000	000	000	000	000	000	000
OT TAWA	0	000	000	000	000	000	000	000	000	000	000	000	000	000
GOOSE	0	000	000	000	000	000	000	000	000	000	000	000	000	000
COLLEG	0	000	000	000	000	000	000	000	000	000	000	000	000	000
CAPE	0	000	000	000	000	000	000	000	000	000	000	000	000	000
CHURCH	0	000	000	000	000	000	000	000	000	000	000	000	000	000
NASSA	0	000	000	000	000	000	000	000	000	000	000	000	000	000
GO DHAV	0	000	000	000	000	000	000	000	000	000	000	000	000	000
RE SOLU	0	000	000	000	000	000	000	000	000	000	000	000	000	000

Figure 35h. Ionospheric sounder data for 21 September 1979.

during the second half of the Zulu day when more sunlight is present and an absence of absorption reports in the Western Hemisphere during the first half of the day. The opposite situation exists for the Asian sector where sporadic absorption is observed during the first half of the day. By 18/0900Z nearly the entire polar cap is affected by the PCA, but this is relatively short-lived, and by 18/1800Z the PCA starts to become patchy once again. The general pattern of absorption being reported by high latitude stations in the daylight sector only is resumed. The absorption occurrence become more sporadic until the last sign of the PCA is observed near 21/1600Z. This type of PCA event is characteristic of relatively small proton events and is difficult to analyse in realtime.

#### Case 2

This PCA occurred during 06-09 June 1979. Figure 36 shows a list of hourly Thule 30 MHz riometer readings. The first indication of absorption shows up between 0900-1000Z on 6 June. The absorption values increase gradually and finally exceed the daytime PCA threshold of 2.0 decibels at 06/2300Z. The peak value of 5.9 db is reached several hours later at 07/0215Z. The PCA gradually decays to less than 2.0 db by 07/1600Z, but significant absorption persists for nearly 24 hours. The absorption continues to decline and reaches pre-event levels near 09/1900Z. In Figure 37 a-d, the high latitude absorption (qualifier 2) recorded by the ionospheric sounder begins near 06/2000Z and spreads rapidly to encompass the entire polar cap. While some auroral zone absorption persists through 9 June, the PCA has ended by 08/1900Z Jun.

#### Case 3

This PCA event covers the period 19-23 August 1979 (Figures 38a-e). During the first half of the Zulu day, on the 19th, several features are present in the high latitude ionosphere. Blanketing E (qualifier 1) and absorption (qualifier 2) are present at the auroral zone latitudes associated with moderate geomagnetic substorm activity (3 hourly  $a_p$  values  $\geq 30$ ). Goose Bay and Murmansk are good examples of stations exhibiting Blanketing E occurrence. The "2" qualifier is identifiable as auroral zone absorption (AZA) only through its location and the correlation of auroral and geomagnetic activity. While the polar stations such as Godhavn and Resolute Bay are dominated by Spread F conditions early in the day, "2" qualifiers are observed as early as 19/0900Z. The absorption qualifiers at these stations signal the onset of the PCA event. The absorption persists at Godhavn and Resolute Bay and also appears at Narsarauak, Greenland as the daytime ionosphere sweeps over Greenland and North America. Note the absorption values at College, Alaska during the latter part of the 19th. The distinction between the occurrence of AZA or PCA is not possible here because AZA would be common at this time of day during geomagnetic substorm activity. This fact, combined with the lack of absorption at Churchill and the occurrence of Blanketing E at Murmansk, indicate the auroral ionosphere is still dominated by substorm effects rather than the PCA. During 20-21 August, the PCA and geomagnetic substorm activity (see Figure 39) both affect the high latitude ionosphere. The absorption from the PCA dominates, but occasional reports of Blanketing E (qualifier 1) are also present. By early on 22 August the PCA shows some sign of breaking up as Spread F reports (qualifier 6) again show up in the polar regions. By midday the absorption reports have diminished considerably, and by 23/0100Z the PCA has ended.

Thule 30 MHz Riometer Absorption (decibels)

<u>Time (Z)</u>	<u>06 Jun 1979</u>	<u>07 Jun</u>	<u>08 Jun</u>	<u>09 Jun</u>
0000	0.0	3.4	1.3	0.3
0100	0.0	4.7	1.3	0.2
0200	0.0	5.5	1.1	0.2
0300	0.0	4.8	1.1	0.2
0400	0.0	4.2	1.1	0.2
0500	0.0	3.7	1.0	0.2
0600	0.0	4.1	0.9	0.1
0700	0.0	3.7	0.8	0.1
0800	0.0	3.7	0.7	0.1
0900	0.0	3.6	0.7	0.1
1000	0.1	3.5	0.7	0.1
1100	0.2	3.2	0.6	0.0
1200	0.1	2.9	—	0.0
1300	0.1	2.4	—	0.1
1400	0.1	2.1	0.5	0.0
1500	0.2	1.9	0.5	0.1
1600	0.2	1.8	0.6	0.1
1700	—	1.9	0.4	0.0
1800	—	1.9	0.4	0.1
1900	1.7	—	0.4	0.0
2000	1.3	1.9	0.5	0.0
2100	—	1.7	0.4	0.0
2200	—	1.6	0.3	0.0
2300	2.2	1.4	0.3	0.0

Figure 36. Thule 30 MHz riometer absorption during the period 06-09 June 1979.

06 Jun	Station	00Z	01Z	02Z	03Z	04Z	05Z	06Z	07Z	08Z	09Z	10Z	11Z	12Z
	Goose Bay	0	0	6	6	6	6	6	6	6	6	6	6	6
	College	9	3	8	0	0	0	0	3	0	8	6	4	4
	Cape Schmidt	0	0	0	0	0	0	0	0	0	0	0	6	6
	Murmansk	0	0	0	0	0	0	0	0	0	0	0	0	0
	Churchill													
	Narssarsuaq													
	Sallékhárdt													
	Dixon													
	Krenkel													
	Godhavn													
	Resolute													
	Qaraq													
	Goose Bay													
	College	2	1	1	1	1	1	1	1	1	9	0	0	2
	Cape Schmidt	2	1	1	1	1	1	1	1	1	6	0	0	2
	Murmansk	0	0	0	0	0	0	0	0	0	0	0	0	2
	Churchill													
	Narssarsuaq													
	Sallékhárdt													
	Dixon													
	Krenkel													
	Godhavn													
	Resolute													
	Qaraq													

Figure 37a. High latitude ionospheric sounder observations (qualifiers)  
for 06 June 1979.

07 Jun

<u>Station</u>	<u>00Z</u>	<u>01Z</u>	<u>02Z</u>	<u>03Z</u>	<u>04Z</u>	<u>05Z</u>	<u>06Z</u>	<u>07Z</u>	<u>08Z</u>	<u>09Z</u>	<u>10Z</u>	<u>11Z</u>	<u>12Z</u>
Goose Bay	2	2	2	2	2	2	2	2	2	2	2	2	0
College	2	2	2	2	2	2	2	2	2	2	2	2	2
Cape Schmidt	0	2	2	2	2	2	2	2	2	2	2	2	2
Murmansk	2	2	0	2	2	2	2	2	2	2	2	2	2
Churchill	2	2	2	0	2	2	2	2	2	2	2	2	2
Narssarsuaq	2	2	2	2	2	2	2	2	2	2	2	2	2
Salekhardt	0	2	2	2	2	2	2	2	2	2	2	2	0
Dixon	2	2	2	2	2	2	2	2	2	2	2	2	2
Krenkel	2	2	2	2	2	2	2	2	2	2	2	2	2
Godhavn	2	2	2	2	2	2	2	2	2	2	2	2	2
Resolute	2	2	2	2	2	2	2	2	2	2	2	2	2
Quang	2	2	2	2	2	2	2	2	2	2	2	2	2
	<u>13Z</u>	<u>14Z</u>	<u>15Z</u>	<u>16Z</u>	<u>17Z</u>	<u>18Z</u>	<u>19Z</u>	<u>20Z</u>	<u>21Z</u>	<u>22Z</u>	<u>23Z</u>		
Goose Bay	2	2	0	2	2	2	2	2	2	0	0	0	0
College	2	2	2	2	2	2	2	2	2	2	2	2	2
Cape Schmidt	2	2	2	2	2	2	2	2	2	2	2	2	2
Murmansk	2	2	2	2	2	2	2	2	2	2	2	2	2
Churchill	2	2	2	2	2	2	2	2	2	0	1	2	2
Narssarsuaq	2	2	2	2	2	2	2	2	2	0	2	2	2
Salekhardt	0	2	0	2	2	2	2	2	2	0	1	2	2
Dixon	2	2	2	2	2	2	2	2	2	2	2	2	2
Krenkel	2	2	2	2	2	2	2	2	2	2	2	2	2
Godhavn	2	2	2	2	2	2	2	2	2	2	2	2	2
Resolute	2	2	2	2	2	2	2	2	2	2	2	2	2
Quang	2	2	2	2	2	2	2	2	2	2	2	2	2

Figure 37b. High latitude ionospheric sounder observations (qualifiers)  
for 07 June 1979.

08 Jun

Station	<u>00Z</u>	<u>01Z</u>	<u>02Z</u>	<u>03Z</u>	<u>04Z</u>	<u>05Z</u>	<u>06Z</u>	<u>07Z</u>	<u>08Z</u>	<u>09Z</u>	<u>10Z</u>	<u>11Z</u>	<u>12Z</u>
Goose Bay	0	6	1	6	6	6	6	6	6	6	6	0	6
College	2	2	2	2	2	2	2	2	2	2	2	2	2
Cape Schmidt	2	0	2	0	0	0	0	0	0	0	0	0	0
Murmansk	2	0	2	0	0	0	0	0	0	0	0	0	0
Churchill													
Narsarsuak													
Salekhardt	0	0	2	2	2	2	2	2	2	2	2	2	0
Dixon	2	2	2	2	2	2	2	2	2	2	2	2	2
Krenkel	2	2	2	2	2	2	2	2	2	2	2	2	2
Godhavn	2	2	2	2	2	2	2	2	2	2	2	2	2
Resolute	2	2	2	2	2	2	2	2	2	2	2	2	2
Quaq	2	2	2	2	2	2	2	2	2	2	2	2	2
	<u>13Z</u>	<u>14Z</u>	<u>15Z</u>	<u>16Z</u>	<u>17Z</u>	<u>18Z</u>	<u>19Z</u>	<u>20Z</u>	<u>21Z</u>	<u>22Z</u>	<u>23Z</u>		
Goose Bay	0	0	6	6	6	6	6	6	6	6	6	0	6
College	2	2	2	2	2	2	2	2	2	2	2	2	2
Cape Schmidt	0	0	0	0	0	0	0	0	0	0	0	0	0
Murmansk	0	0	0	0	0	0	0	0	0	0	0	0	0
Churchill													
Narsarsuak													
Salekhardt	0	0	0	0	0	0	0	0	0	0	0	0	0
Dixon	2	2	2	2	2	2	2	2	2	2	2	2	2
Krenkel	2	2	2	2	2	2	2	2	2	2	2	2	2
Godhavn	2	2	2	2	2	2	2	2	2	2	2	2	2
Resolute	2	2	2	2	2	2	2	2	2	2	2	2	2
Quaq	2	2	2	2	2	2	2	2	2	2	2	2	2

Figure 37c. High latitude ionospheric sounder observations (qualifiers)  
for 08 June 1979.

<u>09 Jun</u>	<u>00Z</u>	<u>01Z</u>	<u>02Z</u>	<u>03Z</u>	<u>04Z</u>	<u>05Z</u>	<u>06Z</u>	<u>07Z</u>	<u>08Z</u>	<u>09Z</u>	<u>10Z</u>	<u>11Z</u>	<u>12Z</u>
<u>Station</u>													
Goose Bay	6	6	6	6	6	6	6	6	6	6	6	6	6
College	2	2	0	0	0	0	0	0	0	0	0	0	0
Cape Schmidt	0	0	0	0	0	0	0	7	7	7	7	7	7
Murmanik	0	0	0	0	0	0	0	0	0	0	0	0	0
Churchill	0	0	0	0	0	0	0	0	0	0	0	0	0
Narsarsuak	0	0	0	0	0	0	0	0	0	0	0	0	0
Salekhardt	0	0	0	0	0	0	0	0	0	0	0	0	0
Dixon	0	2	0	0	0	0	0	6	6	6	6	6	6
Krenkel	6	0	6	6	6	6	6	6	6	6	6	6	6
Godhavn	6	6	6	6	6	6	6	6	6	6	6	6	6
Resolute	6	6	9	6	6	6	6	7	6	7	7	7	7
Quang	6	6	6	9	6	6	6	6	6	6	6	6	6
	<u>13Z</u>	<u>14Z</u>	<u>15Z</u>	<u>16Z</u>	<u>17Z</u>	<u>18Z</u>	<u>19Z</u>	<u>20Z</u>	<u>21Z</u>	<u>22Z</u>	<u>23Z</u>		
Goose Bay	0	0	0	6	0	6	6	6	0	6	6	6	6
College	2	2	1	2	2	2	2	2	2	2	2	2	2
Cape Schmidt	6	6	0	0	0	0	0	0	0	0	0	0	0
Murmanik	9	9	0	0	0	0	0	0	0	1	1	1	1
Churchill	0	0	0	2	0	0	0	0	0	0	0	0	0
Narsarsuak	0	0	0	0	1	1	0	0	0	0	0	0	0
Salekhardt	0	0	0	0	0	0	0	0	0	0	0	0	0
Dixon	0	0	0	0	0	0	0	0	0	0	0	0	0
Krenkel	6	6	6	6	6	6	6	6	6	6	6	6	6
Godhavn	6	6	6	6	6	6	6	6	6	6	6	6	6
Resolute	7	6	6	7	6	7	7	7	6	7	6	6	6
Quang	7	6	6	7	6	7	7	7	6	7	6	6	6

169-

Figure 37d. High latitude ionospheric sounder observations (qualifiers)  
for 09 June 1979.

Figure 38a. Ionospheric sounder observations (qualifiers) for 19 August 1979.

QUAL	20 AUG												10Z	12Z	13Z	14Z
MANILA	007	017	027	037	047	057	067	077	087	097	107	117	000	000	000	000
TAIPEI	000	000	000	000	000	000	000	000	000	000	000	000	000	000	000	000
MAUI	000	000	000	000	000	000	000	000	000	000	000	000	000	000	000	000
KOKOBU	000	000	000	000	000	000	000	000	000	000	000	000	000	000	000	000
NIOSI	000	000	000	000	000	000	000	000	000	000	000	000	000	000	000	000
ASHKHA	000	000	000	000	000	000	000	000	000	000	000	000	000	000	000	000
VANDEN	000	000	000	000	000	000	000	000	000	000	000	000	000	000	000	000
ALMAA	000	000	000	000	000	000	000	000	000	000	000	000	000	000	000	000
POITIE	000	000	000	000	000	000	000	000	000	000	000	000	000	000	000	000
BOULDE	000	000	000	000	000	000	000	000	000	000	000	000	000	000	000	000
WALLOP	000	000	000	000	000	000	000	000	000	000	000	000	000	000	000	000
KIEV	000	000	000	000	000	000	000	000	000	000	000	000	000	000	000	000
IRKUTS	000	000	000	000	000	000	000	000	000	000	000	000	000	000	000	000
MOSCOW	000	000	000	000	000	000	000	000	000	000	000	000	000	000	000	000
DOURBE	000	000	000	000	000	000	000	000	000	000	000	000	000	000	000	000
SLUGH	000	000	000	000	000	000	000	000	000	000	000	000	000	000	000	000
MAGADA	000	000	000	000	000	000	000	000	000	000	000	000	000	000	000	000
SVERDL	000	000	000	000	000	000	000	000	000	000	000	000	000	000	000	000
TOISK	000	000	000	000	000	000	000	000	000	000	000	000	000	000	000	000
OTAWA	000	000	000	000	000	000	000	000	000	000	000	000	000	000	000	000
CHURCH	000	000	000	000	000	000	000	000	000	000	000	000	000	000	000	000
NARSIA	000	000	000	000	000	000	000	000	000	000	000	000	000	000	000	000
SALEKH	000	000	000	000	000	000	000	000	000	000	000	000	000	000	000	000
GODHAW	000	000	000	000	000	000	000	000	000	000	000	000	000	000	000	000
RECOLU	000	000	000	000	000	000	000	000	000	000	000	000	000	000	000	000
MANILA	127	137	147	157	167	177	187	197	207	217	227	237	000	000	000	000
TAIPEI	6	6	6	6	6	6	6	6	6	6	6	6	000	000	000	000
MAUI	000	000	000	000	000	000	000	000	000	000	000	000	000	000	000	000
KOKOBU	000	000	000	000	000	000	000	000	000	000	000	000	000	000	000	000
NIOSI	000	000	000	000	000	000	000	000	000	000	000	000	000	000	000	000
ASHKHA	000	000	000	000	000	000	000	000	000	000	000	000	000	000	000	000
VANDEN	000	000	000	000	000	000	000	000	000	000	000	000	000	000	000	000
ALMAA	000	000	000	000	000	000	000	000	000	000	000	000	000	000	000	000
POITIE	000	000	000	000	000	000	000	000	000	000	000	000	000	000	000	000
BOULDE	000	000	000	000	000	000	000	000	000	000	000	000	000	000	000	000
WALLOP	000	000	000	000	000	000	000	000	000	000	000	000	000	000	000	000
KIEV	000	000	000	000	000	000	000	000	000	000	000	000	000	000	000	000
IRKUTS	000	000	000	000	000	000	000	000	000	000	000	000	000	000	000	000
MOSCOW	000	000	000	000	000	000	000	000	000	000	000	000	000	000	000	000
DOURBE	000	000	000	000	000	000	000	000	000	000	000	000	000	000	000	000
SLUGH	000	000	000	000	000	000	000	000	000	000	000	000	000	000	000	000
MAGADA	000	000	000	000	000	000	000	000	000	000	000	000	000	000	000	000
SVERDL	000	000	000	000	000	000	000	000	000	000	000	000	000	000	000	000
TOISK	000	000	000	000	000	000	000	000	000	000	000	000	000	000	000	000
OTAWA	000	000	000	000	000	000	000	000	000	000	000	000	000	000	000	000
CHURCH	000	000	000	000	000	000	000	000	000	000	000	000	000	000	000	000
NARSIA	000	000	000	000	000	000	000	000	000	000	000	000	000	000	000	000
SALEKH	000	000	000	000	000	000	000	000	000	000	000	000	000	000	000	000
GODHAW	000	000	000	000	000	000	000	000	000	000	000	000	000	000	000	000
RECOLU	000	000	000	000	000	000	000	000	000	000	000	000	000	000	000	000

Figure 38b. Ionospheric sounder observations (qualifiers) for 20 August 1979.

QUAL	21 AUG												10Z	11Z
MANILA	002	012	022	032	042	052	062	072	082	092	102	112	0000	0000
TAIPEI	000	000	000	000	000	000	000	000	000	000	000	000	3	0
MAUI	000	000	000	000	000	000	000	000	000	000	000	000	000	0
KOKOBU	000	000	000	000	000	000	000	000	000	000	000	000	000	0
NIKOSI	000	000	000	000	000	000	000	000	000	000	000	000	000	0
AKHCHA	000	000	000	000	000	000	000	000	000	000	000	000	000	0
VANDEN	000	000	000	000	000	000	000	000	000	000	000	000	000	0
ALMAA	000	000	000	000	000	000	000	000	000	000	000	000	000	0
POITIE	000	000	000	000	000	000	000	000	000	000	000	000	000	0
BOULDE	000	000	000	000	000	000	000	000	000	000	000	000	000	0
WALLOP	000	000	000	000	000	000	000	000	000	000	000	000	000	0
KIEV	000	000	000	000	000	000	000	000	000	000	000	000	000	0
IRKUTS	000	000	000	000	000	000	000	000	000	000	000	000	000	0
MOSCOW	000	000	000	000	000	000	000	000	000	000	000	000	000	0
BOURBE	000	000	000	000	000	000	000	000	000	000	000	000	000	0
QLOUGH	000	000	000	000	000	000	000	000	000	000	000	000	000	0
MAGADA	000	000	000	000	000	000	000	000	000	000	000	000	000	0
OTAWA	000	000	000	000	000	000	000	000	000	000	000	000	000	0
SVERDL	000	000	000	000	000	000	000	000	000	000	000	000	000	0
TOMSK	000	000	000	000	000	000	000	000	000	000	000	000	000	0
GOOSE	000	000	000	000	000	000	000	000	000	000	000	000	000	0
YAKUTS	000	000	000	000	000	000	000	000	000	000	000	000	000	0
COLLEG	000	000	000	000	000	000	000	000	000	000	000	000	000	0
CAPES	000	000	000	000	000	000	000	000	000	000	000	000	000	0
MURMAN	000	000	000	000	000	000	000	000	000	000	000	000	000	0
CHIUCH	000	000	000	000	000	000	000	000	000	000	000	000	000	0
NAPSSA	000	000	000	000	000	000	000	000	000	000	000	000	000	0
SALEKH	000	000	000	000	000	000	000	000	000	000	000	000	000	0
KRENKE	000	000	000	000	000	000	000	000	000	000	000	000	000	0
GOOHA	000	000	000	000	000	000	000	000	000	000	000	000	000	0
RESOLU	000	000	000	000	000	000	000	000	000	000	000	000	000	0
	122	137	147	152	167	177	182	192	207	217	222	232	0000	0000
MANILA	8	8	8	8	0	0	0	0	0	0	0	0	0000	0000
TAIPEI	0	0	0	0	0	0	0	0	0	0	0	0	0000	0000
MAUI	6	0	0	0	0	0	0	0	0	0	0	0	0000	0000
KOKOBU	0	0	0	0	0	0	0	0	0	0	0	0	0000	0000
NIKOSI	0	0	0	0	0	0	0	0	0	0	0	0	0000	0000
VANDEN	0	0	0	0	0	0	0	0	0	0	0	0	0000	0000
ALMAA	0	0	0	0	0	0	0	0	0	0	0	0	0000	0000
POITIE	0	0	0	0	0	0	0	0	0	0	0	0	0000	0000
BOULDE	0	0	0	0	0	0	0	0	0	0	0	0	0000	0000
WALLOP	0	0	0	0	0	0	0	0	0	0	0	0	0000	0000
KIEV	0	0	0	0	0	0	0	0	0	0	0	0	0000	0000
IRKUTS	0	0	0	0	0	0	0	0	0	0	0	0	0000	0000
MOSCOW	0	0	0	0	0	0	0	0	0	0	0	0	0000	0000
BOURBE	0	0	0	0	0	0	0	0	0	0	0	0	0000	0000
QLOUGH	0	0	0	0	0	0	0	0	0	0	0	0	0000	0000
MAGADA	0	0	0	0	0	0	0	0	0	0	0	0	0000	0000
OTAWA	0	0	0	0	0	0	0	0	0	0	0	0	0000	0000
SVERDL	0	0	0	0	0	0	0	0	0	0	0	0	0000	0000
TOMSK	0	0	0	0	0	0	0	0	0	0	0	0	0000	0000
GOOSE	0	0	0	0	0	0	0	0	0	0	0	0	0000	0000
YAKUTS	0	0	0	0	0	0	0	0	0	0	0	0	0000	0000
COLLEG	0	0	0	0	0	0	0	0	0	0	0	0	0000	0000
CAPES	0	0	0	0	0	0	0	0	0	0	0	0	0000	0000
MURMAN	0	0	0	0	0	0	0	0	0	0	0	0	0000	0000
CHIUCH	0	0	0	0	0	0	0	0	0	0	0	0	0000	0000
NAPSSA	0	0	0	0	0	0	0	0	0	0	0	0	0000	0000
SALEKH	0	0	0	0	0	0	0	0	0	0	0	0	0000	0000
KRENKE	0	0	0	0	0	0	0	0	0	0	0	0	0000	0000
GOOHA	0	0	0	0	0	0	0	0	0	0	0	0	0000	0000
RESOLU	0	0	0	0	0	0	0	0	0	0	0	0	0000	0000

Figure 38c. Ionospheric sounder observations (qualifiers) for 21 August 1979.

QUAL	22 AUG												107	117
MANILA	007	012	017	022	027	032	047	052	062	077	087	097	107	000
TAIPEI	000	000	000	000	000	000	000	000	000	000	000	000	000	000
MAUI	000	000	000	000	000	000	000	000	000	000	000	000	000	000
KOKOBU	000	000	000	000	000	000	000	000	000	000	000	000	000	000
NI COSI	000	000	000	000	000	000	000	000	000	000	000	000	000	000
ASHKHA	000	000	000	000	000	000	000	000	000	000	000	000	000	000
VANDEN	000	000	000	000	000	000	000	000	000	000	000	000	000	000
ALMAA	000	000	000	000	000	000	000	000	000	000	000	000	000	000
POITIE	000	000	000	000	000	000	000	000	000	000	000	000	000	000
KHABAR	000	000	000	000	000	000	000	000	000	000	000	000	000	000
BOULDE	000	000	000	000	000	000	000	000	000	000	000	000	000	000
WALLOP	000	000	000	000	000	000	000	000	000	000	000	000	000	000
KIEV	000	000	000	000	000	000	000	000	000	000	000	000	000	000
IRKUTS	000	000	000	000	000	000	000	000	000	000	000	000	000	000
MOSCOW	000	000	000	000	000	000	000	000	000	000	000	000	000	000
DOURBE	000	000	000	000	000	000	000	000	000	000	000	000	000	000
PLUGH	000	000	000	000	000	000	000	000	000	000	000	000	000	000
MAGADA	000	000	000	000	000	000	000	000	000	000	000	000	000	000
SVERDL	000	000	000	000	000	000	000	000	000	000	000	000	000	000
TMMSK	000	000	000	000	000	000	000	000	000	000	000	000	000	000
GOOSE	000	000	000	000	000	000	000	000	000	000	000	000	000	000
YAKUTS	000	000	000	000	000	000	000	000	000	000	000	000	000	000
COLLEG	000	000	000	000	000	000	000	000	000	000	000	000	000	000
CAPE S	000	000	000	000	000	000	000	000	000	000	000	000	000	000
MIRMAN	000	000	000	000	000	000	000	000	000	000	000	000	000	000
CHURCH	000	000	000	000	000	000	000	000	000	000	000	000	000	000
NAPSSA	000	000	000	000	000	000	000	000	000	000	000	000	000	000
SALEKH	000	000	000	000	000	000	000	000	000	000	000	000	000	000
DIXON	000	000	000	000	000	000	000	000	000	000	000	000	000	000
KRENKE	000	000	000	000	000	000	000	000	000	000	000	000	000	000
GODHAW	000	000	000	000	000	000	000	000	000	000	000	000	000	000
RESOLU	000	000	000	000	000	000	000	000	000	000	000	000	000	000
MANILA	127	132	142	147	152	167	172	187	192	207	217	227	237	237
TAIPEI	000	000	000	000	000	000	000	000	000	000	000	000	000	000
MAUI	000	000	000	000	000	000	000	000	000	000	000	000	000	000
KOKOBU	000	000	000	000	000	000	000	000	000	000	000	000	000	000
NI COSI	000	000	000	000	000	000	000	000	000	000	000	000	000	000
ASHKHA	000	000	000	000	000	000	000	000	000	000	000	000	000	000
VANDEN	000	000	000	000	000	000	000	000	000	000	000	000	000	000
ALMAA	000	000	000	000	000	000	000	000	000	000	000	000	000	000
POITIE	000	000	000	000	000	000	000	000	000	000	000	000	000	000
KHABAR	000	000	000	000	000	000	000	000	000	000	000	000	000	000
BOULDE	000	000	000	000	000	000	000	000	000	000	000	000	000	000
WALLOP	000	000	000	000	000	000	000	000	000	000	000	000	000	000
KIEV	000	000	000	000	000	000	000	000	000	000	000	000	000	000
IRKUTS	000	000	000	000	000	000	000	000	000	000	000	000	000	000
MOSCOW	000	000	000	000	000	000	000	000	000	000	000	000	000	000
DOURBE	000	000	000	000	000	000	000	000	000	000	000	000	000	000
PLUGH	000	000	000	000	000	000	000	000	000	000	000	000	000	000
MAGADA	000	000	000	000	000	000	000	000	000	000	000	000	000	000
SVERDL	000	000	000	000	000	000	000	000	000	000	000	000	000	000
TMMSK	000	000	000	000	000	000	000	000	000	000	000	000	000	000
GOOSE	000	000	000	000	000	000	000	000	000	000	000	000	000	000
YAKUTS	000	000	000	000	000	000	000	000	000	000	000	000	000	000
COLLEG	000	000	000	000	000	000	000	000	000	000	000	000	000	000
CAPE S	000	000	000	000	000	000	000	000	000	000	000	000	000	000
MIRMAN	000	000	000	000	000	000	000	000	000	000	000	000	000	000
CHURCH	000	000	000	000	000	000	000	000	000	000	000	000	000	000
NAPSSA	000	000	000	000	000	000	000	000	000	000	000	000	000	000
SALEKH	000	000	000	000	000	000	000	000	000	000	000	000	000	000
KRENKE	000	000	000	000	000	000	000	000	000	000	000	000	000	000
GODHAW	000	000	000	000	000	000	000	000	000	000	000	000	000	000
RESOLU	000	000	000	000	000	000	000	000	000	000	000	000	000	000

Figure 38d. Ionospheric sounder observations (qualifiers) for 22 August 1979.

QUAL	23 AUG	007	012	027	032	047	052	062	072	087	097	107	112
MANILA												000	000
TA IPEI												000	000
MAUI												000	000
KO KOBU												000	000
NI COSI												000	000
AS HKHA												000	000
VA NDEN												000	000
AL MA A												000	000
PO ITIE												000	000
KH AB AR												000	000
BOULDE												000	000
WALL OP												000	000
KI EV												000	000
IR KUTS												000	000
MOSCOW												000	000
DO UR BE												000	000
Q LOUGH												000	000
MA GADA												000	000
SV ER DL												000	000
TO MSK												000	000
GO OS E												000	000
YAKUTS												000	000
COLLEG												000	000
CA PE S												000	000
MIRMAN												000	000
CH URCH												000	000
NARSSA												000	000
SA LEKH												000	000
DI XON												000	000
KRENKE												000	000
RE SOLU												000	000
		127	132	142	152	162	172	18.2	192	202	212	222	232
MANILA												000	000
TA IPEI												000	000
MAUI												000	000
KO KOBU												000	000
NI COSI												000	000
AS HKHA												000	000
VA NDEN												000	000
AL MA A												000	000
PO ITIE												000	000
BOULDE												000	000
WALL OP												000	000
KI EV												000	000
IR KUTS												000	000
MOSCOW												000	000
DO UR BE												000	000
Q LOUGH												000	000
MA GADA												000	000
OT TAWA												000	000
SV ER DL												000	000
TO MSK												000	000
GO OS E												000	000
YAKUTS												000	000
COLLEG												000	000
CA PE S												000	000
MIRMAN												000	000
CH URCH												000	000
NARSSA												000	000
SA LEKH												000	000
DI XON												000	000
KRENKE												000	000
RE SOLU												000	000

Figure 38e. Ionospheric sounder observations (qualifiers) for 23 August 1979.

3-Hourly  $a_p$  (GWC specified)

<u>DATE</u>	<u>03Z</u>	<u>06Z</u>	<u>09Z</u>	<u>12Z</u>	<u>15Z</u>	<u>18Z</u>	<u>21Z</u>	<u>24Z</u>
19 Aug 79	58	44	34	36	21	23	14	20
20 Aug 79	13	10	16	12	16	68	79	19
21 Aug 79	57	39	39	26	15	16	22	9
22 Aug 79	14	21	16	14	13	18	10	8
23 Aug 79	6	3	7	8	10	14	10	8

Figure 39. Geomagnetic activity during the period 19 - 23 August 1979.

## MUF FORECASTING

Variations in the maximum usable frequency are dependent on changes in the critical frequency and reflection heights (or the scale factor  $M$  of the critical frequencies at MUF). For the short term forecast, MUF variations are expressed in percent of deviation from the median values. Using this approach, changes in MUFs can be approximated by changes in  $foF_2$  values. Only for large negative MUF deviations (greater than 20 percent) does a correction factor need be applied. In this instance the change in MUF is approximately 1.1 times the change in  $foF_2$ .

Changes in the critical frequency tend to preserve their sign and order of magnitude over a period of 3 to 4 hours in the middle latitudes. This is true during both quiet and disturbed conditions. At the higher latitudes, this period is reduced to 1 to 2 hours due to increased ionospheric variability, particularly in the auroral zone.

Thus, under generally quiet conditions,  $foF_2$ /MUF deviations at the middle latitudes can be predicted 3 to 4 hours in advance by extrapolation of observed values. By comparing the trend of the  $foF_2$  variations during the previous 3 to 4 hours, the predicted deviations can be moderated. For example, if the observed deviations were negative and the absolute values were increasing, a corresponding greater value of  $foF_2$ /MUF deviations would be forecast.

The spatial extent over which observed values can be extended is limited. Changes in  $foF_2$  will retain their sign and order of magnitude over a latitudinal distance of 5 to 10 degrees and a longitude distance of 15 to 20 degrees in the middle latitudes. At other latitudes the spatial extent is less. It is also less during disturbed ionospheric conditions. MUF forecasting during ionospheric storms will be discussed in the next section.

Another approach to MUF forecasting is to identify synoptic patterns from displays of  $foF_2$  variations. This can be done by identifying patterns either in local time or in different latitude and longitude regions, and extending them in time. This technique is applicable during undisturbed conditions. Application of such techniques in the equatorial region should be with caution.

MUF forecasting in the equatorial region is complicated by the so called equatorial anomaly. The anomaly region is located within roughly 20 degrees of the geomagnetic equator and is characterized by higher than normal  $foF_2$  values. The largest  $foF_2$  values are not found at the geomagnetic equator, but closer to 15 degrees geomagnetic latitude. In some parts of this region, the highest  $foF_2$  values are observed in the evening hours near 2000 local (figure 40). Large ionospheric gradients occur in the morning and postmidnight hours. In general, one can expect a high degree of variability combined with high daytime MUFs.

## IONOSPHERIC STORMS

The term "ionospheric storm" generally refers to disturbances that affect HF communication on a worldwide basis. In addition to the previously discussed effects associated with the expansion of the auroral oval, increased

15 JANUARY 1980

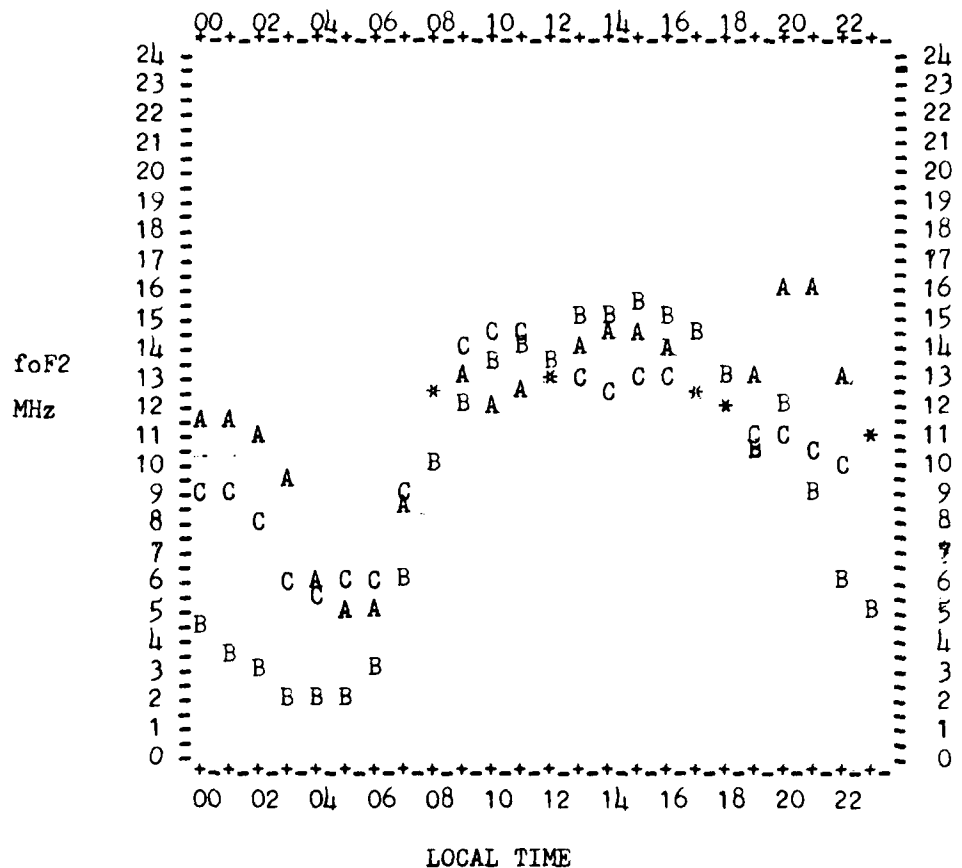


Figure 40. The local time variation of foF2 values at three low latitude stations.  
A = Taiwan B = Maui C = Manila

absorption, and Sporadic E occurrence; ionospheric storms are primarily described in terms of the changes in  $foF_2$ . Most ionospheric storms are associated with worldwide geomagnetic disturbances. The generalized effects on the range usable frequencies are shown in Figure 41. Briefly stated, these effects are a decrease in MUF and an enhancement in the LUF resulting in a narrow frequency window, particularly near local sunrise.

The storms sometimes appear unrelated to the severity of the geomagnetic disturbance and in some cases, rapid dropouts of the MUF (MUF crashes) occur on a large scale basis with no geomagnetic disturbances in progress. The storm characteristics are a function of latitude, season, and time of day. Occasionally, significant differences are observed between the Eastern and Western Hemispheres. Although each storm has its own individual characteristics, two types of storms have been classified on the basis of the behavior of  $foF_2$ . These are:

1. Negative storm. At middle latitudes, this type of storm is characterized by a relatively sharp increase in  $foF_2$  for several hours following the onset of the disturbance. This is followed by a significant and gradual decrease corresponding to the main phase onset of the disturbance. The identification of this main phase onset is important for determining  $foF_2$  variations. On the day side of the earth, the middle latitude decreases will initially be slight and have a limited duration. In the night sector,  $foF_2$  will show more severe and persistent decreases. As the storm progresses, the depressed  $foF_2$  area will expand into the morning and daytime sectors.

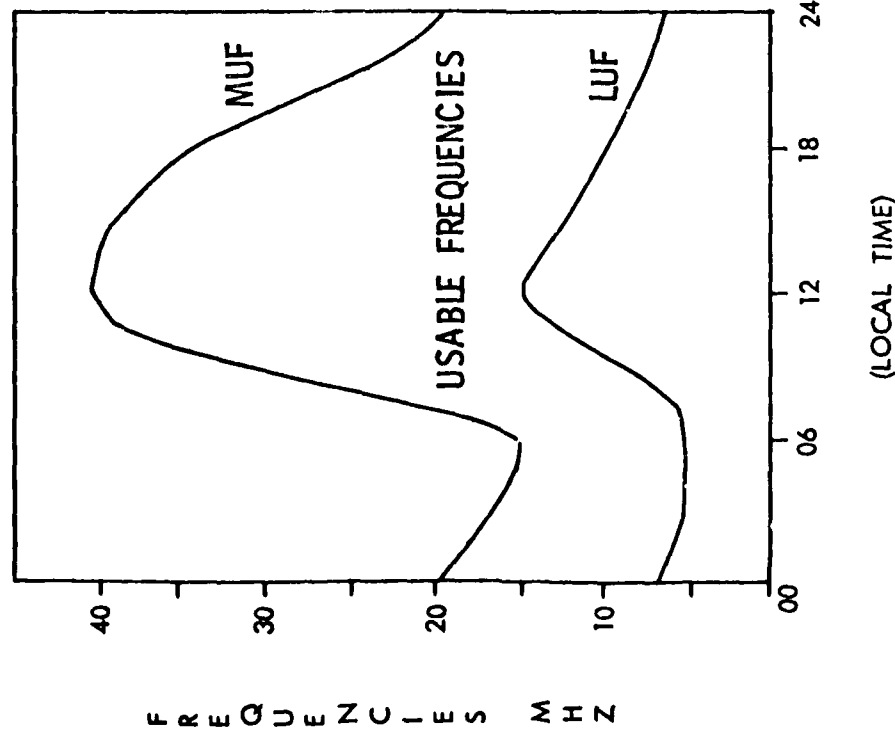
2. Positive storms. These disturbances are less frequent but occasionally occur at the middle and low latitudes during the winter.

Overall,  $foF_2$  variations during a storm can be described as follows:

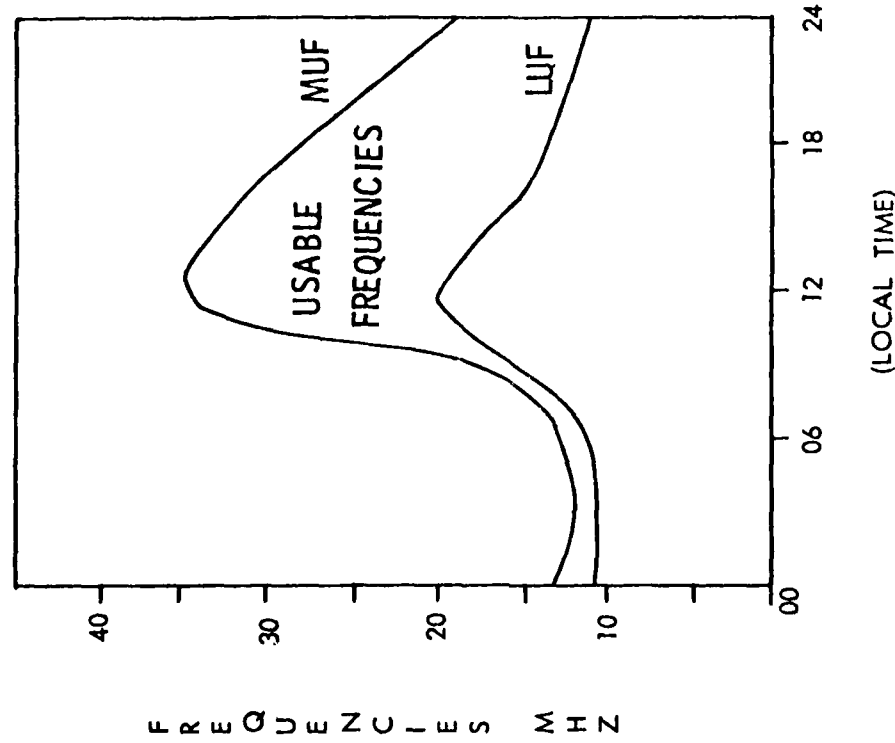
Geomagnetic Latitude	Hours After Storm Sudden Commencement	Percent Decrease		Local Time of Max	Max Decrease(%)
		During Hrs	After S.C.		
56 - 60	17 - 42	20%		14 - 22	30 - 50
50 - 55	10 - 41	20%		22 - 04	30 - 45
46 - 50	10 - 42	20%		01 - 07	30 - 45
40 - 45	19 - 55	10%		03 - 13	15 - 25
30 - 40	20 - 48	8%		03 - 13	15 - 20

Figure 42 illustrates the areas of maximum decrease by local time and latitude. Typical storm-time variations of  $foF_2$  are illustrated for strong ( $A_p \geq 50$ ) and weak ( $A_p < 50$ ) storms in Figure 43. When forecasting MUF deviations during an ionospheric storm, the percentage changes previously illustrated should be used depending upon the expected/observed severity of the geomagnetic disturbance. Generally, the larger decreases occur in the summer rather than the winter. Computer generated MUF deviations can be obtained in a few minutes for a given month, sunspot number, and K-index value (Figure 44). These should be the basis for MUF forecasts at the onset of the main phase of the storm. While the onset of the disturbance is usually

## HF RADIO PROPAGATION



## QUIET IONOSPHERIC CONDITIONS



## DISTURBED IONOSPHERIC CONDITIONS

Figure 41. Ionospheric storm effects on the range of usable HF frequencies.

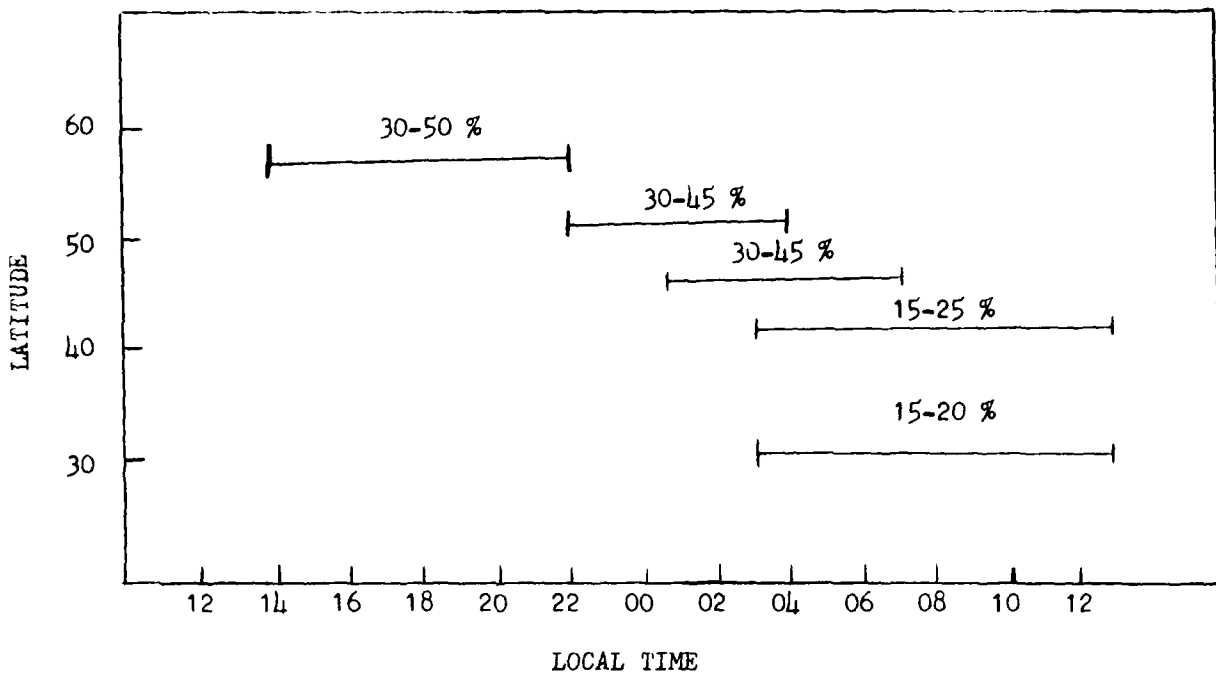


Figure 42. Time of peak foF2 depression during ionospheric storms.

## STORM-TIME foF2 DEVIATIONS

## foF2 Changes

## Equinox

21 Mar - 20 Jun

21 Sep - 20 Dec

Geomag	Strong ( $A_p \geq 50$ )											
Lat	6	12	18	24	30	36	42	48	54	60	66	72
45-62	10	-25	-30	-30	-25	-25	-15	-15	-15	-15	-15	-15
10-45	+5	+5	+5	+0	-5	-5	-5	-5	-5	-5	-5	+0
< 10	+0	+5	+5	+10	+10	+10	+10	+10	+5	+5	+10	+10

Geomag	Weak ( $A_p < 50$ )											
Lat	+10	+10	-5	-5	-5	-5	-5	-5	-5	-5	-5	-5
45-62	+5	+10	+10	+5	+5	+10	+10	+5	+0	+5	+5	+5
10-45	+10	+10	+0	+5	+10	+10	+10	+10	+10	+10	+10	+10

## Winter 21 Dec - 20 Mar

Geomag	Strong ( $A_p \geq 50$ )											
Lat	6	12	18	24	30	36	42	48	54	60	66	72
45-72	+0	-15	-20	-30	-25	-25	-25	-20	-20	-15	-15	-15
10-45	+0	+10	+10	+10	+10	+10	+10	+10	+10	+10	+5	+5
< 10	+0	+10	+10	+10	+10	+10	+10	+10	+5	+5	+5	+5

Geomag	Weak ( $A_p < 50$ )											
Lat	+5	+5	-15	-15	-10	-10	-10	-10	-10	-10	-10	-10
45-72	+5	+15	+20	+20	+20	+10	+10	+10	+10	+5	+5	+5
10-45	+10	+15	+20	+20	+20	+10	+10	+10	+10	+5	+5	+5
< 10	+5	+5	+5	+10	+10	+10	+10	+10	+0	+0	+0	+0

## Summer 21 Jun - 20 Sep

Geomag	Strong ( $A_p \geq 50$ )											
Lat	+5	-30	-40	-45	-45	-40	-30	-20	-20	-15	-15	-15
45-62	+10	-10	-20	-25	-30	-25	-20	-15	-15	-15	-10	-10
10-45	+0	+5	+5	+5	+10	+10	+10	+5	+5	+5	+5	+5

Geomag	Weak ( $A_p < 50$ )											
Lat	+5	-5	-20	-20	-20	-10	-10	-5	-5	-5	-5	-5
45-62	+5	+5	+0	+0	-10	-20	-10	-5	-5	-5	+0	+0
10-45	+5	+5	+10	+5	+5	-20	+0	+10	+10	+0	+0	+0
< 10	+5	+5	+10	+5	+5	-20	+0	+10	+10	+0	+0	+0

Figure 43. Storm - time foF2 deviations

Local Lat	00-03	03-06	06-09	09-12	Percentage MUF Deviations			
					K Value 6	12-15	15-18	18-21
0-14	99.0	117.9	104.6	103.8	102.6	101.9	99.9	100.3
15-34	90.5	85.7	94.6	93.3	92.9	92.7	96.0	94.5
35-49	90.5	86.3	79.8	80.6	83.1	84.6	89.1	91.8
50-59	76.4	75.7	73.2	75.9	79.9	85.1	88.2	83.6
60-67	77.8	87.4	81.6	77.4	77.9	82.3	83.9	76.2
68-74	89.3	89.9	85.4	85.7	85.5	91.8	91.1	92.1
75-90	88.4	86.2	84.8	92.0	92.5	95.9	96.5	93.3

Figure 44. Forecaster display of predicted MUF variations at different latitudes and local times. For example: A value of 117.9 indicates a predicted value 17.9 percent above the quiet day MUF.

apparent from routine magnetometer data, the main phase onset is more difficult to detect. Large variations of the middle latitude magnetometer observations may signal the onset of this phase. Total electron content (TEC) data can also be used to detect the onset of the decrease in  $foF_2$ . Comparisons of hourly observations of middle latitude ionospheric sounder data ( $foF_2$ ) with the pre-storm values are also needed. Stations such as Vandenberg, Dourbes, and Patrick are best suited for this purpose. Once the decrease in  $foF_2$ /MUF is observed, the predicted MUF deviations can be moderated with consideration of the current state of geomagnetic field and the previously illustrated variations with respect to storm-time and local time. Complete recovery to normal conditions may take a day or more after the geomagnetic disturbance has ended. Occasionally, ionospheric storms during the equinoxes serve as a transition mechanism for the seasonal change of the ionosphere, e.g., a recovery from a storm in the early spring may result in post-storm ionospheric characteristics more typical of the summer ionosphere than the pre-storm wintertime characteristics.

The period of 29-30 August 1979 provides an interesting example of how the ionosphere responds to geomagnetic activity. In Figures 45 and 46 we see the onset of the disturbance near 29/0500Z. At maximum storm intensity, 3-hourly  $a_p$  values approach 100, and the duration of the disturbance is slightly over 30 hours, ending about 30/1200Z.

From Figures 47 and 48 we can see that despite high 3-hourly  $a_p$  values immediately following the storm sudden commencement (SSC),  $foF_2$  and MUF deviations show little change during the following 5-7 hours. Beginning about 1100Z, significant decreases in the MUF begin to appear in the Western Hemisphere as indicated by Vandenberg and Boulder values. At the same time the European and Asian area retains slightly enhanced MUFs. During the period of 29/1200-2300Z a pattern of decreased MUFs emerges. Vandenberg and Boulder MUF deviations continue to be more negative. Overall, the higher latitude MUFs become depressed earlier and the effect spreads to the middle and lower latitudes such that by 29/1800Z a global pattern of MUF depression of 20-40 percent exists.

This pattern of depressed MUFs continues into the first part of 30 August (Figures 49 and 50). In comparing MUF deviations for the period 0000-0600Z on the 29th and 30th, drastic differences are noted. MUFs at Taiwan and Manila are significantly enhanced on the 30th as compared to the 29th. At the same time, Maui, another low latitude station, shows MUFs depressed by forty percent. By midday on the 30th the disturbance is subsiding. MUFs at the upper-middle and middle latitudes in Asia are showing MUF enhancements. The European area (Dourbes, Belgium) is also beginning to experience positive MUF deviations. At the same time, the Western hemisphere represented by Vandenburg is still experiencing negative MUF deviations. Not until 30/1500Z do the MUF deviations become positive. Note that the MUFs at Maui remain depressed for several hours beyond this time. By the end of the day there is no discernible MUF pattern.

Sporadic E conditions early on the 29th (Figure 51) present a typical summer pattern. Beginning about 29/1800Z, higher than normal  $foEs$  values (7 MHz) begin to appear at the higher latitudes. Dixon, Murmansk and later Narssarsuak show strong Sporadic E effects after 29/1200Z. This pattern

## GEOMAGNETIC INDEX DISPLAY FOR 790829

STATION	NUMBER	K-INDICES										REMARKS
		03	06	09	12	15	18	21	24			
THULE	04205	3	4	6	4	5	5	5	5			3
KOPENHAGEN	36801	5	6	7	6	6	5	5	5			6
DI XON	38701	4	6	6	6	7	8	7	6			
TI XIE BAY	43701											
COLLEGE	25602	2	5	5	5	6	7	6	4			
GOOSE BAY	71816	4	7	6	6	6	6	6	6			
MIRMANSK	33702	3	4	5	5	6	7	7	6			
ANCHORAGE	25601	3	5	7	6	7	7	7	5			
LORING	72712	3	6	6	6	6	6	8	5			
TJINGUSKA	39601	2	5	6	5	8	8	9	6	*SSC*		(04571)
LENINGRAD	33603	3	4	4	5	6	7	8	6	*SSC*		(05001)
MAGADAN	45601											
SVERDLOVSK	36502	2	4	4	4	5	6	6	6			
IPPERHFFORD	03655	2	3	5	4	4	6	5	5			
WINGST	31523	4	4									
MOSCOW	34502	3	4	4	5	6	6	7	5	*SSC*		(05001)
FREDRICKSBURG	18403	2	5	4	5	5	6	5	5	*SSC*		(04591)
Boulder	72469	2	4	5	5	5	5	5	4			
IRKUTSK	40501	2	3	4	4	6	6	6	5			
PE TROPAVLOVSK	46501											
CHAMBON	30503	4	4							*SSC*		(04591)
KAKIOKA	44402	1	3							*SSC*		(05001)
KE RGUELFN	77501				4	7	8	8	7	BAY (PSC)		(12121)
3-HMIRLY AP		14	52	60	56	67	94	93	45			
3-HMIRLY KP		3-	50	5+	5+	6-	6+	60	5-			
24-HD AVE AP		14	20	26	30	36	46	56	60			

Figure 45. Forecaster display of geomagnetic activity on 29 August 1979.

## GEOMAGNETIC INDEX DISPLAY FOR 790830

STATION		K-INDICES								
STATION	NUMBER	03	06	09	12	15	18	21	24	REMARKS
THULE	04205	5	4	3	4	4	5	5	4	
KRKENKEL	36801	4	5	5	5	2	2	3	3	
DIXON	38701	6	4	5	4	3	3	3	4	
TI XIE BAY	43701									
COLLEGE	25602	4	4	4	4	3	2	2	1	
GOOSE BAY	71816	6	5	3	3	1	2	2	1	
MURMANSK	33702	6	4	3	3	2	1	1	1	STORM END (1400)
ANCHORAGE	25601	6	6	5	4	2	3	3	2	
LORING	72712	4	5	3	3	3	3	3	2	
TINGUSKA	39601	5	3	4	4	2	1	1	1	
LE宁INGRAD	33603	5	3	3	3	2	1	2	1	STORM END (0100)
MAGADAN	45601									
SVERDLOVSK	36602	4	2	2	3	1	1	1	1	
IPPERHEYFORD	03655	5	2	3	3	3	3	2	2	
WINGST	31523									
MOSCOW	34502	4	4	2	3	3	2	2	2	STORM END (1100)
FREDRICKSBURG	18403	4	4	3	2	2	2	2	2	
BEDFORD	72469	3	4	3	3	3	2	3		
IP KUTSK	40501	3	3	2	2	1	1	1	1	
PE TROPAVLOSK	46501									
CHAMBON	30503			2	2	1	2	1	1	
KA KIOKA	44402			2	2	1	1	1	2	STORM END (1200)
KERGUELEN	77501	6	4	3	2	1	0	0	1	
3-HOURLY AP	37	32	18	15	12	11	10	6		
3-HOURLY KP	4+	4+	3+	30	3-	2+	2+	2-		
24-HR AVE AP	63	61	55	50	43	33	23	18		

Figure 46. Forecaster display of geomagnetic activity on 30 August 1979.

## VERTICAL INCIDENCE IONOSONDE DATA DISPLAY

STATION	29 AUG	00Z	01Z	02Z	03Z	04Z	05Z	06Z	07Z	08Z	09Z	10Z	11Z
MANILA	-5	1	6	1	-7	-8	-9	-12	-7	-4	-7	-7	-11
TAIPEI	10	-13	-5	9	8	9	6	5	-1	-3	3	2	
MAUI	-2	-3	-3	-2	-1	0	1	17	19	7	14	1	
KOKOHO	6					-4				5			
NIOSI	-8										3		
ASIAKH											44		54
VANDEN	2	2	6	-8	-4	-3	-13	-11	-5	-2	-2	-13	
ALMAA	-7					16				8	21	31	
KAABAR								1	4				
BONNIE	9	12	10	4	0	7	2	4	17	25	0	-35	
WALLOP	18	14	13	9	11	25	18	6	12	2	16	-23	
KIEV	-4	-2	-2	0	10	13	14	7	13	20	16	17	
IRKUTS	-10					10							
MOSCOW	2					8							
CHURBE	0	3	13	6	8	5	5	7		23	22	22	
CHIUCH	7	10	13	10	14	6							
AGADA	-8	-5	-5	-2	2	-1	-3	0	-3	4	-11	-23	
SEVERDL	-6	0	19	9	1	3	5	17	13	20	16	13	
TOMSK	3	-2	7	0	0	3	9	14	14	13	8	9	
GOOSE	-14	-15	-7	-5	-3	3	0	-3	-3	0	-10	-8	
YAKUTS	-22		-5	-5	-3	3							
CHLEG	-2	-27	-13	-13					-42				
MIRMAN	-20	-2	2	-4			-14	-38	-1	0	-4	-3	
CHLEKH	-4	0	-3	-1	-1	-32		-7	-7				
CHYON	14	2	0	2		-6	-13	1					
KOPENKE	-5	-11	-38	-33	-15	-15	-16	-13	-13	-20	-37		
CHOLU	19	14	14	9	9								
MANILA	127	137	147	157	167	177	187	197	207	217	227	232	
TAIPEI	-8	-8	-8	-3	-5	-20	-23	-13	-8	-3	5	11	
MAUI	22	29	30	36	15	17	3	4	-4	-1	-4	31	
KOKOHO	-16	-14	-7	7		-21	-37	-33	-37	-38	-40	-25	
NIOSI	8					18							
ASIAKH	16	16	25		12		-18	-26	-26	-28	-25	-11	
VANDEN	-18	-31	-24	-36	-44	-45	-45	-47	-47	-48	-45	-49	
ALMAA	22					-18							
KAABAR	27	26	31	2		8	2	-9	-15	3	-5	-17	
BONNIE	-37												
WALLOP	-29	-37	-29	-18	-20	-17	-19	-10	-6	4	9	2	
KIEV	20	13	12	9	10	-27	-32	-36	-39	-41	-35	-34	
IRKUTS	6					-18							
MOSCOW	23					-42							
CHURBE	29	25	17	17	19	1	-9	-26	-38	-58	-47	-43	
AGADA	-60	-61	-45	-42	-41	-42	-41	-43			-36	-35	
CHTAWA	-36		-21	-31	-31	-33	-33	-7	-7				
SEVERDL	11	-1	9	-12	12	-54	-64	-46	-47	-39	-35	-29	
TOMSK	-3	-18	16										
GOOSE			-31	-25								-41	
YAKUTS	-7	-29	-39	-40	-38					-31		-41	
CHLEG	-16			-23	-39	-38	-24	-30	-10	-13	-15	-27	-28
MIRMAN													
CHIUCH													
AGADA													
CHYON													
KOPENKE	-10	-41	-33	-32	-25	-28	-13	-31	-43	-38	-38	-37	
CHDAV		-30	2		-10		-21	-21	-23	-25	-25	-17	
CHOLU						-17			-19	-2			

Figure 47. Forecaster display of foF2 deviations on 29 August 1979.

VERTICAL INCIDENCE IONOSONDE DATA DISPLAY

CM MUF 4	29 AUG											
MANILA	007	012	027	037	047	057	062	072	087	097	107	117
TAIPEI	21	-7	-12	13	25	18	15	17	6	8	22	9
MAIDI	2	1	4	6	10	11	5	35	15	31	16	7
NI CO SI	-15			9		25	11	3	12	4	24	53
AS HK HA									-9	-6	-2	-16
VA NDEN	6	14	14	19	-1	-3	-9	-19	1	8	26	
KA BAR									4	15	-4	-37
BO ULD E	13	16	18	4	7	7	2	-4	13	29	21	21
KI EV	4	6	2	11	28	13	22	19	13	19	26	18
DO HOB E	4	8	17	6	4	9	8	7		1	-14	-29
MA GADA	-4	-9	-1	6	9	6	1	4	-3	1	16	13
SV EPO L	1	8	27	13	5		13	22	13	20	16	5
TO NSK	15	13		15	8	10	13	14	18	17	4	
SO DSE	2	-9	-10									
YA KU TS	-1		-5			-3	7	0	1	-3	-4	-20
COLLEG	2	-7	1	-3						-35		
MIRMAN	9	-5	6	-4						-1	-4	-12
SA LFK H	4		19	12	2	6	-18		1		-3	
PI XON	28	14	8	8	14	5	-3	14				
KO ENKE	6	-7	-21	-17	-5			-9		-9	-17	-15
PE SOLII	32	22	27	26								
MANILA	127	137	142	157	167	177	187	197	207	217	227	237
TAIPEI	-16	-16	-4	9		-17	-29	-16	-21	-19	-9	11
MAIDI	26	55	45	51	27	43	11	4	-8	-12	-14	31
NI CO SI	-13	-211	-11	-5		-34	-32	-49	-43	-44	-43	-40
AS HK HA	16	16			9		-27	-37	-35	-37	-34	-21
VA NDEN	-21	-37	-37	-43	-59		-19	-211	5	30		-31
KA BAR	22	16	31	-14			8	-15	-16	-21	-1	-5
BO ULD E	-46											
KI EV	24	21	24	5	10	-29	-32	-41	-46	-50	-40	-37
DO HOB E	29	30		21	33	5	1	-32	-22	-61	-51	-47
MA GADA	-62	-66		-41	-42	-37	-43				-41	-45
SV EPO L	11	-5	9	-15	6	-56	-66	-55	-43	-39	-30	-27
TO NSK	-3	-24	12									-47
SO DSE				-4	-1							
YA KU TS	-37	-51	-47	-45						-24		-17
COLLEG	-19				-7						12	8
MIRMAN										-16		
KO ENKE	-19	-43	-33	-37	-20	-25	-9	-15	-38	-25	-19	-22
SO DHA V				-13		-24		-34		-6	-20	
PE SOLII												

Figure 48. Forecaster display of MUF deviations on 29 August 1979.

STATION	30 AUG											
	00Z	01Z	02Z	03Z	04Z	05Z	06Z	07Z	08Z	09Z	10Z	11Z
MANILA	13	23	21	8	-4	-4	11	2	-2	-5	-8	
TAIPEI	22	31	33	28	18	9	3	5	6	-4	-5	
MAINT	-44	-47	-42	-40	-31	-33	-38	-33	-36	-37	-33	-33
NICOSIA	-17			21			29	7	1	4	3	
ASHKHA	-13	-15	0		13	19	22	21	24	21	15	8
VANDEN	-31	-36	-29	-33	-35	-28	-34	-37	-32	-28	-30	-33
ALMAA	-15						5					
KHABAR	-12	-12	-13		-16	-14	-12	-7	0	5	10	13
WALLOP	-9	-14	-4								0	
KIEV	-23	-26	-35	-29	-24	-25	-23	-11	-2	16	-7	4
IRKUTS	30						-26					
MOSCOW	-42						-25					
DOURBE	-40	-34	-31	-31	-31	-23	-22	-16	-7	-1	0	
MAGADA	-34	-31	-29	-28	-15	-12	-7	-3	7	9	0	-9
SVFRDL	-27	-26	-25	-29	-20	-13	-4	0	11	11	17	9
TOYSK	-29	-25	-16	-3	10	16	16	14	22	16	10	-50
YAKUTS	-39	-38	-11		3	0	11	18	18	0		-3
COLLEG			-19	-5								
CAPES			7	2	-2							
MIRMAN	-18				-26	-30						
SALEKH												
DTXON												
KOPENKE	-40	-41	-43		-25	-34	-24	-24	-19	-17	-16	-23
MANILA	127	137	147	157	167	177	187	197	207	217	227	237
TAIPEI	-8	-3	-2	-3	-3	-12	-7	6	3	-32	-11	-1
MAINT	12	26	30	29	33	44	0	-4	-3	-23	-9	3
NICOSIA	-37	-31	-28	-30	-30	-14						
ASHKHA	13			17		-5						
VANDEN	-33	-35	-11	7	11	11	-13	-8	-7	6	9	13
ALMAA	6							5	4	17	16	13
KHABAR	13	11	9	11	11	13	0	-18	-28	-22	-20	-21
WALLOP	-3							-1	-7	-11	-8	-5
KIEV	-2	-15	9	10								
IRKUTS	-61											
MOSCOW	0											
DOURBE	0	5	8	10	14	14	12	9	3	-1	-6	-5
MAGADA	-17	-22	-27	-30	-26	-34	-30	15	-12	-15	-22	-17
OTTAWA	-8	-8	-7	-1	10	6	11					
SVFRDL	0	5	9	16	10	19	9	2	-3	-2	-6	-6
TOYSK	-26	5	8	14	13			-6	-4	7		
YAKUTS	-1	-3	-2	-3	11	7	-4	-6	-24	-21	-16	-2
COLLEG			-49	-4	-30	0	-8					
MIRMAN	-7	-4	-3	5	5	3	-10			11	-6	-8
CHIRCH			-7	-7	-5	-8						
SALEKH	-14	-11	0	3	5	0	-2	3	4	6		-4
DTXON	-25	-24	-14	-8	-2	0	0	0	9	6	6	
KOPENKE	-6	-5	0	2	7	3	2	7	7	7	6	
PESELII			-9				5				-12	-12

Figure 49. Forecaster display of foF2 deviations on 30 August 1979.

AD-A096 833

AIR FORCE GLOBAL WEATHER CENTRAL OFFUTT AFB NE  
SHORT TERM HF FORECASTING AND ANALYSIS. (U)

F/G 4/1

JAN 81 J A MANLEY  
AFGWC/TN-81/001

UNCLASSIFIED

SBIE-AD-E850 033

NL

2  
202-364-18

END  
PAGE  
4  
DTIC

30 AUG													
DMUF 4	007	017	027	037	047	057	067	077	087	097	107	117	
MANILA	9	23	21	8	-4	-4	11	12	17	14	3	-1	-12
TAIPEI	18	26	33	33	26	18	11	20	17	14	3	2	
MAUI	-44	-47	-42	-40	-23	-26	-45	-33	-36	-37	-30	-31	
NICOSI	-20				21			24	7	-7	-10	-21	
ASHKHA	-10	-8	0		21	19	27	25	33	30	20	8	
VANDEN	-33	-34	-29	-31	-37	-31	-32	-35	-26	-22	-19	-28	
KHABAR	-15	-21	-20		-22	-34	-22	-10	-7	5	10	25	
KIEV	-26	-26	-30	-29	-18	-17	-20	-11	-10	30	14	20	
DOLIBE	-45	-34	-29	-29	-31	-15	-14	-10	-10	-1	11		
MAGADA	-36	-31	-26	-25	-18	-12	-4	1	11	25	4	-2	
VERDL	-25	-24	-25	-27	-20	-6	4	12	24	28	36	17	
TOMSK	-24	-25	-13	8	27	34	30	18	36	30	22	-28	
YAKUTS	-39	-38	-40	-7			19	19	7	27	9	11	4
COLLEG				-7	-12								
CAPE				28	13	6							
MIRMAN	-28				-32								
SALEKH													
DI XON													
KOENKE	-30	-41	-45	-19	-16	-21	-19	-27	-22	-14	-5	-11	-5
	127	137	142	157	167	177	182	192	207	217	227	237	
MANILA	-8	14	14	16	8	-3	-1	17	16	-28	-5	13	
TAIPEI	21	46	55	48	53	65	22	3	11	-13	-3	11	
MAUI	-35	-26	-23	-30	-32	-14							
NICOSI	-5		12			4				-18		-14	
ASHKHA	15		22	35	28	6	-6	-8	-11	2	6	13	
VANDEN	-33	-35	-14	22	28	19	25	9	31	22	30	26	
KHABAR	13	3	9	11	11	18	8	-18	-22	-16	-14	-26	
KIEV	14	-9	17	18			6	4	-5		-8	3	
DOLIBE	11	-13	20	19	-31	-26	-20	17	17	11	6	-2	
MAGADA	-11	-22	-33	-33	-23	-31	-25	-5	1	-15	-28	-7	
VERDL	4	10	13	20	23	23	17	5	8	-15	-6	-2	
TOMSK	-23	9	12	14	13								
YAKUTS	2	-6	-5	-3	0	7	-10	1	4	3	-16	11	
COLLEG			-45	-4	-13	8	3		-14	-14	-6	-4	
MIRMAN	-4	-4	-14	12	5	3							
SALEKH	5	-5	14	7	12	7	-5	3	8	10			
DI XON	-28	-18	-11	-8	13	4	-4	3	22	5			
KOENKE	4	9	11	17	15	15	13	23	24	14			
RE SOLU											-12	-5	

Figure 50. Forecaster display of MUF deviations on 30 August 1979.

VERTICAL INCIDENCE IONOSONDE DATA DISPLAY

FOES	29 AUG											
MANILA	007	017	027	037	047	057	067	077	087	097	107	117
TAIPEI	6.	4.	4.	6.	4.	4.	4.	4.	6.	3.	3.	3.
MAHII	3.	4.	3.	4.	4.	6.	4.	5.	5.	5.	3.	3.
NI COSI	5.	5.	5.	4.	5.	3.	4.	5.	2.	3.	2.	2.
AS HKHA	4.				3.		4.	5.		5.	5.	4.
VA NDEN	3.	4.	3.	5.	5.		3.	5.	4.	4.	2.	
WA ABAP												
KI EV	2.	2.		2.	5.	3.	4.	5.	4.	5.	5.	
DO UIRBE	2.						3.	4.		5.	4.	4.
WA GADA	3.	3.	3.	3.	3.	3.	4.	3.	2.		2.	2.
SV ERDL	3.	2.	3.	3.	3.	3.	4.	5.	4.	3.	4.	
TO YSK	4.	4.			4.		4.	4.				
GO OSE	2.		3.	5.			4.	4.	7.			7.
WA KIITS	5.		3.	3.	3.	4.			2.	5.	7.	3.
COLLEG		4.	3.								5.	
CAPE S												
MURMAN	3.	3.	4.	3.			4.					
NA RESSA	5.	4.	4.		5.	3.	5.		5.	3.	3.	5.
WA LEKH	2.			3.	3.	3.						
DI XON	4.							4.				
KI ENKE	3.											
127	137	147	157	167	177	187	197	207	217	227	237	
MANILA	3.			4.	4.	3.	6.	4.	4.	9.	5.	
TAIPEI	3.	4.	5.	5.	3.	6.	4.	3.	3.	4.	3.	
MAHII	2.	2.	2.	2.	2.	3.	4.	5.	8.	7.	4.	4.
NI COSI	4.	4.	4.	2.	2.	2.	4.	10.	4.	2.	4.	2.
AS HKHA	4.	6.	5.				4.					
VA NDEN					3.	3.	3.	3.	3.	3.	3.	3.
WA ABAP				2.	3.	3.	4.	3.	3.	3.	3.	3.
KI EV		3.	4.	3.	3.	7.	3.	4.	3.	3.	3.	3.
DO UIRBE		4.	4.	4.	4.	3.	3.	3.	2.	4.		
WA GADA	2.	1.	2.	2.	2.	2.	2.	2.	3.	3.	3.	3.
SV ERDL	4.	3.	3.	2.								
TO YSK	4.	3.										
GO OSE	5.	5.	5.	4.	4.	5.			8.	5.		5.
WA KIITS	3.	4.	4.	3.								
COLLEG	4.	4.			4.				3.		3.	3.
CAPE S		5.		5.	5.			6.				
MURMAN				9.	4.		3.	8.	4.	5.	6.	5.
NA RESSA	5.					3.	3.	4.	3.	5.	12.	2.
WA LEKH											6.	4.
DI XON	10.	1.	10.	10.	10.	9.	6.	3.	5.	4.	3.	3.
KI ENKE		6.					3.	3.	8.	3.		
GO DHAU							4.	3.	3.	3.		
RE SOLII				3.	3.	3.	3.	3.	3.	3.	3.	3.

Figure 51. Forecaster display of foEs values for 29 August 1979.

extends into the first part of the 30th (Figure 52), although the North American stations do not exhibit as strong an effect as the Asian ones. At the middle and lower latitudes, the foEs tends to show slightly higher values during the disturbance, although nowhere near the dramatic changes in the auroral zone.

Examination of the qualifiers (Figures 53 and 54) accompanying the vertical incidence sounder reports adds to our knowledge of the disturbed ionosphere during this period. Throughout the entire disturbed period 29/0500Z-30/1200Z, the high latitude stations are dominated by qualifier 2 indicating of auroral zone absorption and qualifier 1 indicating Blanketing E. Good examples of this are Murmansk, Salekhardt, and Dixon.

#### COMMUNICATOR REPORTS AS A DIAGNOSTIC TOOL

Additional information concerning the state of HF propagation conditions can be obtained through contacts with HF communicators. Such information is limited in its applicability to short-term forecasts. Voice contacts with various communicators can prove useful but must be used with caution. Infrequent monitoring, inexperienced operators, and equipment problems may contribute to misleading reports from communicators. Therefore, communicator contacts should be used as a diagnostic tool for the prepared forecast. If HF propagation conditions, as described by communicators, do not confirm the analysis and forecast prepared from ionospheric observations, then the forecast should be re-evaluated for indicators that may have been overlooked. Some quantified data can be obtained from HF communicators through the use of the internationally recognized SINPO code. There are five variables in this code, and each of these varies on a scale of one to five. These are:

S = strength. This is the observed signal strength.

I = interference. This covers man-made interference.

N = noise. Natural noise and static including that produced by lightning.

P = propagation disturbance. This includes fading and other irregularities in propagation.

O = overall rating. This is the sum total, dependent on the other four.

There is a five digit quality classification associated with the five letters. For example SINPO 55555 would indicate the highest quality reception. The five ratings for signal strength and overall rating are:

- 5 = excellent
- 4 = good
- 3 = fair
- 2 = poor
- 1 = barely audible, unacceptable signal

foEs	30 AUG											
MANILA	002	017	027	032	047	052	062	072	082	092	102	112
TAIPEI	8.	5.	5.	5.	4.	5.	4.	7.	5.	4.	2.	2.
MAUI	4.	7.	8.	8.	7.	6.	4.	2.	2.	2.	2.	2.
NIHON	3.	4.	3.	3.	2.	2.	4.	2.	2.	2.	2.	3.
ASHKHA	2.	3.	3.	5.	5.	5.	6.	4.	4.	4.	4.	4.
VANDEN	3.	3.	3.	5.	5.	5.	3.	3.	2.	4.	4.	4.
KHABAR	3.	4.	4.		3.	4.	3.	3.	2.	2.	4.	4.
KIEV	3.	2.			2.	3.	5.	4.	4.	4.	4.	4.
DOURBE	3.							6.	4.	4.	4.	4.
MAGADA	4.	3.				3.	3.	2.	2.	2.	1.	5.
COVERDL		2.	2.	2.	4.	3.	4.	5.			5.	5.
TMMSK	2.	2.										
GOOSE	5.	5.			4.	5.	8.	5.	4.			
COLLEG	3.		5.	4.		2.	3.	3.	3.	3.	4.	4.
MIRMAN	4.	5.	5.	4.								
NAPCCA	8.	6.	4.	5.	5.	5.	6.	5.	4.			
CALEKH												
DIxon	5.	4.	3.	3.	3.	3.	3.	2.	2.			
KPENKE		3.	3.	3.								
GODHAW												
RESOLU	3.	2.			1.							
	127	137	147	157	167	177	187	197	207	212	222	232
MANILA							1.	3.	4.	6.	7.	5.
TAIPEI					3.	3.	4.	3.	3.	3.	4.	3.
MAUI	2.	2.	2.	1.	1.	3.	3.	3.	3.	3.	3.	3.
NIHON	4.	4.	4.	1.		4.						2.
ASHKHA	4.	4.	3.	2.	2.	3.	4.	7.	7.	5.	7.	7.
VANDEN	3.	3.	3.	3.	2.	5.	6.	3.	3.	3.	4.	4.
KHABAR	2.	2.	2.	2.	2.	2.	3.	3.	3.	3.	4.	4.
KIEV	5.	3.	3.	3.	2.	2.	4.	3.	4.	4.	3.	3.
DOURBE	2.	1.	2.	1.	2.	2.	2.	2.	3.	3.	3.	3.
MAGADA	2.	4.	3.	3.	3.	3.	3.	2.	3.	3.	3.	2.
COVERDL	5.	4.	3.	3.	3.	3.	3.	2.	3.	3.	3.	2.
TMMSK												
YAKUTS	3.						4.					
COLLEG	5.	6.	5.	5.	3.	3.	3.	3.	3.	3.	4.	4.
MIRMAN					3.	2.					3.	3.
CALEKH						2.						
DIxon	3.	3.	3.	3.	5.	5.		7.	9.	7.		
KPENKE	3.	5.	5.	5.	4.	4.	4.	3.	6.	6.		
RESOLU	2.	2.	2.	2.	3.	3.	5.		6.	6.	2.	2.

Figure 52. Forecaster display of foEs values for 30 August 1979.

VERTICAL INCIDENCE IONOSONDE DATA DISPLAY

QUAL	29 AUG												137
	00	01	02	03	04	05	06	07	08	09	10	11	
MANILA	00	01	02	03	04	05	06	07	08	09	10	11	237
TAIPEI	00	00	00	00	00	00	00	00	00	00	00	00	00
MAUI	00	00	00	00	00	00	00	00	00	00	00	00	00
KOKOBU	00	00	00	00	00	00	00	00	00	00	00	00	00
NI CO SI	00	00	00	00	00	00	00	00	00	00	00	00	00
AS HK HA	00	00	00	00	00	00	00	00	00	00	00	00	00
VAN DEN	00	00	00	00	00	00	00	00	00	00	00	00	00
AL MA A	00	00	00	00	00	00	00	00	00	00	00	00	00
KAHABAR	00	00	00	00	00	00	00	00	00	00	00	00	00
BOULDE	00	00	00	00	00	00	00	00	00	00	00	00	00
WALLOP	00	00	00	00	00	00	00	00	00	00	00	00	00
KI EV	00	00	00	00	00	00	00	00	00	00	00	00	00
IP KIITS	00	00	00	00	00	00	00	00	00	00	00	00	00
MA SCOW	00	00	00	00	00	00	00	00	00	00	00	00	00
DA LIOPBE	00	00	00	00	00	00	00	00	00	00	00	00	00
MA GADA	00	00	00	00	00	00	00	00	00	00	00	00	00
AT TAWA	00	00	00	00	00	00	00	00	00	00	00	00	00
SV ERDL	00	00	00	00	00	00	00	00	00	00	00	00	00
TA MSK	00	00	00	00	00	00	00	00	00	00	00	00	00
GO OSE	00	00	00	00	00	00	00	00	00	00	00	00	00
VA KIITS	00	00	00	00	00	00	00	00	00	00	00	00	00
CL LEG	00	00	00	00	00	00	00	00	00	00	00	00	00
CAPE S	00	00	00	00	00	00	00	00	00	00	00	00	00
MIPMAN	00	00	00	00	00	00	00	00	00	00	00	00	00
CHIOPCH	00	00	00	00	00	00	00	00	00	00	00	00	00
NA DCC	00	00	00	00	00	00	00	00	00	00	00	00	00
SA LEKH	00	00	00	00	00	00	00	00	00	00	00	00	00
DE XON	00	00	00	00	00	00	00	00	00	00	00	00	00
KRENKE	00	00	00	00	00	00	00	00	00	00	00	00	00
GO DHAV	00	00	00	00	00	00	00	00	00	00	00	00	00
RE SOLII	00	00	00	00	00	00	00	00	00	00	00	00	00
	127	137	147	157	167	177	187	197	207	217	227	237	
MANILA	6000	00000	00000	00000	00000	00000	00000	00000	00000	00000	00000	00000	
TAIPEI	00000	00000	00000	00000	00000	00000	00000	00000	00000	00000	00000	00000	
MAUI	00000	00000	00000	00000	00000	00000	00000	00000	00000	00000	00000	00000	
KOKOBU	00000	00000	00000	00000	00000	00000	00000	00000	00000	00000	00000	00000	
NI CO SI	00000	00000	00000	00000	00000	00000	00000	00000	00000	00000	00000	00000	
AS HK HA	00000	00000	00000	00000	00000	00000	00000	00000	00000	00000	00000	00000	
VAN DEN	00000	00000	00000	00000	00000	00000	00000	00000	00000	00000	00000	00000	
AL MA A	00000	00000	00000	00000	00000	00000	00000	00000	00000	00000	00000	00000	
KAHABAR	00000	00000	00000	00000	00000	00000	00000	00000	00000	00000	00000	00000	
BOULDE	00000	00000	00000	00000	00000	00000	00000	00000	00000	00000	00000	00000	
WALLOP	00000	00000	00000	00000	00000	00000	00000	00000	00000	00000	00000	00000	
KI EV	00000	00000	00000	00000	00000	00000	00000	00000	00000	00000	00000	00000	
IP KIITS	00000	00000	00000	00000	00000	00000	00000	00000	00000	00000	00000	00000	
MA SCOW	00000	00000	00000	00000	00000	00000	00000	00000	00000	00000	00000	00000	
DA LIOPBE	00000	00000	00000	00000	00000	00000	00000	00000	00000	00000	00000	00000	
MA GADA	00000	00000	00000	00000	00000	00000	00000	00000	00000	00000	00000	00000	
AT TAWA	00000	00000	00000	00000	00000	00000	00000	00000	00000	00000	00000	00000	
SV ERDL	00000	00000	00000	00000	00000	00000	00000	00000	00000	00000	00000	00000	
TA MSK	00000	00000	00000	00000	00000	00000	00000	00000	00000	00000	00000	00000	
GO OSE	00000	00000	00000	00000	00000	00000	00000	00000	00000	00000	00000	00000	
VA KIITS	00000	00000	00000	00000	00000	00000	00000	00000	00000	00000	00000	00000	
CL LEG	00000	00000	00000	00000	00000	00000	00000	00000	00000	00000	00000	00000	
CAPE S	00000	00000	00000	00000	00000	00000	00000	00000	00000	00000	00000	00000	
MIPMAN	00000	00000	00000	00000	00000	00000	00000	00000	00000	00000	00000	00000	
CHIOPCH	00000	00000	00000	00000	00000	00000	00000	00000	00000	00000	00000	00000	
NA DCC	00000	00000	00000	00000	00000	00000	00000	00000	00000	00000	00000	00000	
SA LEKH	00000	00000	00000	00000	00000	00000	00000	00000	00000	00000	00000	00000	
DE XON	00000	00000	00000	00000	00000	00000	00000	00000	00000	00000	00000	00000	
KRENKE	00000	00000	00000	00000	00000	00000	00000	00000	00000	00000	00000	00000	
GO DHAV	00000	00000	00000	00000	00000	00000	00000	00000	00000	00000	00000	00000	
RE SOLII	00000	00000	00000	00000	00000	00000	00000	00000	00000	00000	00000	00000	

Figure 53. Forecaster display of qualifiers for 29 August 1979.

QIAL	30	AUG	007	017	027	037	047	057	067	077	087	097	107	117
MANILA														
TAIPEI														
MAUI														
NICOSIA														
ASIAHKHA														
VANDEN														
ALMAA														
KHABAR														
WALLOP														
KIEV														
IRKUTS														
MOSCOW														
DOURBE														
MAGADA														
OTAWA														
VERDL														
TONSK														
YAKUTS														
COLLEG														
CAPE														
MURMAN														
NAPCCA														
SALEKH														
DIKON														
KRENKE														
RECOLU														
	127	6	000	00	00	00	00000000000000000000	00000000000000000000	00000000000000000000	00000000000000000000	00000000000000000000	00000000000000000000	00000000000000000000	00000000000000000000
	137	6	000	00	00	00	00000000000000000000	00000000000000000000	00000000000000000000	00000000000000000000	00000000000000000000	00000000000000000000	00000000000000000000	00000000000000000000

Figure 54. Forecaster display of qualifiers for 30 August 1979.

For the I, N, and P values the ratings are:

5 = nil  
4 = slight  
3 = moderate  
2 = severe  
1 = extreme

Such reports for individual HF circuits can help fill gaps in other data sources; however, caution should again be exercised in interpreting such reports as indicators of the general state of HF propagation conditions.

#### HF EFFECTS FROM A NUCLEAR EXPLOSION

The effects of a nuclear explosion on the ionosphere and HF communication can be severe and highly variable. While there are many unknown factors involved, the forecaster may be able to provide useful information to users of HF communication. These assessments should be considered order of magnitude estimates. Much of our knowledge concerning the ionosphere effects of nuclear explosions came from the high altitude TEAK and ORANGE explosions in the Pacific Ocean during the summer of 1958. These and other effects are described in detail in Glasstone's "The Effects of Nuclear Weapons." The information in this section has been extracted from this source to serve as a brief reference for HF forecasting and analysis.

The effects of the ionization produced by nuclear explosions varies with the height of the detonation. As the height of the detonation varies, the manner in which the changes in electron density are produced also changes. For radio and radar waves, the maximum attenuation occurs mainly within a 10 mile altitude range centered around an altitude of 45 miles, i.e., the D-region of the normal ionosphere.

For nuclear detonations at altitudes below 10 miles, much of the ionization produced will be contained within several hundred yards of the fireball. The large number of neutral particles present will result in rapid recombination, such that the large increase in ionization will last only a fraction of a second. This is sufficient to cause some attenuation of electromagnetic signals passing through the immediate vicinity of the burst, but its effects will disappear in a matter of seconds.

In the case of megaton range detonations, however, the radioactive cloud may rise to heights of 20 miles or more. An appreciable portion of the gamma radiation associated with fission products and other weapon debris will travel upward into regions of lower air density. The continued emission of this radiation will result in an increased electron density in the D-region and will persist for several hours.

In the altitude range of 10 to 40 miles, additional amounts of radiation will reach the D-region and cause significant amounts of ionization. The electron densities resulting from a one megaton explosion at various heights are illustrated in Figure 55 as a function of horizontal distance. Note that the electron densities are only those produced by the explosion and do not include the normal ionization produced by solar radiation. Also of

significance is that the horizontal distance over which the ionization occurs is limited by the curvature of the earth to that portion of the D-region that is in line-of-sight of the explosion. This is shown by the broken curve in Figure 55.

Additional ionization will result as a consequence of gamma and beta (electron) radiation associated with the debris cloud. For a one megaton burst to an altitude of 20 miles, the radioactive debris can reach an altitude of 40 miles. The ionizing particles will have a spatial extent of about 20 miles, so that the associated absorption will be generally confined to that area.

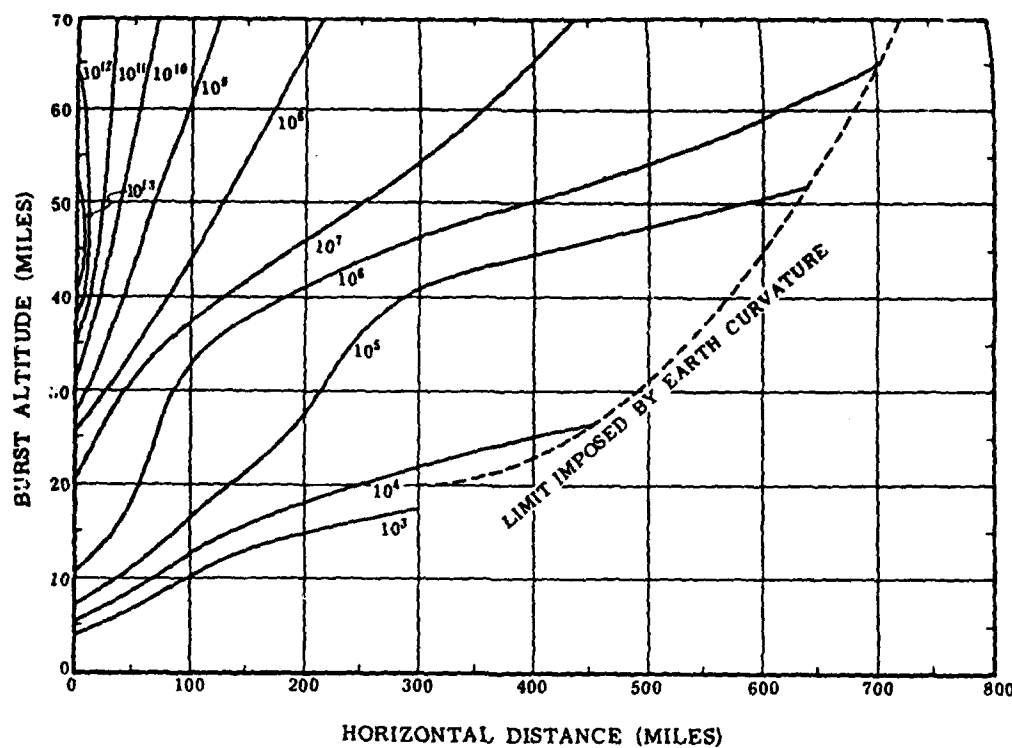
For detonations that occur at altitudes between approximately 40 and 70 miles, the ionization produced by thermal x-rays and ultraviolet light becomes more significant. Since the x-rays may carry as much as two thirds of the explosion energy, the electron densities produced will be high. The distance over which the ionization effects occur, as noted above, is limited by the curvature of the earth. For example, a detonation at 70 miles altitude will only produce radiation out to a horizontal distance of roughly 700 miles.

The ionization associated with the delayed gamma and beta radiation also becomes more important at these altitudes. The weapon debris can reach an altitude of several hundred miles, but the low atmospheric density will result in the particles rapidly falling, reaching an altitude of about 85 miles within an hour. Widespread ionization will occur, but the electron densities will be relatively low because of the large volume involved.

For example, the gamma rays, associated with the weapon debris, reaching an altitude of 300 miles will produce significant D region ionization as far out as 3000 miles.

A new situation arises for the beta particle radiation at the higher altitudes. These particles will follow a spiral path along the earth's magnetic field lines with about one half moving toward the corresponding point in the opposite hemisphere (See Figure 56). Thus, two conjugate volumes of ionization, one in each hemisphere, will be produced where the earth's magnetic field lines pass through the D-region. Each of the ionized areas will have roughly one half that of the radioactive cloud at the location of the explosion. "Artificial" aurora and strong D-region absorption can be expected to accompany the ionization in each of the conjugate areas.

At altitudes above 70 miles an additional phenomenon occurs. The lower atmospheric density at these altitudes will allow the weapon debris to expand rapidly, "stretching" the earth's magnetic field lines. As the debris is stopped and falls back toward the earth, the gamma and beta radiation will irradiate the D region from above, causing widespread but low intensity ionization. Part of the debris will also be trapped by the earth's magnetic field. As a result, beta particles will spiral back and forth along the field lines. As the particles drift eastward in longitude they will form, in a matter of hours, a shell of high energy electrons completely around the earth. During the ARGUS experiments in 1958, a detonation on the order of 3 kilotons resulted in a well defined shell, about 60 miles thick persisting for many days.



Calculated electron densities at an altitude of 45 miles produced by 1-megaton fission yield explosion at various burst heights as a function of horizontal distance.

Figure 55. (from Glasstone)

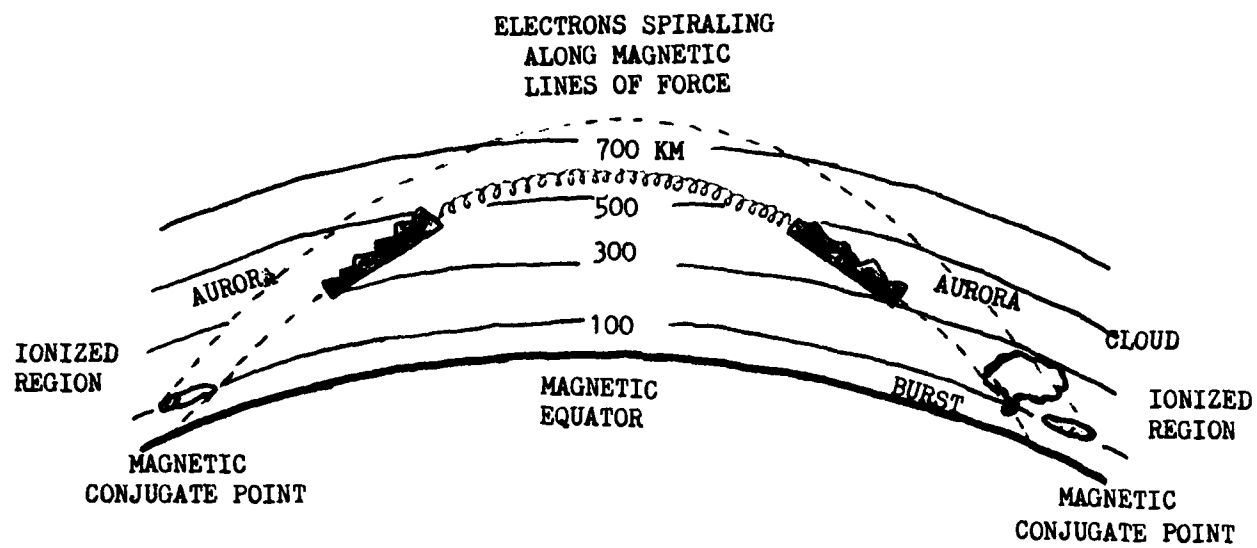


Figure 56. Phenomena associated with high-altitude nuclear explosions ( after Glasstone ).

The time history of ionization produced by the initial nuclear radiation of a one megaton explosion can be estimated using Figure 55 with the data below. From this data we see the time required for various electron densities to decrease by a factor of 10. For example: after 1 second, day or night, all electron densities of  $10^8$  electrons per cubic centimeter or more will be decreased to  $10^7$ ; densities of  $10^7$  or less will be essentially unchanged. For densities below  $10^6$  the recovery times for day and night are different. Note also, that densities below  $10^5$  will decrease relatively slowly during the daytime. For the D-region, a normal daytime electron density is  $10^3$  and nearly zero at night. By adding the recovery times necessary to achieve those densities, it can be seen that it would take about 3 hours in the day and about 100 seconds at night for the D region to recover completely from the initial ionization.

#### CALCULATED RECOVERY TIMES IN THE D REGION OF THE IONOSPHERE.

Electron Density (electron/cm <sup>3</sup> )	Time for density to decrease by factor of 10	
	Day (Sec)	Night (Sec)
$10^8$ (decreased to $10^7$ )	Less than 1	Less than 1
$10^7$	10	10
$10^6$	100	15
$10^5$	1,000	15
$10^4$	10,000	15

The ionization associated with the residual beta and gamma radiation extends over a longer period of time, making it difficult to estimate electron densities. Figures 57 and 58 can be used to make estimates of electron density as a function of the debris radius. Figure 57 is for a one megaton explosion in the 10 to 40 mile altitude range. It is postulated that the debris cloud rises to a height of 20 miles above the burst level and that the cloud radius increases at a rate of 100 miles per hour. So the radius (R) of the cloud (miles) at any time t (hours) after the explosion is given by

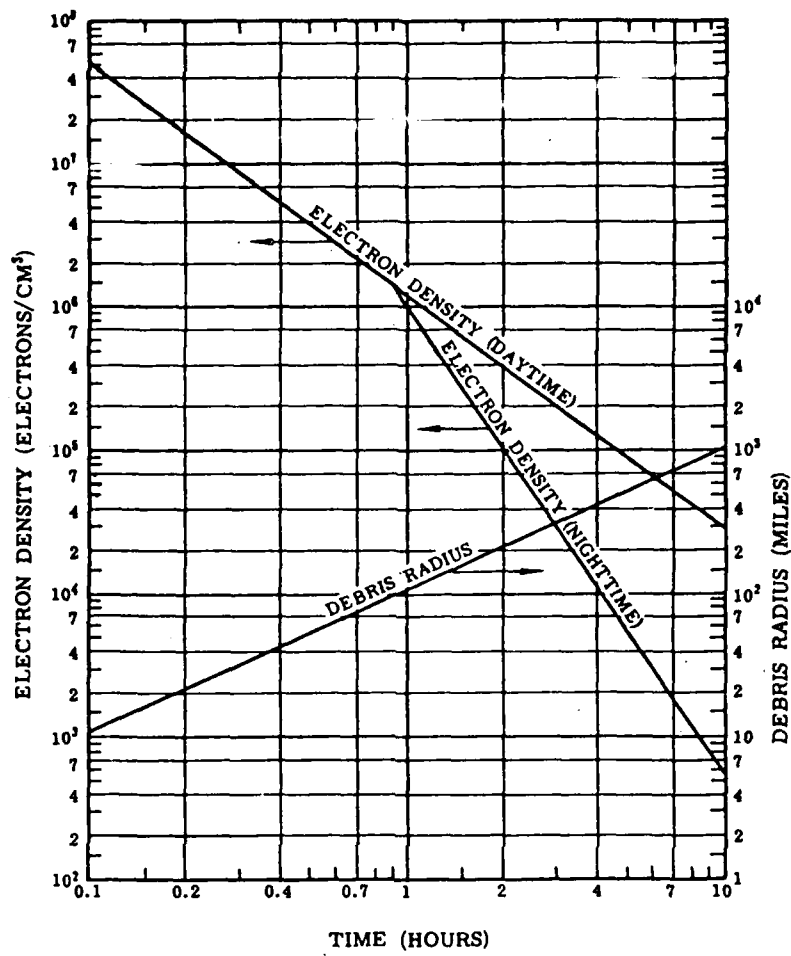
$$R = 100t$$

Figure 58 illustrates the same parameters for the 40 to 70 mile altitude range. It is assumed that the cloud rises to heights of greater than 100 miles and then drops to 85 miles within a few minutes. The cloud radius is assumed to increase at a rate of 2,000 miles per hour for 30 minutes and 100 miles per hour thereafter such the R in miles is expressed by:

$$R = 2000t \text{ for } t \leq 0.5 \text{ hours}$$

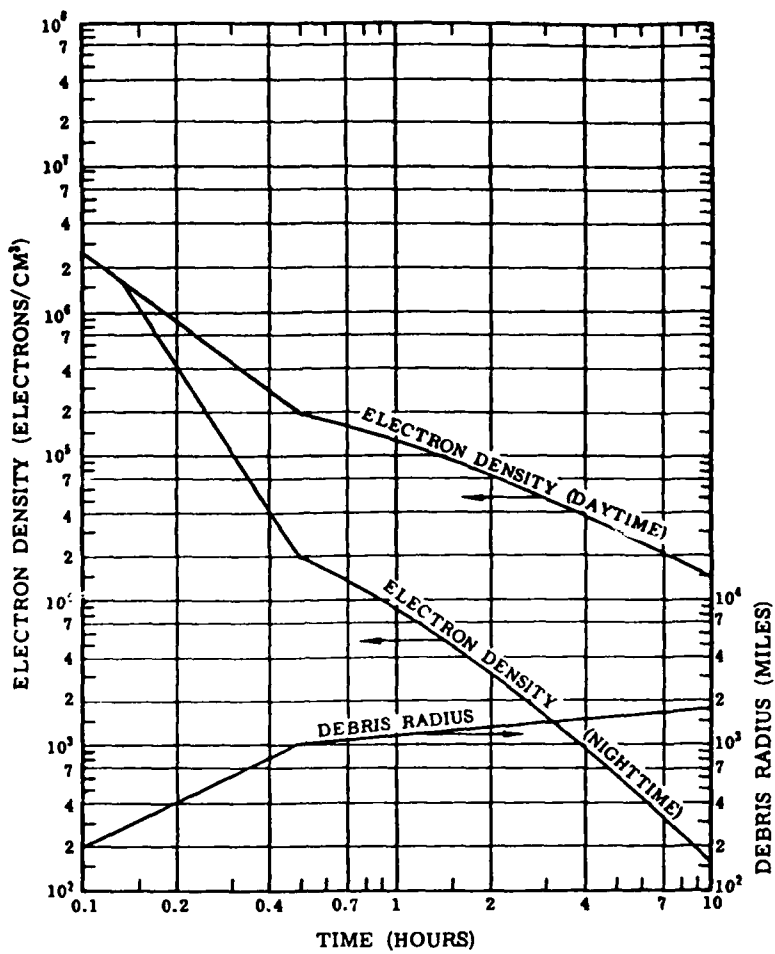
$$R = 950 + 100t \text{ for } t > 0.5 \text{ hours.}$$

To illustrate: Figure 57 shows that at one hour after a one megaton burst in the 10 to 40 mile altitude range, an electron density of about  $10^6$  will extend over an area of radius 100 miles around the burst point, day or night. At 3 hours after the detonation, a density of  $2 \times 10^5$  will extend to a radius of 300 miles in the daytime, but at nighttime the density would only be  $3 \times 10^4$  electrons per cubic centimeter.



Radius of debris expansion and corresponding D-region electron density as functions of time for a 1-megaton fission detonation in the altitude range of 10 to 40 miles.

Figure 57. (from Glasstone)



Radius of debris expansion and corresponding D-region electron density as functions of time for a 1-megaton fission detonation in the altitude range of 40 to 70 miles.

Figure 58. (from Glasstone)

Signal attenuation at various frequencies can be calculated using the equation:

$$A = 4 \times 10^{-3} \frac{N}{f^2} \sec \phi \text{ where}$$

A = absorption in decibels per mile

N = electron density (electrons per cubic centimeter)

f = wave frequency (megahertz)

$\phi$  = angle of incidence of the radio signal with the vertical.

An operational HF circuit will normally have a value of  $\sec \phi$  equal to about 5. Assuming the signal traverses a vertical distance of 10 miles at a frequency of 5 megahertz, an electron density of about  $5 \times 10^3$  electrons per cubic centimeter will yield a signal attenuation of nearly 40 decibels. At a frequency of 20 megahertz, an electron density of nearly  $10^5$  is required to produce the same attenuation. These values can be considered nominal values for making an HF circuit inoperable. Additional areas of strong absorption can be expected at the conjugate points for bursts at 40 to 70 miles altitude range. Artificial aurora will also be produced near these locations to add to the disruption of HF communication.

There are two main ways in which an HF circuit can be affected by the ionization produced by a nuclear explosion. First, if the signal passes through the D-region at a point where sufficient ionization is present, severe attenuation can result. A density of  $10^3$  electrons per cubic centimeter in the region is usually sufficient to affect transmission of the lower frequencies on the HF band, whereas  $10^4$  electrons per cubic centimeter will interfere with the higher frequency end. For bursts at altitudes below 10 miles, no widespread interference with HF communication is to be expected. For megaton range detonations above 10 miles, it is seen from Figure 55 that the initial nuclear radiation and thermal x-rays are sufficient to cause instantaneous disruption of HF signals passing sufficiently close to the burst point.

For example, using Figure 55, for a megaton burst at a height of 50 miles in the daytime, the effect would be felt out to a distance of 600 miles. Using the previously mentioned recovery times, recovery from this would require from about 1,000 seconds (17 minutes) to roughly 10,000 seconds (3 hours) according to the frequency. In addition to the effects of the initial radiation, the ionization due to the delayed nuclear radiation must also be considered. From Figure 57 it can be seen that a signal passing 500 miles from a megaton burst in the altitude range from 10-40 miles will be disrupted by radiation from the debris cloud 5 hours after the burst in the daytime and will not recover until several hours later. For a burst at altitude of 40-70 miles, Figure 58 indicates that a signal 500 miles distant will be affected within 15 minutes and will not recover for 10 hours or more. At night, the electron density would drop below  $10^4$  electrons per cubic centimeter in 1 hour and below  $10^3$  in 4 hours. In comparing Figures 57 and 58 with respect to nuclear radiation, bursts at higher altitudes influence larger areas, but the effects are of shorter duration.

The second and quite different manner in which HF communications may be affected by a nuclear explosion is the disturbance of the ionosphere by

hydromagnetic motions. If the ionosphere is disturbed in any manner in the vicinity of one of the control points of an HF circuit, disruption of the circuit can be expected. For burst altitudes above 40 miles, such disturbances can be expected to occur despite the low atmospheric density. Just as for lower altitude bursts, a shock wave will be formed and transmitted radially in all directions from the burst. When that part of the shock front traveling upward and outward reaches altitudes corresponding to E and F layer heights, it will encounter air of such low density that further propagation can occur with very little loss of energy. Thus, it will move outward for very long distances - possibly thousands of miles for a megaton burst--carrying with it most of the atmosphere in the upper E and lower F regions. The disturbance travels at about 2,000 miles per hour and after its passage the ionosphere will require from one to several hours to recover. If a HF system has one of the control points within 1,000 miles of a megaton burst in the altitude range from 40 to 70 miles, it will probably be disrupted for an hour or more.

#### REFERENCES

AFCWCP 105-1, Volume IV, "Space Environment Products" HQ Air Force Global Weather Central, Offutt AFB, NE 68113

AWSP 105-36, "Guide to Solar-Geophysical Activity", HQ Air Weather Service (MAC), Scott AFB, IL 62225, 12 Jul 1977, 38 p.

Beard, E. D., 1978: AFGWC Technical Memorandum 78-001, "High Frequency Radio Users Guide to AFGWC Products", Jan 1978.

CCIR Report 322, "World Distribution and Characteristics of Atmospheric Radio Noise", Geneva, 1963.

Davies, K., 1965: NBS Monograph 80, "Ionospheric Radio Propagation", U.S. Department of Commerce, Washington, D.C., April 1, 1965, 470 p.

Glasstone, S. (Editor) 1962: The Effects of Nuclear Weapons, U.S. Government Printing Office, Washington, D.C., April 1962.

Pike, C.P. (Editor), 1975: AFCRL-TR-75-0191 "Defense Meteorological Satellite Program Auroral - Ionospheric Interpretation Guide", Air Force Surveys in Geophysics No. 306, 4 Apr 1975.

Rose, R.B., Jr. Hill, and M.P., Bleiweiss, NELC TR 1938, "Sudden Ionospheric Disturbance Grid", Dec 1974.

Smith, E. K., 1978: "Temporate Zone Sproadic - E Maps ( $foEs \geq 7$  MHz)", Radio Science, Vol 13, No 3, pp 571-575, May-June 1978.

